Novel therapies for hypertension and associated cardiovascular risk

A DISSERTATION
SUBMITTED TO THE FACULTY OF THE GRADUATE SCHOOL
OF THE UNIVERSITY OF MINNESOTA
BY

Elizabeth M. Annoni

IN PARTIAL FULFILLMENT OF THE REQUIREMENTS
FOR THE DEGREE OF
DOCTOR OF PHILOSOPHY

Advisor: Alena Talkachova

August 2018

Acknowledgements

This has been an incredible journey, and I owe many thanks to those who have helped me along the way. First and foremost I would like to thank my advisor, Dr. Alena Talkachova, for all the support and guidance she has provided throughout my graduate school career. You taught me to be a successful researcher, team member and leader. I am forever grateful for all of the time and resources you have devoted to me and my project.

I would also like to thank the rest of my committee members, Dr. John Osborn, Dr. Bruce KenKnight, and Dr. Matthew Johnson, for their advice and encouragement throughout the project. Thank you for all of your time and contributions to this project, and thank you for helping me become a well-rounded scientist.

I would like to thank my lab mates in Dr. Talkachova's lab as well as Dr. Osborn's lab. You have all made my graduate school experience fun and exciting. I greatly appreciate all of the time you spent discussing science and for all of your assistance throughout my time at the University of Minnesota. I would especially like to thank Dusty Van Helden for all of your time and expertise you contributed to the project.

I would like to thank my friends for their support throughout this journey. Thank you for the countless talks over tea, coffee, volleyball, and even boxing. Thanks for keeping me sane throughout this process. I greatly appreciate the support you all have provided and the breaks from work when things got stressful.

Lastly, I would like to thank my family for all of their support, love and encouragement. First, my sister, Jen, thank you for always being my sounding board for all things related and unrelated to graduate school. Thank you for always being there for me, keeping me grounded, and making sure I find time for fun. To my parents, who have supported my dreams to become a scientist from the start, thank you for believing in me and encouraging me in all of my pursuits. Thank you for reading countless drafts of everything from emails to this thesis. To Mark, thank you for all of your love and support over these past few years. For all the encouragement and stress relieving adventures, I am so grateful that you have been by my side throughout this process.

Dedication

To My Family

Abstract

This thesis is comprised of two parts. The first part investigates a novel therapy, vagus nerve stimulation, for hypertension and hypertension-induced heart disease. Hypertension impacts over 1 billion people worldwide, and clinical management is challenging. Left uncontrolled, high blood pressure can significantly increase the risk of cardiovascular events. The majority of hypertensive patients are treated with anti-hypertensive drugs to control blood pressure, but many limitations exist including resistant hypertension, inability to tolerate therapy, and non-compliance with the medication regime. For these patients, an alternative approach is needed to control blood pressure. Recently, the imbalance in the autonomic nervous system, evident in hypertension, has been the target of novel device-based therapies such as vagus nerve stimulation. The main goal of this research is to evaluate the efficacy of vagus nerve stimulation to treat hypertension and hypertension-induced heart disease. This thesis investigates the impact of vagus nerve stimulation on disease progression, survival, and cardiovascular remodeling in Dahl salt-sensitive hypertensive rats. Overall, the results of this work provide evidence for the beneficial therapeutic effects of vagus nerve stimulation in hypertension and motivate future studies to optimize therapy parameters and further understand therapeutic mechanisms.

The second part of this thesis focuses on atrial fibrillation and the evaluation of new mapping techniques for improving rotor localization for ablation procedures. Currently, success rates for ablation procedures for non-paroxysmal atrial fibrillation are low and require repeat procedures or a lifetime of pharmacological agents to reduce the risk of stroke. Improved signal processing techniques for mapping electrical activity in the atrium can help further our understanding of the generation and maintenance of atrial fibrillation and ultimately improve ablation procedure success rates and terminate the arrhythmia. The main goal of this work was to validate new signal processing techniques – multiscale frequency, kurtosis, Shannon entropy, and multiscale entropy – to identify regions of abnormal electrical activity. The results of this work demonstrate improved accuracy of these novel techniques in mapping rotors in cardiac arrhythmias and motivates further studies evaluating more complex arrhythmias and human intracardiac electrograms.

Contents

Part 2: Investigating novel mapping techniques to identify rotors in cardiac arrhythmias

List of Tables

List of Figures

Abbreviations and Acronyms

ACE	Angiotensin converting enzymes
AF	Atrial fibrillation
ANS	Autonomic nervous system
ARB	Angiotensin receptor blocker
APD	Action potential duration
BCL	Basic cycle length
BP	Blood pressure
BPV	Blood pressure variability
BRS	Baroreflex sensitivity
CCB	Calcium channel blocker
CFAE	Complex fractionated atrial electrograms
CNS	Central nervous system
CRP	C-reactive protein
CV	Conduction velocity
CVD	Cardiovascular disease
DBP	Diastolic blood pressure
DF	Dominant frequency
DSI	Data Science Inc.
DSS	Dahl salt-sensitive
ECG	Electrocardiogram
ERP	Effective refractory period
FN	False negative
FP	False positive
HF	Heart failure
HR	Heart rate
HRV	Heart rate variability
HTN	Hypertension
HW	Heart weight
HW/TL	Heart weight normalized to tibia length
Kt	Kurtosis
LAT	Local activation time
LV	Left ventricle
MAP	Mean arterial pressure
MI	Myocardial infarction
MSE	Multiscale entropy
MSF	Multiscale frequency
PP	Pulse pressure
PVI	Pulmonary vein isolation
PVC	Premature ventricular contraction
QTc	Corrected QT interval
ROC	Receiver operating characteristics
RV	Right ventricle
SBP	Systolic blood pressure
SE	Shannon entropy
TL	Tibia length
TN	True negative
TP	True positive

tVNS	Transcutaneous vagus nerve stimulation
VF	Ventricular fibrillation
VNS	Vagus nerve stimulation
VT	Ventricular tachycardia

Chapter 1

Introduction

Hypertension (HTN) and atrial fibrillation (AF) are two very prevalent conditions with over 1 billion and 33.5 million people affected worldwide, respectively [1, 2] with these numbers only predicted to rise with the aging population. In the case of HTN, the most common treatment approach is antihypertensive medications. Despite a large body of research demonstrating efficacy of pharmaceuticals, almost half of the patient population does not have controlled blood pressure, which increases their risk of cardiovascular and cerebral events [3]. In AF, patients are often treated using ablation to isolate the pulmonary veins. For patients with paroxysmal AF, this approach has the highest success rates with termination of the arrhythmia in over 70% of patients [4]. However for those with persistent AF, pulmonary vein isolation ablation procedures are only successful in 21-22% of patients, often requiring repeat procedures or prescription medications to limit the associated risk if the arrhythmia is unable to be terminated [5, 6]. New therapies are needed to help overcome limitation associated with the current clinical approach to help improve patient outcomes.

HTN poses a unique challenge to clinicians to treat as appropriate therapy requires a combination of controlling blood pressure and associated risks while also accounting for comorbidities, drug resistance, non-compliance, and intolerance. Recently, research has turned to modulation of the autonomic nervous system (ANS) as a potential therapy for HTN and hypertension-induced heart disease (HHD). A large body of literature exists demonstrating the imbalance in the ANS, with sympathetic hyperactivity driving the pathophysiology of HTN [7]. Novel device-based therapies, such as vagus nerve stimulation (VNS), baroreceptor activation therapy, and renal nerve denervation, target this imbalance to reduce global sympathetic outflow and enhance parasympathetic tone. Rebalancing the ANS can have numerous beneficial effects in hypertensive patients including blood pressure control, cardioprotection, and anti-inflammatory response. However, research is needed to investigate novel therapies and evaluate the efficacy in controlling blood pressure and addressing adverse cardiovascular remodeling.

AF is a prevalent condition worldwide and often can develop as a result of unmanaged high blood pressure and the subsequent cardiac remodeling. One key challenge today is understanding the spatial organization of the arrhythmia. Multiple theories exist, including multiple wavelet theory and focal sources (i.e. rotors). However, to date, there is still a lack of understanding around

the substrate responsible for the initiation and maintenance of the arrhythmia due to its complex evolution and inconsistencies between patients. Thus, properly targeting the responsible tissue and terminating the arrhythmia is challenging. One treatment option for patients with AF is ablation to isolate the pulmonary veins. However, for many patients the arrhythmia is not terminated after a single procedure, requiring repeat ablations or to continue pharmacological agents to minimize risk of long-term complications such as of stroke. Improving mapping techniques for ablation therapies can help advance our understanding of the underlying spatial organization of the arrhythmia and improve localization of ablation targets to ultimately improve procedure outcomes.

The present dissertation is presented in two parts. Part 1 (Chapters 2-6) is the main contribution of this thesis and aims to evaluate the efficacy of a novel device-based therapy, VNS, in treating HTN and HHD. Part 2 (Chapters 7-9) investigates novel mapping techniques in their ability to locate rotors in cardiac arrhythmias and its associated implications for clinical electrophysiological mapping in AF.

1.1 PART 1

Chapter 2 provides detailed background on HTN management and the development of new therapies. This chapter discusses pharmaceutical options for patients, the limitations with current approaches, and the recent development of novel device-based therapies targeting the ANS imbalance present in HTN. Chapter 2 provides background on VNS and the current experimental and clinical findings relevant to HTN and associated cardiovascular disease.

Chapter 3 details the experimental study investigating the effects of VNS in Dahl salt-sensitive (DSS) rats. This initial study investigated the effects of four weeks of VNS therapy in hypertensive rats to investigate safety and efficacy. In-vivo and ex-vivo effects of VNS in HTN are presented, providing evidence for VNS as an effective therapy.

Further experiments were performed to evaluate chronic effects of VNS in DSS hypertensive rats on long-term survival and relevant cardiovascular and hemodynamic parameters and are presented in Chapters 4 and 5. Chapter 4 details the experimental methods and results of the survival study investigating the impact of VNS therapy on long-term survival, blood pressure, heart rate, autonomic tone, and cardiac structural properties. Chapter 5 provides the methods and results for acute evaluation of individual episodes of VNS therapy to better understand the cardiovascular and hemodynamic changes that occur during low-level, intermittent vagal stimulation.

Chapter 6 summarizes the main findings and contributions of this thesis, providing evidence for the efficacy of VNS to treat HTN and HHD. In addition, recommendations for future work and scientific investigations are discussed.

1.2 PART 2

Chapter 7 provides the background information for the second part of the thesis, investigating novel mapping techniques for rotor identification in cardiac arrhythmias, including AF. Chapter 7 describes AF and the current clinical management and treatment. Several key limitations with the current approaches to guide ablation procedures are discussed. In addition, mapping techniques to better locate areas of abnormal electrical activity that may help lead to new therapeutic targets for patients with AF are presented.

In Chapter 8, the experimental results for new signal processing techniques to map rotors in cardiac arrhythmias are presented. Four novel mapping techniques – multiscale frequency, kurtosis, Shannon entropy, and multiscale entropy – are evaluated using arrhythmias captured during ex-vivo animal experiments driven by rotors on the epicardial surface. The accuracy of the rotor identification was compared to the traditional mapping technique, dominant frequency analysis, as well as phase movies derived from optical mapping recordings. Further analysis quantified the performance of these techniques under simulated clinical limitations.

Chapter 9 summarizes the key findings from my work in AF and mapping rotors. This chapter also presents future work and clinical translation.

Part 1

Investigating novel device-based therapy, vagus nerve stimulation, for hypertension and hypertension-induced heart disease

OBJECTIVE

The objective of Part 1 of my dissertation is to demonstrate the efficacy of a novel therapy, vagus nerve stimulation, for the treatment of hypertension and hypertension-induced heart disease. Through direct activation of the parasympathetic nervous system, vagus nerve stimulation provides a novel approach to target the imbalance in the autonomic nervous system, which is known to play a critical role in the pathogenesis of hypertension. The acute and chronic effects of low-level, intermittent vagus nerve stimulation are demonstrated through two studies investigating the progression of hypertension in Dahl salt-sensitive rats. In-vivo and ex-vivo results provide evidence of the beneficial impact of vagus nerve stimulation on several key aspects of hypertension including long-term survival, blood pressure control, and heart rate, autonomic tone, along with electrophysiological and structural cardiac properties.

Chapter 2

Background

2.1 Introduction

This chapter provides the background on hypertension (HTN) and hypertension-induced heart disease (HHD), and also summarizes experiments performed to investigate the efficacy of a novel device-based therapy, vagus nerve stimulation (VNS), to treat various cardiovascular and metabolic diseases. Chapter 2 discusses the current prevalence and impact of HTN while also presenting the current standard of care for patients with HTN and limitations with the current approach, which have motivated investigations into new therapies.

2.2 Hypertension & Hypertension-Induced Heart Disease

HTN, or high blood pressure (BP), affects over 1 billion people around the world and is the leading risk factor for cardiovascular disease (CVD), stroke, and global disease burden [1, 8]. With the aging population, this number is expected to continue to climb, reaching over 1.5 billion by 2025 [9]. In the United States alone, over 75 million adults are diagnosed with HTN and results in an annual cost of $42.9 billion, with over $20 billion spent on antihypertensive medication [10]. Left uncontrolled, the rise in BP can result in target organ damage in the myocardium, brain, vasculature, and kidney (Figure 2.1) [8, 11-13].

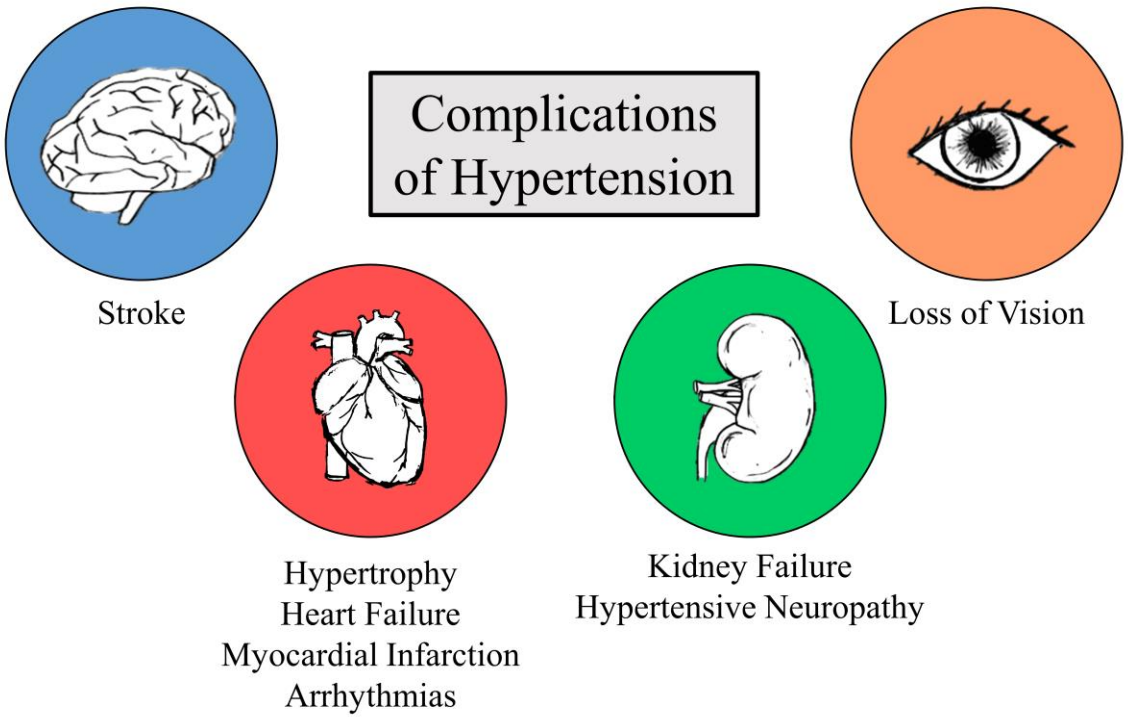

Figure 2.1 Major complications associated with hypertension.

Cardiovascular remodeling and the development of CVD is a major concern for patients with HTN and includes a wide range of abnormalities such as left ventricular hypertrophy, systolic and diastolic dysfunction, arrhythmias and heart failure (HF) [14]. Common structural cardiac remodeling due to HTN is shown in Figure 2.2 [15]. In fact, 51% of adults with CVD have HTN, and 40.6% of CVD-related deaths have been attributed to HTN [10]. In addition, HTN is present in 75% of patients with chronic HF [16]. These electrical and structural cardiac changes occur early in HTN and ultimately increase the hearts susceptibility to the development of atrial and ventricular arrhythmias as well as increases in the risk of death, making early detection, treatment, and management of HTN critical.

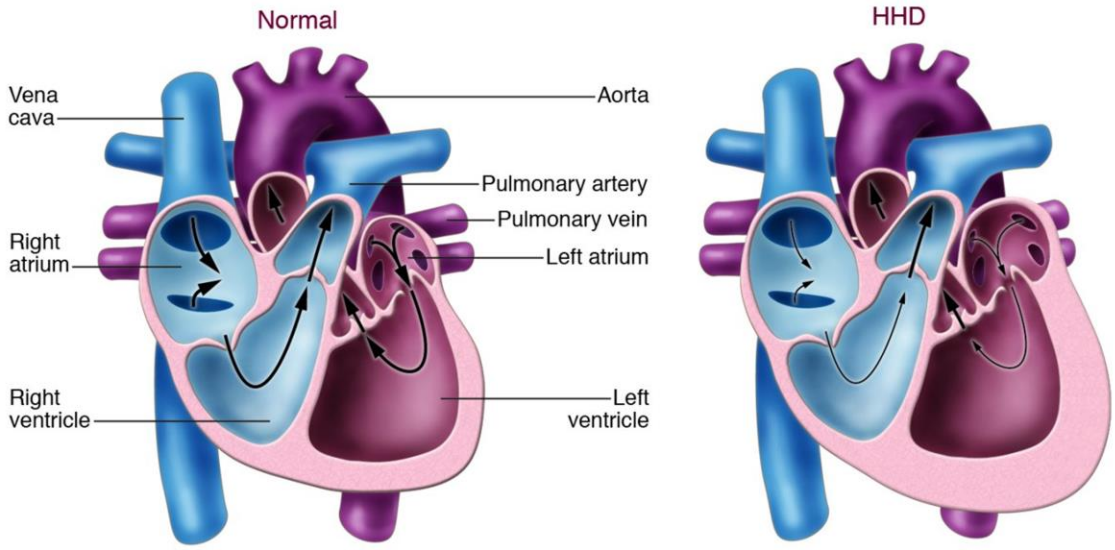

Figure 2.2 Common cardiac remodeling including atrial dilation left ventricular hypertrophy occurring in hypertension-induced heart disease (HHD; right) in comparison with the normal, healthy heart (left). Adapted from Berk et al. 2007 [15].

The classic progression to HHD is through left ventricular wall thickening in compensatory response to elevated BP to minimize the stress on the walls of the heart, shown in Figure 2.3 [17]. This hypertrophy can result from numerous alterations including increased cardiomyocyte size, changes in the extracellular matrix, and accumulation of fibrosis, both interstitial and perivascular. The increase in left ventricular mass can than lead to left ventricular dilation and reduced ejection fraction as the heart “transitions to failure” [14].

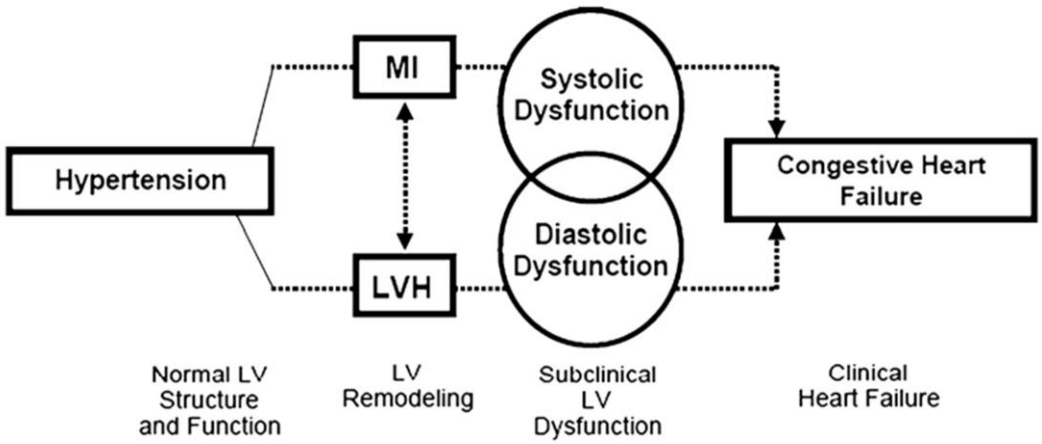

Figure 2.3 The role of hypertension in the development of heart failure. Adapted from Vasan & Levy, 1996 [17].

Recently, the American College of Cardiology and American Heart Association updated the guidelines for detection, prevention, management, and treatment of high BP in the hopes of attaining lower, controlled BP levels and reducing the associated cardiovascular complications. The new classifications are shown in Table 2.1 [3]. This change in standards increased the number of HTN diagnoses by 31.1 million adult in the United States alone, increasing the percent of adults with HTN from 32% to 46% [18]. It has been shown that with an increase in 20 mmHg systolic blood pressure (SBP) or 10 mmHg diastolic blood pressure (DBP), the risk of death from CVD and stroke doubles [1, 3]. Decreasing BP down to normotensive levels can greatly diminish the patient's risk of a cardiovascular event.

Table 2.1 New hypertension classifications

Classification	**Systolic Blood Pressure**	**Diastolic Blood Pressure**
Normal	120 mmHg	80 mmHg
Elevated	120-129 mmHg	< 80 mmHg
Stage 1 HTN	130-139 mmHg	80-89 mmHg
Stage 2 HTN	>140 mmHg	> 90 mmHg

2.3 Current Treatment Options

Currently, the primary basis for treating HTN is with pharmacological agents in addition to lifestyle changes including diet and exercise. Currently, there are a large variety of pharmaceutical options available to treat patients. The primary classes of antihypertensive drugs used to treat HTN

include thiazide diuretics, angiotensin converting enzymes (ACE) inhibitors, angiotensin receptor blockers (ARBs) and calcium channel blockers (CCBs). A summary of classes of HTN medications are included in Table 2.2 [9].

Table 2.2 Classes of antihypertensive drugs and their associated mechanism of action

Class of Antihypertensive Medication	Mechanisms of Action
Diuretics	Inhibits the reabsorption of sodium, preventing fluid retention
ACE Inhibitors	Inhibits the conversion of the inactive angiotensin I to the active angiotensin II
ARBs	Blocks angiotensin II from binding to its receptor, preventing it from causing vasoconstriction and fluid retention.
Renin Inhibitors	Inhibits the conversion of angiotensin to angiotensin I
CCBs	Prevents the entry of calcium into the vascular smooth muscles, resulting in vasodilation and reduced contractility in the vasculature
Beta-blockers	Blocks beta-1 adrenergic receptors, resulting in slower heart rate, decreased contractility, and reduced cardiac output Inhibits renin release, resulting in reduced angiotensin II production
Alpha-blockers	Blocks alpha-1 adrenorecpetors which are responsible for vasoconstriction in vascular smooth muscles
Direct Vasodilators	Relaxes smooth muscles, primarily arterioles

These medications can be used individually or in combination to achieve controlled BP levels. Despite a large body of research demonstrating the efficacy of these antihypertensive medications, there still exists a large portion of the hypertensive population who do not reach their target BP levels. Although the percentage of adults with HTN who have achieved controlled BP levels has increased from 49.3% in 2009 to 55.2% in 2012 [3], still approximately half of the patients with HTN do not reach target BP levels. Several key factors contribute to this alarming statistic including resistance, compliance, cost, side effects, and physician inertia [19].

Patients are considered to have resistant HTN if they are unable to achieve BP values of 140/90 mmHg or less while on 3 or more antihypertensive drugs or those who are able to control BP, but require at least 4 antihypertensive drugs. The exact prevalence of resistant HTN is unknown, but studies estimate between 10-30% of hypertensive patients have resistant HTN. This number is expected to increase due to the combination of the new standard of care of HTN increasing the number of patients diagnosed with HTN and decreasing the target blood pressure levels from 140/90 to 130/80 mmHg [3, 20, 21]. The large range in prevalence demonstrated in studies is due

to the difficulty in true diagnosis of resistant HTN, as numerous hypertensive patients have uncontrolled BP due to noncompliance, intolerance, and inadequate treatment regime.

Noncompliance is a prominent challenge clinician's face when trying to reach target BP for the hypertensive patient population. Recently, it was reported that 40% of patients discontinued antihypertensive medications within the first year of treatment [22]. Further follow up revealed that by 10 years after the start of treatment, less than 40% of patients continued with their prescribed antihypertensive medications [23].

New therapeutic options are necessary for hypertensive patients to address the limitations of current treatment options. An optimal therapy for HTN would address the inappropriate rise in BP while also addressing adverse cardiovascular remodeling and associated risks. In addition, new therapies that are able to reduce costs and side effects while also encouraging compliance can help increase the number of patients reaching target BP levels and ultimately reduce their risk of cerebral and cardiovascular events.

2.4 Device-Based Therapies

Recently, novel device-based therapies have been investigated for treating HTN. These therapies target the imbalance in the autonomic nervous system (ANS) present in hypertensive patients, which manifests as an inappropriate increase in sympathetic nervous activity and a withdrawal of parasympathetic nervous activity [7]. Increased sympathetic nerve activity plays a critical role in the development, maintenance and acceleration of HTN [7, 20]. Several studies have demonstrated that this imbalance is present even before BP reaches hypertensive values, and the increase in sympathetic activity continues to rise in parallel as HTN advances [7, 24, 25]. One hypothesis for the rise in sympathetic activity is the excessive adrenergic response, which initially increases BP variability, but over time may contribute to a sustained increase in BP. Another proposed mechanism contributing to an overactive sympathetic nervous system (SNS) is through the reduction in the influence or function of arterial baroreceptors [7]. Targeting this imbalance in the ANS, through either the parasympathetic or sympathetic branch, may provide a novel therapy for HTN to prevent its progression and possibly reverse any adverse remodeling associated with a sustained increase in BP.

Several therapies being investigated for the treatment of HTN and HHD directly target the over activity in the SNS with the goal of inhibiting efferent and afferent sympathetic nervous activity (Figure 2.4). These therapies include baroreceptor activation therapy (BAT) and renal denervation

(RDNx). In contrast, vagus nerve stimulation (VNS) stimulates the parasympathetic branch with the goal of rebalancing the ANS through a combination of efferent and afferent parasympathetic activation and resulting inhibition of sympathetic activity.

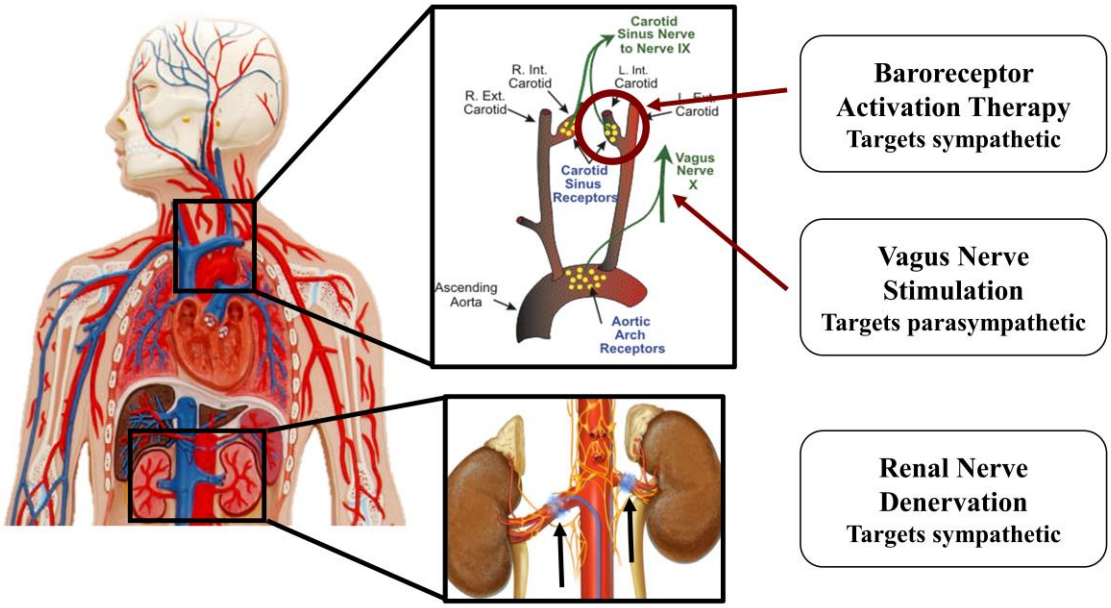

Figure 2.4 Device-based therapies targeting the sympathetic branch (BAT & RDNx) and parasympathetic branch (VNS) of the autonomic nervous system as a therapy for HTN. Figures adapted from Klabunde, 2011 [26] and Fischell et al. 2016 [27].

2.4.1 Baroreceptor Activation Therapy

Baroreceptors play a critical role in short- and long-term BP control. BAT directly stimulates the carotid baroreceptors to increase firing rate of baroreceptors as their function is often altered in HTN resulting in a rise the homeostatic BP set point and reduced sensitivity to blood pressure fluctuations [28, 29]. One hypothesis of impaired or altered function of baroreceptors is due to stiffening of the arterial walls in response to increased BP leading to a diminished response from the baroreceptors. Electrically stimulating the baroreceptors results in increased parasympathetic activity and decreased sympathetic outflow which is the primary mechanism for BP reduction (Figure 2.5) [30].

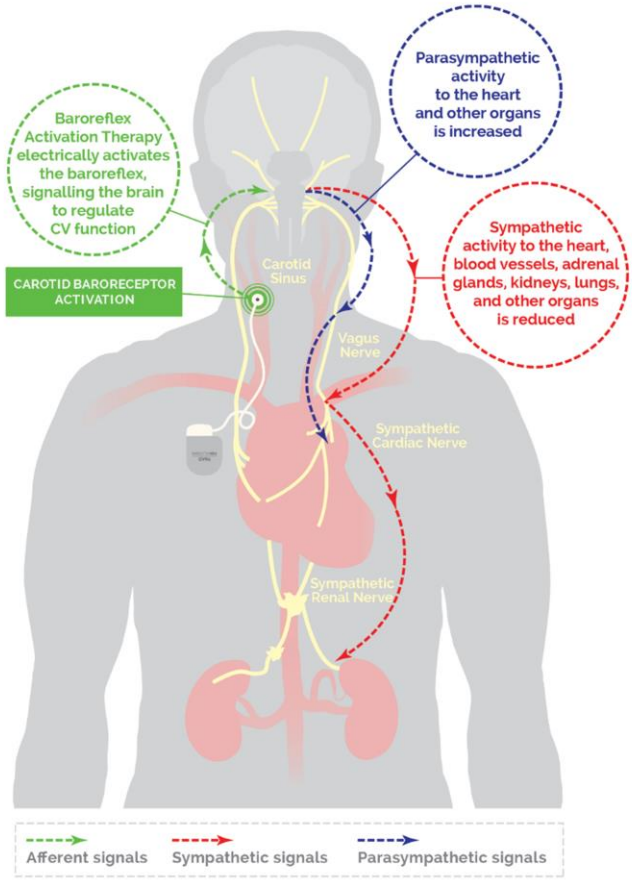

Figure 2.5 Mechanisms of BAT for the treatment of resistant HTN. Adapted from Yoruk et al. 2016 [30].

BAT has been investigated in several key clinical trials. The DEBut-HT trial implanted 45 patients with BAT and demonstrated a significant drop in BP which was reported at 6 months, 1 year, and 2 years post-implant [31]. However, during this study, there were 8 procedure or device-related serious adverse events. The Rheos Pivotal trial, a larger clinical trial with 265 patients with resistant HTN, failed to meet several efficacy and safety endpoints [32]. These clinical results motivated further advancements in technology and improvements in the baroreflex activation device including a smaller but longer lasting battery, smaller electrodes, and a reduction in the number of electrodes (Figure 2.6). These modifications will hopefully address the limitations revealed by these trials, and subsequently reduce the number of serious adverse events. With this new technology, a small clinical trial was performed with 30 patients showing a reduction in BP at 6 months and a reduction in complications [33]. This therapy and newer technology will be further evaluated in the upcoming Barostim Hypertension Pivotal Trial.

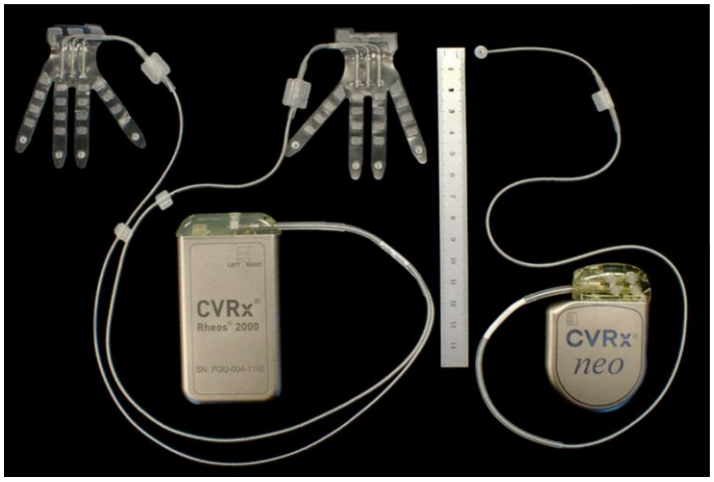

Figure 2.6 Comparison of the original CVRx Rheos device (left) and the newer Barostim neo (right) technology for BAT. Adapted from Yoruk et al. 2016 [30].

2.4.2 Renal Denervation

Renal nerves are responsible, in part, for the development and progression of HTN. The efferent renal nerves innervating the kidney are responsible for the modulation of renin release, sodium reabsorption, and vascular resistance [34, 35]. Many pharmaceutical agents target one or more of these components. However with RDNx, the advantage is to provide localized therapy acting on the kidney and renal nerve directly as opposed to a global therapy which may lead to undesirable side effects. RDNx applies energy to ablate the afferent and efferent sympathetic nerves. Ablating efferent renal nerves results in a reduction in renin release, sodium reabsorption, and vascular resistance, ultimately lowering BP. The ablation of afferent nerves are also suspected to play a role in controlling BP through a reduction in global sympathetic activity (Figure 2.7) [34, 36-38].

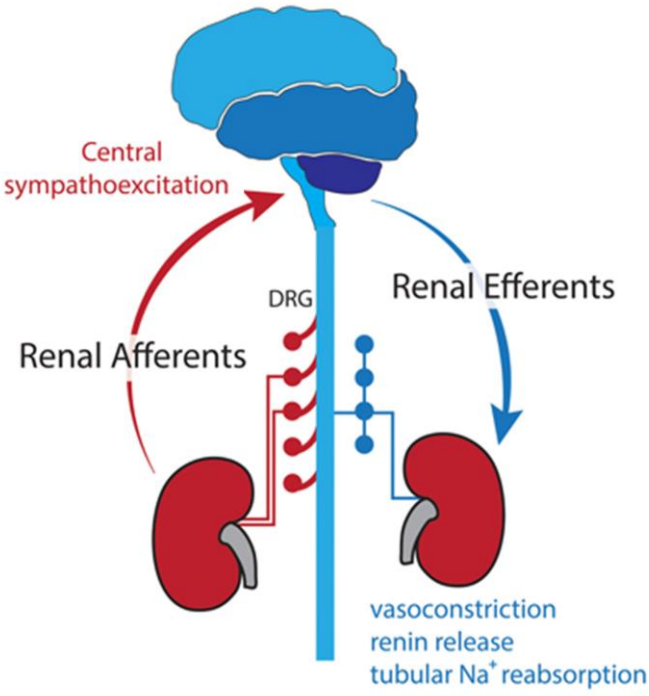

Figure 2.7 Role of renal afferent and efferent nerves in the pathogenesis of HTN. Adapted from Booth et al. 2015 [39].

Several clinical trials have been performed to evaluate this therapy in humans. SYMPLICITY HTN-1 and SYMPLICITY HTN-2 demonstrated reductions in BP in resistant HTN patients [40-42]. However, the third clinical trial, SYMPLICITY HTN-3, failed to meet its efficacy endpoint [43, 44] due to numerous pitfalls including failure to properly perform the procedure and potential confounding factors from changes in medication and compliance [45]. The result of SYMPLICITY HTN-3 highlighted one of the major limitations of the RDNx procedure, which is the lack of a method to confirm the completeness and effectiveness of the ablation procedure. In addition, another limitation in achieving complete RDNx is the secondary branches of the renal artery, which also play a role in the pathogenesis of HTN. The outcome of SYMPLICITY HTN-3 made the field hesitate and question the validity of the technique. However, with the recent SPYRAL HTN Global Clinical Trial using a new ablation catheter design and reporting positive effects 3 months post-operative [46], research into RDNx therapy for HTN has been rejuvenated. Further studies will continue with the improved catheter design (Figure 2.8) and physician training implemented in the newest SPYRAL trial in hopes of achieving more complete and consistent ablation results [47].

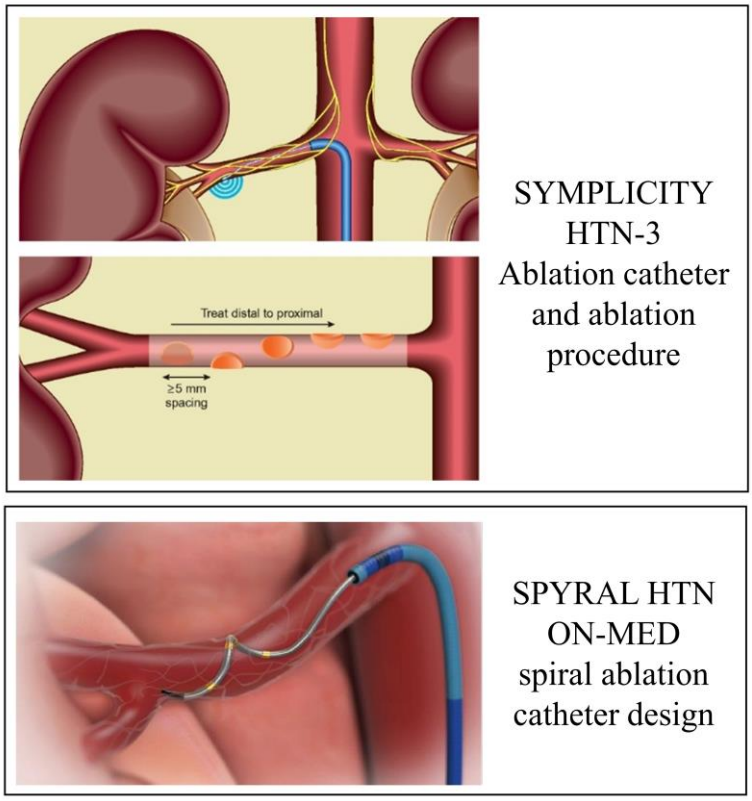

Figure 2.8 Catheter ablation technologies for the SYMPLICITY HTN-3 trial (top) and the new design for the SPYRAL HTN ON-MED trial (bottom). Adapted from Patel et al. 2014 [48] and Kandzari et al. 2016 [47].

2.4.3 Vagus Nerve Stimulation

Another treatment approach for HTN is to target the parasympathetic branch of the ANS through stimulation of the vagus nerve. VNS is applied at the cervical level and is hypothesized to work through numerous mechanisms including afferent signaling suppressing sympathetic activation and efferent signaling enhancing cardiac parasympathetic tone (Figure 2.9). With the direct innervation to the heart, while also playing a major role in BP control, modulation of vagal activity is hypothesized to provide efficacious therapy for HTN, allowing patients to achieve target BP levels while also treating HTN-associated cardiovascular complications.

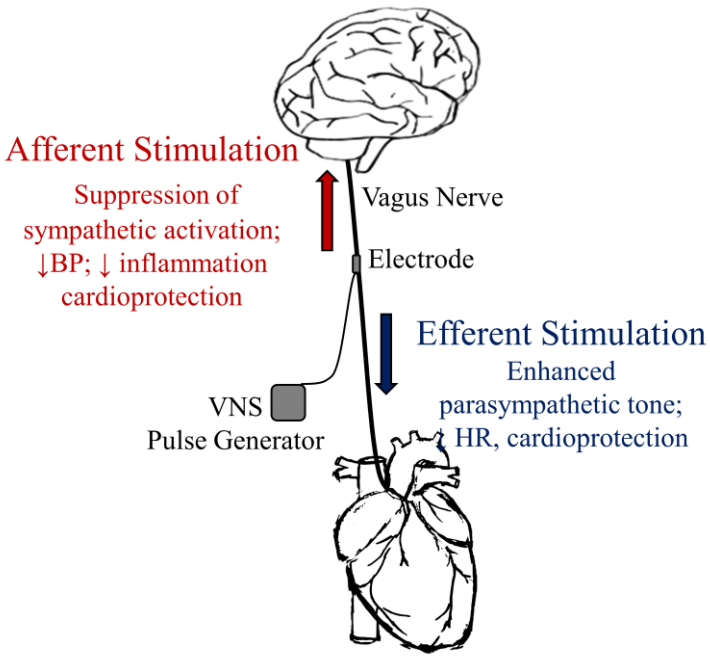

Figure 2.9 Proposed mechanisms of VNS therapy through efferent and afferent nerve activation.

This therapy is the focus of my thesis in investigating its efficacy to treat HTN and HHD. The following sections will go into detail on the anatomy of the vagus nerve, clinical applications, and experimental findings of VNS demonstrating its potential to provide an effective therapy for HTN and HHD.

2.5 Vagus Nerve Stimulation

2.5.1 Vagus Nerve Anatomy & Physiology

The vagus nerve is the tenth cranial nerve (CN X), a complex, parasympathetic nerve originating from the medulla. Named the "great wandering protector" [49], the vagus innervates numerous major organs in the body and is involved in the autonomic, cardiovascular, endocrine, gastrointestinal, immune, and respiratory systems making it the most extensively distributed cranial nerve (Figure 2.10) [50, 51].

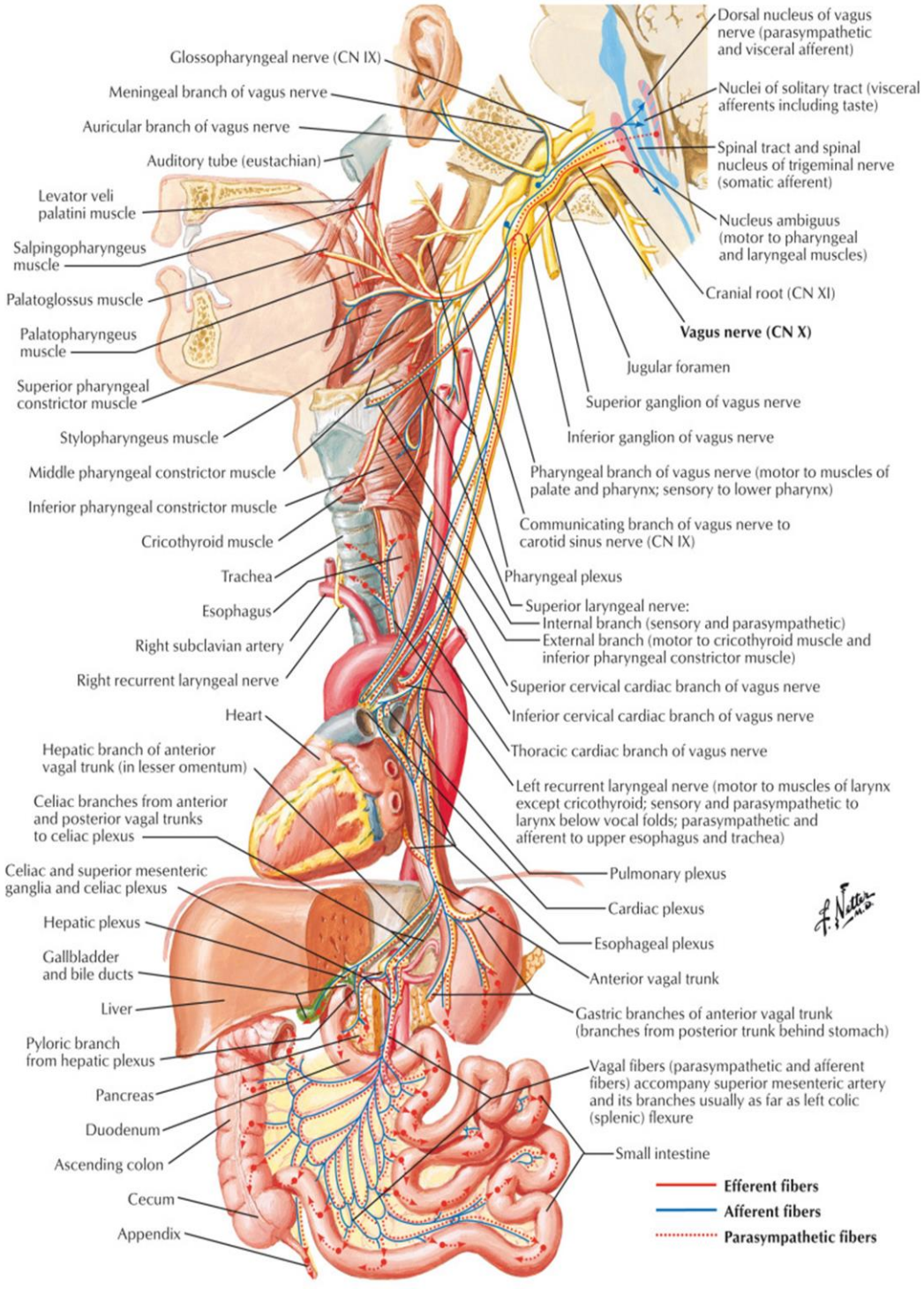

Figure 2.10 Anatomy of the vagus nerve. Adapted from Netter, 2016 [52].

Approximately 80-90% of the fibers in the vagus nerve are sensory, or afferent, fibers communicating to the brain with the remaining 10-20% of fibers in the vagus nerve being efferent fibers, transmitting signals from the brain to the viscera [53]. Vagal afferent fibers carry sensory information from various organs, including the heart, which are then integrated and interpreted by the central nervous system (CNS). The CNS then sends out appropriate sympathetic and parasympathetic motor signals on efferent fibers to adjust organ function and maintain homeostasis [51, 54, 55]. Specifically, in the case of the heart, when activated, the vagus nerve has a cardioinhibitory effect, reducing heart rate and contractility [54, 56]. This effect is mediated through efferent signaling directly to the myocardium. Both the right and left vagus nerves carry cardiac efferent fibers, but anatomical studies in dogs suggest that those on the right side preferentially supply the sinoatrial node of the heart whereas those on the left side preferentially innervate the atrioventricular node [57].

The widespread influence of the vagus nerve and prominent role of the ANS in many disease states has made the vagus nerve a popular target for new research for a variety of indications. However, the complex anatomy presents challenges in clinical applications in fully understanding the intended and unintended effects of VNS therapy.

2.5.2 Clinical Applications

VNS has been clinically available for decades, but has been focused in neurological disorders. Left cervical VNS was first FDA approved to treat refractory epilepsy in 1997 and was later approved for use in treatment-resistant depression in 2005. In addition, several new indications have recently received FDA approval for the use of VNS therapy – morbid obesity (2015), cluster headaches (2017), and migraine headaches (2018). An example of the FDA-approved VNS system from LivaNova PLC is shown in Figure 2.11 (top panel).

VNS continues to be investigated for numerous other conditions including HF, myocardial infarction (MI), diabetes, and chronic inflammation conditions. Here, we investigated the potential of VNS in treating HTN and HHD. This area of research has emerged only in the past several years and is quickly gaining interest leading to several clinical investigations. One clinical trial is currently underway at Massachusetts General Hospital where they are recruiting subjects for a study to investigate the effects of transcutaneous VNS (tVNS) in patients with HTN. The protocol consists of three stimulation sessions to evaluate the impact of tVNS on HR and BP metrics. An example of a transcutaneous VNS system from gammaCore is shown in Figure 2.11 (bottom panel).

Implantable VNS

Transcutaneous VNS

Figure 2. 11 Examples of an invasive VNS system (LivaNova PLC; Figure adapted from http://www.livanova.com) and a noninvasive, transcutaneous VNS system (Gamma Core Inc.; Figure adapted from https://gammacore.com/).

2.5.3 Experimental Findings

The evaluation of VNS in treating HTN is still a new area of research with numerous preclinical studies being conducted to understand the beneficial effects of VNS therapy and its mechanisms of action. A majority of literature supporting the application of VNS in HTN has stemmed from investigations in other disease states including HF, MI, chronic inflammation, and atrial fibrillation (AF). The studies summarized here demonstrating numerous beneficial effects including BP control, autonomic control, cardiac remodeling, arrhythmia suppression, and a reduction in inflammation provide evidence supporting the investigation into the use of VNS for the treatment of HTN and HHD.

2.5.3.1 Blood Pressure Control

The most crucial element of an anti-hypertensive therapy is its ability to control the rise in BP and to help return BP levels back to normotensive values. VNS plays a key role in BP control

through its innervation to baroreceptors in the aortic arch. However, to date, limited studies have investigated the role of VNS in BP control in hypertensive [58-60] and healthy models [61-64]. Further, the majority of these findings are from acute applications of VNS while the animal was anesthetized, which may have confounding effects on VNS therapy. These studies in spontaneously hypertensive rats have shown an acute reduction in BP due to VNS [58, 59]. However, using this same HTN model in a chronic study, four weeks of VNS therapy did not alter the rise in systolic BP (SBP). Although BP was not affected, other beneficial effects were demonstrated such as improved endothelial function and the prevention of aortic stiffening [60].

Acute studies in healthy rats have helped further the understanding of the parameter space and the mechanisms by which VNS can lower BP. Specifically, these studies have been developing more targeted VNS therapy to optimize this BP effect while limiting the occurrence of side effects such as bradycardia and bradypnea. Plachta et al. has evaluated the efficacy of isolating and stimulating the aortic depressor nerve (ADN) within the vagus nerve in healthy rats [62, 63]. The ADN is an afferent nerve that transmits signals from the receptors in the aortic arch to maintain homoeostasis [65]. Through selective ADN stimulation, BP is acutely lowered while avoiding significant changes in heart rate (HR) and respiration rate [62]. Further, this group evaluated the selective stimulation of the ADN while synchronized to the cardiac cycle to the mimic inherent, pulsatile activity of the ADN which proved improved therapeutic efficacy, which accounts for the intended effect, BP reduction, and the unintended effect, HR reduction [63].

In general VNS has been shown to reduce BP, but discrepancies exist in scientific findings which can largely be due to parameter selection, selective versus nonselective stimulation, and disease model. Further acute and chronic studies are needed to HTN models to better understand the parameters space and optimize treatment for HTN and HHD.

2.5.3.2 Autonomic Control

Another critical aspect of VNS therapy is the impact on the ANS. Traditionally, clinical measures of heart rate variability (HRV) and baroreflex sensitivity (BRS) have been used as indicators of autonomic tone and carry strong prognostic value in CVD. HRV provides a measures of the sympathetic and parasympathetic influence in acute changes in HR while BRS evaluates the magnitude of the HR change in response to changes in BP. In the case of impaired autonomic balance, both HRV and BRS decrease, which is significantly associated with increased cardiovascular risk [66, 67].

The effect of VNS on these markers of autonomic tone have been evaluated in a normal physiological state [68] and in a state of altered autonomic balance present in HF [69, 70]. Zhou et al. evaluated the spectral components, specifically high frequency and low frequency components, of HRV in a healthy porcine model. Their results showed that acute application of VNS resulted in a decrease in the low frequency and increase in the high frequency components, demonstrating improved parasympathetic tone [68, 71]. A similar effect on low and high frequency components of HRV was demonstrated by Zhang et al. in a high-rate pacing HF canine model. Additional beneficial autonomic effects were observed in BRS measures which were preserved in the VNS-treated group, with higher BRS values, measured at Weeks 4 and 8 of therapy, in comparison to the untreated group.

The beneficial autonomic effect has also been demonstrated in humans with HF. A previous clinical trial, the ANTHEM-HF Trial, evaluated the efficacy of right- and left-sided VNS in treating HF patients. The ANTHEM-HF trial met their safety and efficacy endpoints and demonstrated an increase in HRV, evident in patients receiving both right- or left-sided VNS [72]. Further analysis on the dynamics of the autonomic HRV response was performed using Poincaré plots, which provides a visual representation of the variability in R-R intervals by plotting each R-R interval against the previous R-R interval [73]. Right-sided VNS resulted in increased SD1, representative of short term variability in R-R intervals, and a significant reduction in the centroid, representative of mean HR. This effect was highly correlated to the amplitude of the simulation. In contrast, the left-sided stimulation did not alter the Poincaré parameters unless stimulation was raised sufficiently high, greater than 2 mA [70]. This laterality was also demonstrated by Zhou et al. in which the spectral measures of HRV were only influenced by right- and not left-sided VNS [68]. These results suggest that a stronger cardiac autonomic effect can be achieved at lower stimulation thresholds through right-sided VNS, which preferentially innervates the sinoatrial node.

2.5.3.3 Cardioprotection

The vagus nerve has a strong influence on the heart through direct innervation to the atria and the ventricles. Parasympathetic activation has negative chronotropic, inotropic, and dromotropic effects [74]. These effects are well documented, and initially the drop in HR was thought to be a necessary component of the cardioprotective effect of VNS. However recent studies have shown beneficial cardiac effects without HR reduction [75]. Numerous studies have been conducted to evaluate the cardioprotective role of VNS in the atria and the ventricles separately and the role of therapy in arrhythmia suppression.

2.5.3.3.1 Atrial Remodeling and Arrhythmia Suppression

A large body of research exists demonstrating the pro- and anti-arrhythmic effects of VNS. Traditionally, VNS has been used to induce AF in acute animal studies [76-78], and the ablation of the vagus nerve was shown to prevent or reduce the occurrence of AF in these models [77]. Specifically, the release of acetylcholine by stimulating the vagus nerve results in shortening of atrial action potential duration (APD) and effective refractory period (ERP) and an increase in spatial heterogeneity, due to the non-uniform distribution of vagal innervation in the atria. Taken together, these effects increase the atria's susceptibility to arrhythmias and the probability of multiple reentrant circuits [79]

However, recent research has shown VNS has cardioprotective and anti-arrhythmic properties in the atria. Ultimately, these antagonistic effects are a result of the intensity of the stimulation. An experiment in canines demonstrated the impact of stimulation intensity and revealed that high intensity stimulation, which slows the heart rate by 60% or more, facilitated AF, while moderate intensity stimulation, slowing the heart rate by no more than 40%, did not affect AF [76]. Animal studies have confirmed this anti-arrhythmic effect in several studies using low-level VNS [80-82]. Specifically, VNS was shown to inhibit intrinsic cardiac autonomic nervous activity in the major ganglionated plexi [82] as well as prevent atrial electrophysiological remodeling induced via rapid atrial pacing [81]. Additional studies have demonstrated this effect in humans [83-85] where acute VNS sessions have shown lasting effects in AF suppression [84, 85]. Further, some of the most compelling evidence demonstrating that VNS is not pro-arrhythmic, in its current clinical application, comes from the thousands of patients implanted with VNS who have not experienced an increase in the risk of developing AF [86-89].

2.5.3.3.2 Ventricular Remodeling and Arrhythmia Suppression

Initially, due to the concentration of vagal fibers in the atria, the ventricles were thought to be unaffected by VNS. However, studies have recently revealed the extensive presence of sympathetic and parasympathetic innervation in the ventricles. Research showing the beneficial ventricular effects has been mostly focused on HF and MI. However, mechanistic insights from HF and MI studies can help inform studies designed to treat HTN and HHD.

Investigating the effects of VNS in ventricular myocardium has resulted in a large number of studies with relatively consistent results demonstrating cardioprotection, maintaining electrical stability and suppressing arrhythmias. Further, several literature reviews have been written

summarizing the results [90, 91]. Briefly, results have shown that the use of VNS in treating cardiac diseases has resulted in an increase in in ventricular ERP [92, 93], APD [94], and ventricular fibrillation (VF) threshold [95, 96], accompanied with a reduction in the spatial dispersion of ventricular refectory period, VF occurrence [95, 96], and the maximum slope of the restitution curve, S_{max} [92]. Studies have also consistently reported improvements in left ventricular function including improved left ventricular ejection fraction, increased left ventricular end-systolic volume, and protection against left ventricular hypertrophy [75]. In addition, this anti-arrhythmic effect has been shown to persist even after the cessation of therapy suggesting a remodeling or memory component of the myocardium as a result of VNS applied over time [97]. Overall, the effects of VNS have demonstrated improvements in structural and electrophysiological properties of the ventricles, providing evidence as an efficacious therapy for not only HF and MI, but also providing promise as a therapy for HTN-associated CVD.

Overall, these studies have shown that VNS is able to provide beneficial structural and electrical cardiac remodeling to and prevent the progression of CVD. VNS has the ability to maintain or restore electrical stability in the atria and ventricles to provide protective effects and reduced arrhythmia susceptibility. There are numerous mechanisms which are postulated to result in the anti-arrhythmic effect observed with VNS therapy including HR reduction [98], the preservation of connexin 43 [98, 99], inhibition of the opening of mitochondrial permeability pore [100], inhibition of SNS [100], and nitric oxide-mediated effects on ventricular APD restitution [92, 93, 95, 101]. Further studies are needed to evaluate which therapeutic mechanisms play a key role in HTN and HHD and whether these effects can be optimized through VNS parameter selection.

2.5.4 Inflammation

Recent research has shed light on the role of inflammation in HTN, particularly on the impact of adaptive immunity in the development and progression of HTN [102]. Although the cause-and-effect relationship between inflammation and HTN remains unclear, research in this field continues to grow. In general, inflammation is a protective response to injury. However, chronic inflammation can have deleterious effects. In fact, increased levels of pro-inflammatory cytokines have been demonstrated in HTN and CVD [103-105]. Several studies have also observed an increase in pro-inflammatory cytokines in patients at risk for HTN and CVD [106]. These results suggest that the systemic inflammation may precede the clinical diagnosis. One current hypothesis is that

inflammation can lead to endothelial dysfunction and increased oxidative stress, which promote the development and progression of HTN (Figure 2.12) [107].

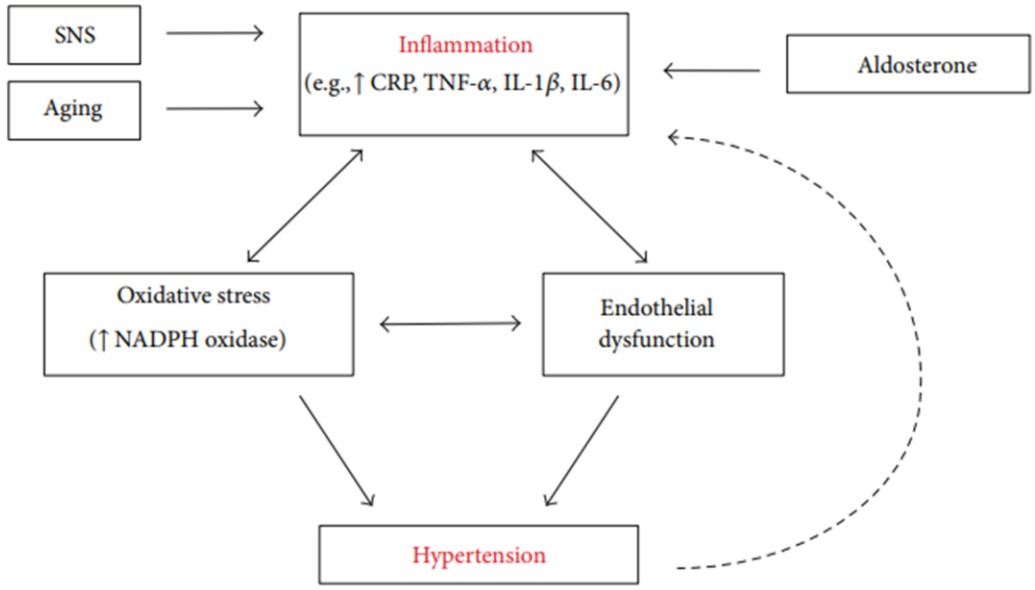

Figure 2.12 Schematic showing the role of inflammation in the pathogenesis of HTN. Adapted from Dinh et al. 2014 [107].

One of the major recent discoveries in VNS therapy is its profound impact on inflammation. VNS has the capability to reduce systemic inflammation through the activation of the cholinergic anti-inflammatory pathway, reducing cytokine synthesis and the inflammatory response [69, 108]. Animal studies in HF models have shown a reduction in pro-inflammatory cytokines as a result of VNS therapy [75, 109]. Specifically, Zhang et al. demonstrated a reduction in C-reactive protein (CRP) in VNS-treated HF canines [110]. Although this experiment was performed in a HF model, elevated CRP is strongly associated with HTN [105, 106]. Additional studies have observed decreases in inflammatory biomarkers of HF including TNF-α, IL-2, Il-6 and IL-18. Experimental evidence suggests that VNS may be able to help treat CVD through a reduction in inflammation [111, 112]. As a therapy for HTN, VNS has to potential to modulate the innate inflammatory response and reduce vascular end organ damage through decreased oxidative stress and subsequent endothelial dysfunction. More work in this area is needed to fully understand the role of these cytokines in the development of CVD and HTN, as they are unlikely to be "innocent bystanders" [113].

Numerous other mechanisms of VNS therapy, including anti-adrenergic effect and inhibition of the renin-angiotensin system, have been evaluated in HTN and CVD models which could provide further understanding of the beneficial effects of VNS. Suppressing central sympathetic outflow through activation of vagal nerve afferent fibers can lead to a reduction in sympathetic nervous system activity, resulting in reductions in HR, vascular resistance, and arterial BP. VNS has also been shown to directly activate the nitric oxide pathway producing nitric oxide in the ventricles, altering cardiac electrophysiology and decreasing arrhythmia susceptibility [101]. Another proposed mechanism of VNS is inhibition of the renin-angiotensin system through afferent vagal nerves, resulting in a reduction in renin in the kidneys and marked reduction in plasm angiotensin II levels [69, 114].

2.6 Conclusion

VNS has demonstrated its ability to modulate key components in the pathogenesis of HTN. These results, taken together, show potential for VNS to treat HTN and associated cardiovascular risk through a combination of afferent and efferent parasympathetic activation. VNS has demonstrated strong beneficial cardiac effects, improving outcomes through electrical and structural remodeling, as well as BP control, specifically demonstrated through direct activation of the afferent ADN. In addition this new therapeutic approach could be leveraged to overcome current treatment limitations, such as treatment resistance and noncompliance, and help achieve improved patient outcomes.

Although numerous studies have been completed investigating VNS as a novel therapy having strong beneficial effects on the heart, autonomic balance, and inflammation, limited research is available on the potential of VNS to treat HTN and associated cardiovascular remodeling. Chronic studies are necessary to evaluate the full potential of VNS therapy in HTN and HHD, specifically evaluating long-term survival, hemodynamic and cardiovascular responses, and the associated cardiac electrical and structural remodeling. In this work, I evaluate these effects of chronic low-level VNS applied to the right cervical vagus nerve in DSS hypertensive rats.

Chapter 3

Intermittent electrical stimulation of the right cervical vagus nerve in salt-sensitive hypertensive rats: effects on blood pressure, arrhythmias and ventricular electrophysiology

3.1 INTRODUCTION

Chapter 3 presents the methods and findings from the first chronic study of vagus nerve stimulation (VNS) therapy in a Dahl salt-sensitive (DSS) hypertensive rat model. The main objective was to evaluate the efficacy of chronic VNS therapy in hypertension (HTN) using in-vivo and ex-vivo analysis techniques. The progression of HTN is quantified over time using in-vivo physiological recorders to get real-time blood pressure (BP) and ECG recordings. Ex-vivo studies using optical mapping were performed to evaluate the impact of VNS therapy on the electrophysiological properties of the hypertensive heart.

HTN is one of the strongest risk factors for sudden cardiac death [115]. Over time, HTN leads to left atrial dilation, left ventricular hypertrophy, and impaired ventricular relaxation (i.e., "diastolic dysfunction"), and thus, affecting ventricular systole, diastolic filling, and increasing the risk of heart failure (HF) [116]. In addition to adverse structural changes in the myocardium, chronically elevated BP also negatively affects autonomic regulation of BP [117], heart period dynamics [118], and electrophysiological properties of neural and myocardial tissues of the heart, causing progressive symptom expression and elicitation of spontaneous cardiac arrhythmias. The presence and the complexities of these cardiac arrhythmias in hypertensive patients significantly influence the morbidity, mortality, and quality of life [119-122].

Currently, the most common treatment option prescribed by physicians for patients with HTN and HTN-induced heart diseases (HHD) is a regimen of antihypertensive drugs along with diet and exercise. However, there are still numerous limitations with this approach and nearly half of all hypertensive patients do not achieve controlled BP levels. As a result, there is a clear need for novel and effective alternative treatments for HTN and HHD.

VNS has the capability of restoring autonomic nervous system (ANS) regulatory function not only in the vascular system but also in the heart at its neural processing hierarchy [123]. Our laboratory and others have shown that VNS is able to alter several electrophysiological properties

of the heart, eventually suppressing arrhythmias and leading to an improved prognosis of HF rats, and significantly improved long-term survival after chronic HF [124, 125].

3.2 AIM

In the present study, we investigated for the first time the potential of VNS to be used as a novel device-based therapy for HTN and HHD. Specifically, this study aimed to determine the effects of VNS on the evolution of mean arterial pressure (MAP) and arrhythmogenesis in-vivo in a genetic model of HTN, the DSS rat. In addition, at the end of the study, the effect of VNS therapy on the electrophysiological properties of the heart were evaluated through ex-vivo optical mapping.

3.3 METHODS

All procedures were approved by the University of Minnesota Animal Care and Use Committee and were conducted in accordance with institutional and NIH guidelines.

Prophylactic antibiotic (gentamicin sulfate; 10 mg/kg, i.m.) was given prior to each surgery. During the surgeries, rats were anesthetized with isoflurane (5% for induction, 2% or 3% for maintenance) in oxygen (2 L/min for induction and 1L/min for maintenance). The rat's body temperature was maintained at 37°C on a temperature-controlled surgery table.

3.3.1 Experimental Design

DSS male rats (n = 12, 5 weeks old) were used for the study. HTN was induced via 8% NaCl high salt diet (S10001, Research Diets, Inc., NJ, USA) and was maintained throughout the entire duration of the study (Figure 3.1A). Vagus nerve stimulators (Cyberonics Model 103, Houston, TX, USA) and telemetry systems (HD-S11, Data Sciences, Inc. (DSI), Minneapolis, MN, USA) were implanted at Week 5 of the study, and the rats were randomly divided into two groups: Sham (n = 6, with nonfunctional VNS stimulator implants of the same mass) and VNS (n = 6, with functional VNS stimulator implants). At the end of Week 6 (Figure 3.1A, "Day 0 VNS"), functional stimulators were activated in the VNS group, and real-time bipolar electrograms and arterial BP were recorded using DSI telemetry for both VNS and Sham groups for 4 weeks (Week 6 through Week 10).

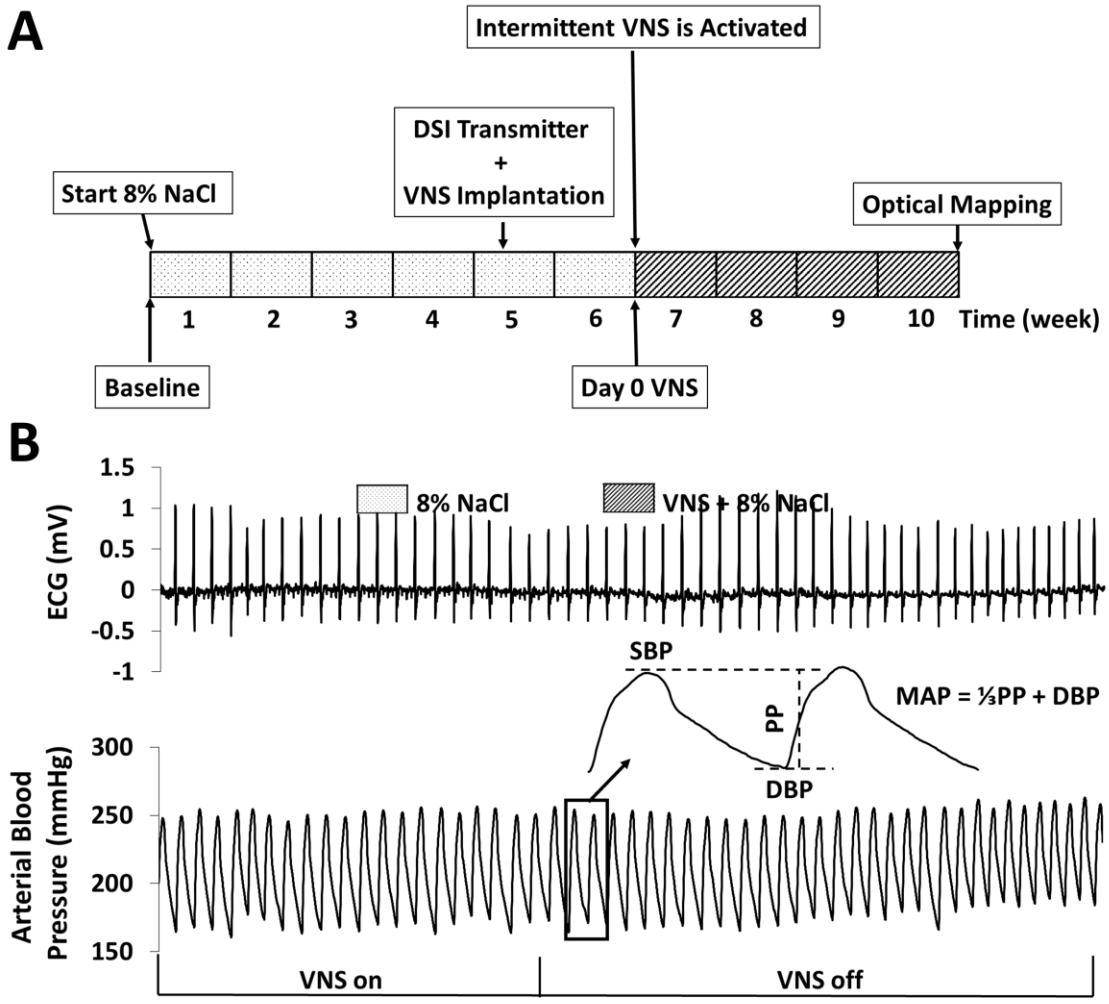

Figure 3.1 A) Experimental design timeline. HTN was induced through 6 weeks of high salt diet (8% NaCl). DSI transmitters and VNS devices were implanted during Week 5. Rats were randomly divided into 2 groups: Sham (n=6) with non-functional VNS stimulators and VNS (n=6) with functional stimulators. VNS therapy was turned on at Week 6, and ECG and blood pressure were monitored in both groups. B) Sample ECG (top) and arterial blood pressure (bottom) recordings from DSI telemetric devices. Insert: MAP is calculated using SBP and DBP measured from the blood pressure recordings.

3.3.2 Vagus Nerve Stimulator Implantation

The VNS pulse generator and lead were implanted as described previously [125, 126]. The back and the neck of the rats were shaved, and the right cervical vagus nerve and common carotid artery bundle were isolated from the surrounding tissue through a small incision on the neck. Bipolar cuff electrodes were placed around the bundle. The pulse generator (8cc, 14g) was implanted subcutaneously and positioned on the back of the rat. Parameters of the intermittent VNS

were set as follows: pulse frequency 20 Hz; pulse width 500 μsec, output current 1.0 mA. The pulse generator was programmed using radio-frequency telemetry to deliver continuously cyclic VNS: 7 seconds "On" and 66 seconds "Off". With a two-second ramp up and ramp down period before and after the stimulation on time, the duty cycle of the VNS therapy applied was 15%. Nonfunctional stimulators were implanted in the Sham rats to provide the same mass (14 g).

3.3.3 DSI Telemetry System Implantation

The DSI transmitter implantation was performed as described previously [127]. Briefly, the surgical regions (chest and inner leg) were shaved and the transmitter pressure catheter was implanted into the descending aorta via the left femoral artery through a small incision in the inguinal area. The two ECG leads were fixed subdermally on the chest muscle. Following recovery from surgery, rats were conscious and freely moving in their home cages for the duration of the in-vivo study. Continuous arterial BP and ECG data acquisition were performed with the use of a commercially available telemetry system (DSI, Inc.). The real-time bipolar electrograms and arterial BP data were collected with a 500 Hz sampling rate. Each cage was placed on a receiver (model RPC1, DSI Inc.) that was connected to a computer via a Data Exchange Matrix (DSI Inc.).

3.3.4 Optical Mapping

Upon completion of the in-vivo protocol (Figure 3.1A), rats were sacrificed for heart extraction through thoracotomy. The hearts were immersed in cold cardioplegic solution and Langendorff-perfused with warm (37 +/- 1°C) oxygenated Tyrode's solution as described in detail previously [128]. After 30 minutes of stabilization, the voltage sensitive dye di-4-ANEPPS (5 ug/mL) was added to the perfusate. Two 532 nm green lasers (Millenia Pro 5su, Spectra-Physics Inc., Mountain View, CA, USA) were used to illuminate both the right (RV) and left ventricles (LV) of the heart, and the fluorescence signal from more than 80% of the total ventricular surface was captured with two 14-bit CCD cameras (Little Joe CCD39, SciMeasure Analytical Systems, Inc., GA, USA), that ran synchronously at 1000 frames per second with 80 x 80 pixel resolution (the field of view was 12 x 12 mm). Blebbistatin (10-15 uM) was added to stop heart contractions and reduce motion artifacts.

3.3.5 Gross Morphology

Tibia length (TL)-normalized heart weight (HW) was used to quantify the effect of VNS on the cardiac structure to avoid the confounding effects of body weight. The left leg of the rat was severed above the knee joint, and the muscle and skin of the tibia were removed by mechanical stripping. The length of the tibia from the condyles to the tip of the medial malleolus was measured using micrometer caliper. HW normalized by TL (HW/TL) was compared between Sham and VNS rats at the end of the study. The RV and LV free-wall thickness was measured after optical mapping experiments to obtain an RV/LV wall thickness to quantify hypertrophy in the HTN hearts.

3.3.6 Data Analysis

3.3.6.1 In-Vivo DSI Telemetry System Data Analysis

Representative examples of simultaneously recorded ECG and arterial BP traces obtained from the DSI telemetry system are shown in Figure 3.1B during VNS "On" and "Off" periods. Note the presence of small artifacts on the ECG traces (arrows) while VNS therapy is applied (Figure 3.1B, top panel).

The ECG traces were used for the estimation of arrhythmia episodes using commercial software (Ponemah Life Science Suite, DSI Inc., MN, USA). Episodes of arrhythmias were counted one day prior to the start of therapy ("Day 0 VNS") and at the end of the study (Week 10) during the same time interval (four hours at night), and were presented as the number of episodes per hour per rat. Several types of arrhythmic events were observed: premature ventricular complexes (PVC), atrial fibrillation (AF), bradycardia, and skipping beats. PVC episodes were separated from all other arrhythmic events, as PVCs can occur in a healthy rat and poses less of a threat to the heart than the other types of arrhythmias.

From the arterial BP traces, the following parameters were calculated using commercial software (Dataquest A.R.T., DSI Inc., MN, USA): heart rate (HR), heart rate variability (HRV), systolic blood pressure (SBP), diastolic blood pressure (DBP), pulse pressure (PP), and MAP, as indicated in Figure 1B. ΔHR was also calculated to determine the relative changes in HR over the duration of VNS therapy. ΔHR was defined as

$$\Delta HR = (HR_n - HR_0),$$

Where $HR_n$is the HR at day n after VNS activation, and HR_0 is the HR measured at "Day 0 VNS." The relative changes in MAP were calculated as

$$\Delta\text{MAP} = (MAP_n - MAP_0),$$

Where MAP_n is the MAP at day n after VNS activation, and MAP_0 is the MAP measured at "Day 0 VNS" (See Figure 1A). The values for ΔMAP and ΔHR were calculated separately for the 12-hour day (7am – 7pm) and night (7pm-7am) time intervals.

3.3.6.2 Ex-Vivo Optical Mapping Data Analysis

Optical action potential durations (APD) were measured at 80% repolarization (APD_{80}), and two-dimensional (2D) APD maps were constructed to reveal the spatial distribution of APDs on both the LV and RV epicardial surfaces. Mean APD was calculated at different basic cycle lengths (BCLs) for the visible RV and LV surfaces by averaging APDs from all pixels. The maximum slope of the APD restitution, S_{max}, was calculated at the smallest diastolic interval. 2D maps of S_{max} were constructed to evaluate its spatial distribution and calculate the mean value of S_{max} on the epicardial surface.

The spatial dispersion of APD was estimated based on the heterogeneity index

$$\mu = \frac{APD^{95} - APD^{5}}{APD^{50}}$$

where APD^{95} and APD^{5} represent the 95^{th} and 5^{th} percentiles of the APD distribution, respectively, and APD^{50} is the median APD distribution.

To measure the local conduction velocity (CV), the distributions of the activation times (AT) over a spatial region of 5 x 5 pixels were fitted with a plane, and the gradients of ATs g_x and g_y were calculated for each plane along the *x* and *y* axes, respectively [128]. The magnitude of the local CV was calculated for each pixel as

$$(g_x^2 + g_y^2)^{-\frac{1}{2}}$$

During sustained ventricular tachycardia (VT) or VF, optical movies were acquired for 10 seconds, and the first 3000 frames (3 seconds) of each episode were used for VT/VF analysis. For each VT/VF episode, fast Fourier transform was applied at each pixel to obtain the power spectrum and determine the distribution of frequencies in the range of 5-35 Hz. The dominant frequency (DF) was defined as the frequency corresponding to the highest peak in the power spectrum [128]. 2D DF maps were constructed and used to determine the maximum DF (DF_{max}) on the epicardial surface, as well as the number of DF domains. The minimum size of the domain was considered to be 100 pixels with resolution of 0.01 Hz between domains.

3.3.7 Statistics

Data are presented as mean +/- standard error. Statistical comparisons between Sham and VNS rats were performed using one-way ANOVA. $P < 0.05$ was considered to be statistically significant.

3.4 RESULTS

3.4.1 In-Vivo Effect of VNS on Blood Pressure, ECG, and Arrhythmias in HTN Rats

Table 3.1 shows in-vivo BP and ECG twenty four-hour mean parameters (MAP, PP, HR, and HRV) at Weeks 5, 6, 8, and 10 for all Sham and VNS rats. Table 1 indicates that 6 weeks of high salt diet successfully induced HTN in both Sham and VNS groups, as indicated by a significant increase in MAP and PP, as well as a significant decrease in HR. Note that there were no significant differences between the groups in any parameter at either baseline or Week 6.

Table 3.1 In-vivo blood pressure and ECG parameters for Sham and VNS rats

		Week 5 (Baseline)	**Week 6: Day 0 VNS (8% NaCl)**	**Week 8 (8% NaCl +VNS)**	**Week 10 (8% NaCl +VNS)**
HR (BPM)	**VNS**	436 ± 10	*408 ± 10	421 ± 9	*407 ± 3
	Sham	442 ± 10	*399 ± 7	*#380 ± 12	*397 ± 9
MAP (mmHg)	**VNS**	120 ± 3.5	*157 ± 6.0	*†171 ± 10.4	*†179 ± 11.6
	Sham	112 ± 2.5	*155 ± 11.7	*†174 ± 10.0	*†200 ± 15.7
PP (mmHg)	**VNS**	47 ± 2.8	*56 ± 2.7	*†62 ± 3.0	*60 ± 1.6
	Sham	38 ± 5.7	*59 ± 3.4	*58 ± 4.0	*61 ± 3.0
HRV	**VNS**	0.091 ± 0.009	0.090 ± 0.007	0.097 ± 0.012	0.108 ± 0.021
	Sham	0.099 ± 0.006	0.097 ± 0.009	*†0.119 ± 0.004	0.099 ± 0.015

* denotes significance with respect to Week 5 ($p < 0.05$)
† denotes significance with respect to Week 6 ($p < 0.05$)
# denotes significance between Sham and VNS groups ($p < 0.05$)

Figure 3.2 shows relative changes of twenty four-hour mean data for MAP (A), PP (B), and HR (C) with respect to baseline (Week 5) for both Sham and VNS groups. The data are shown at different times during VNS stimulation: Week 6 ("Day 0 VNS"), Weeks 8 and 10 (after 2 and 4 weeks of VNS, respectively). Figure 3.2 shows that further development of HTN (Weeks 8 and 10

in comparison to Week 6) did not affect relative change in HR and PP, but significantly increased MAP in the Sham but not the VNS group. Note that the relative changes in HR and PP are larger in the Sham group in comparison to the VNS group, although statistical significance is only present at some weeks.

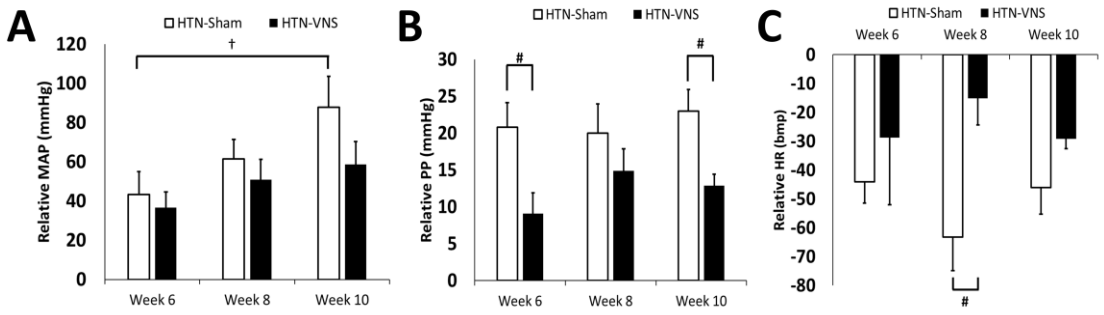

Figure 3.2 Relative change of 24-hour mean data for A) MAP; B) PP; and C) HR with respect to baseline data (Week 5) for both Sham and VNS rats. † indicates statistical significance ($P < 0.05$) with respect to Week 6; # indicates statistical significance ($P < 0.05$) between VNS and Sham.

To further investigate the effect of VNS on MAP and HR, we calculated ΔMAP and ΔHR, which reflect relative change in MAP and HR at each day with respect to "Day 0 VNS." Figure 3.3 shows the change in ΔMAP (Panels A and B) and ΔHR (Panels C and D) for the entire duration of VNS stimulation separately for the day and night time periods, as rats were housed in rooms that have automatic controlled light-dark cycles. Figure 3.3A shows the long-term VNS treatment attenuated the increase in ΔMAP during the day time interval, where parasympathetic system is playing the dominant role in rats. This effect becomes statistically significant toward the end of the study ($P < 0.05$, # in Figure 3.3A). On the other hand, VNS has no significant effect on ΔMAP during the night time interval, where sympathetic activity is dominant. Figure 3.3 panel C and D indicate that the ΔHR in both Sham and VNS groups has similar trend over time suggesting no chronic effect of VNS on HR, which is expected since the duty cycle of the VNS treatment was only 15%.

Lastly, this study investigated the effects of VNS on the development of arrhythmias that are induced in the rats as a result of HTN. Figure 3.4A shows simultaneous recordings of arterial BP and ECG from an implantable DSI transmitter for Sham rats, demonstrating examples of a PVC (left) and a skipped beat (right). Similar types of abnormal cardiac behaviors were observed in VNS rats. However, there were a smaller number of occurrences of these arrhythmias in the VNS rats compared to the Sham rats. Figure 3.4B shows the total numbers of PVCs and arrhythmia episodes counted in both groups at Week 6 ("Day 0 VNS") and Week 10. Note the reduction in both PVCs

and other arrhythmic episodes ($P < 0.05$) in VNS rats, indicating the antiarrhythmic effects of VNS therapy in HTN rats.

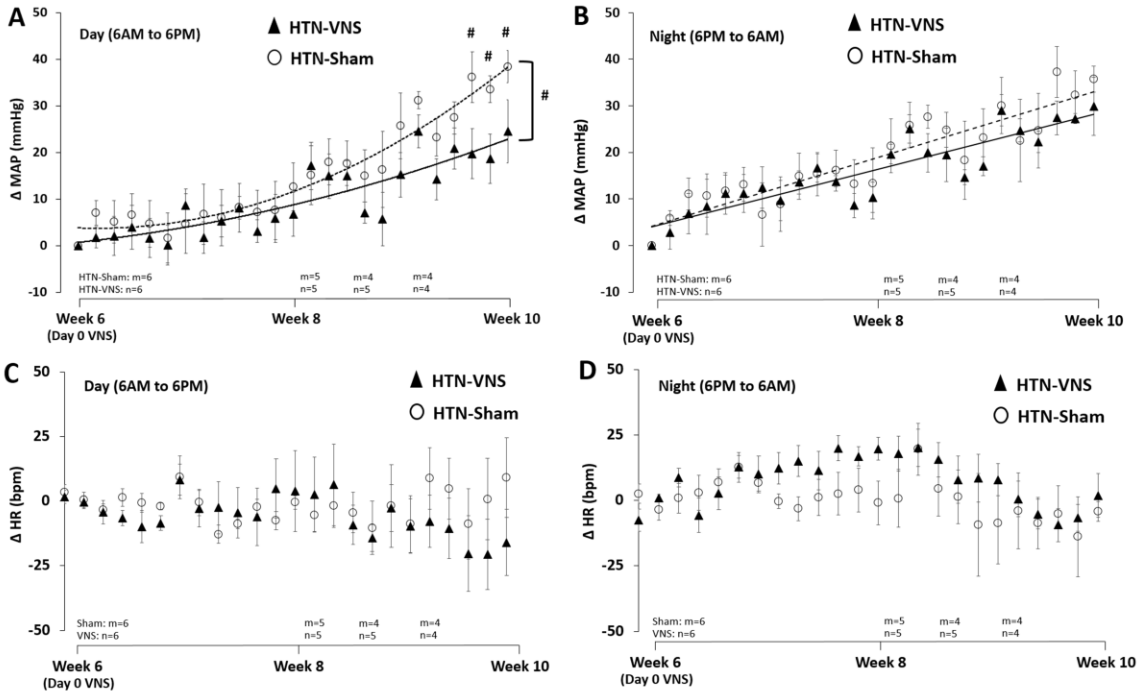

Figure 3.3 A, B) ΔMAP and C, D) ΔHR during the day (7am-7pm) (panels A and C) and night (7pm-7am) (panels B and D) for the Sham and VNS rats. # indicates statistical significance ($P < 0.05$) between VNS and Sham.

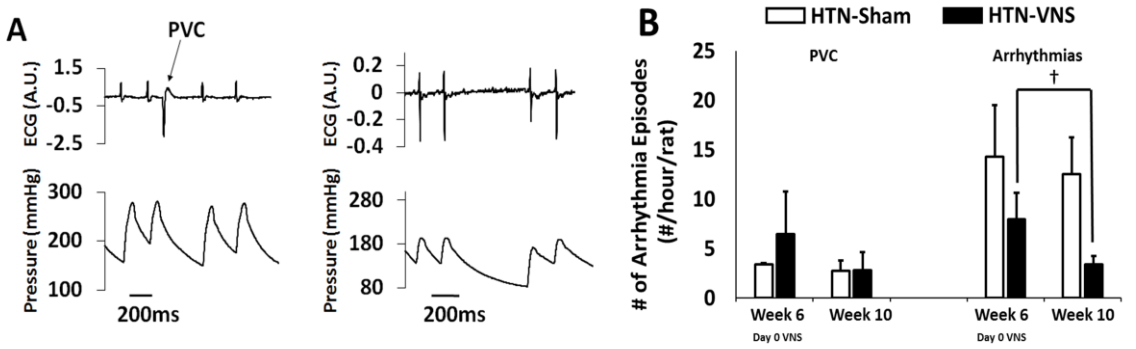

Figure 3.4 A) Examples of episodes of a PVC (left) and other arrhythmias (skipped beats, right) from Sham rat at Week 6. B) Mean number of episodes of PVCs and other arrhythmias between Week 6 and Week 10 for Sham and VNS rats. † indicates statistical significance ($P < 0.05$) between Week 6 and Week 10.

3.4.2 Ex-Vivo Effect on VNS on Electrophysiological Properties of the HTN Hearts

Typical examples of 2D APD maps of the RV and LV of Sham and VNS rat hearts obtained at a BCL of 200 ms are presented in Figure 3.5A. Corresponding traces of action potentials from a representative single pixels are shown in Figure 3.5B. Mean APD_{80} calculated in both groups for various BCLs are presented in Figure 3.5C for RV (left panel) and LV (right panel). Note that VNS reduced APD in the RV, with significant reduction at BCLs 120, 140, and 160 ms, but not in the LV. In addition, the maximum slope of APD restitution curve (S_{max}) was significantly reduced in the RV but not in the LV as a result of VNS therapy, as indicated in Figure 3.5D.

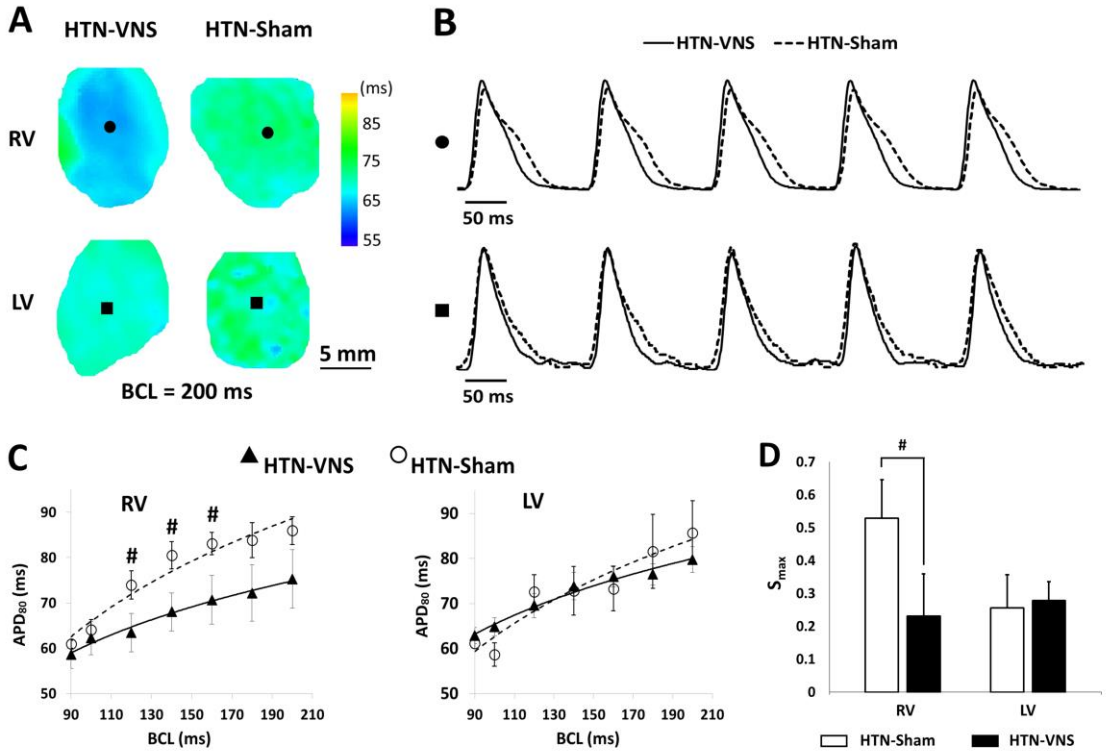

Figure 3.5 A) Representative examples of 2D APD_{80} maps calculated at BCL=200 ms for RV and LV of VNS and Sham hearts. B) Single pixel action potential traces taken from the RV (●) and LV (■) data from panel A for VNS (solid line) and Sham (dashed line) hearts. C) Mean APD_{80} as a function of BCL for the RV and LV of VNS (n=5) and Sham (n=5) hearts. D) Mean S_{max} values for the RV and LV of all VNS and Sham hearts. # indicates statistical significance ($P < 0.05$) between VNS and Sham.

To determine whether VNS affected the spatial dispersion of APD, we calculated the heterogeneity index, μ, separately for the RV and LV at different BCL values. Figure 3.6A indicates that VNS significantly reduced μ in the LV but not in the RV at most BCLs.

To study whether VNS affected CV of action potential propagation, AT maps were constructed for both Sham and VNS groups at various BCLs. A representative example of AT maps at a BCL of 180 ms is shown in Figure 3.6B, indicating normal propagation in the RV of both the Sham and VNS rat hearts. Figure 3.6C shows mean CV data at different BCLs for both groups indicating that VNS increased CV both in the RV and LV, although the effect is significant only at some BCLs.

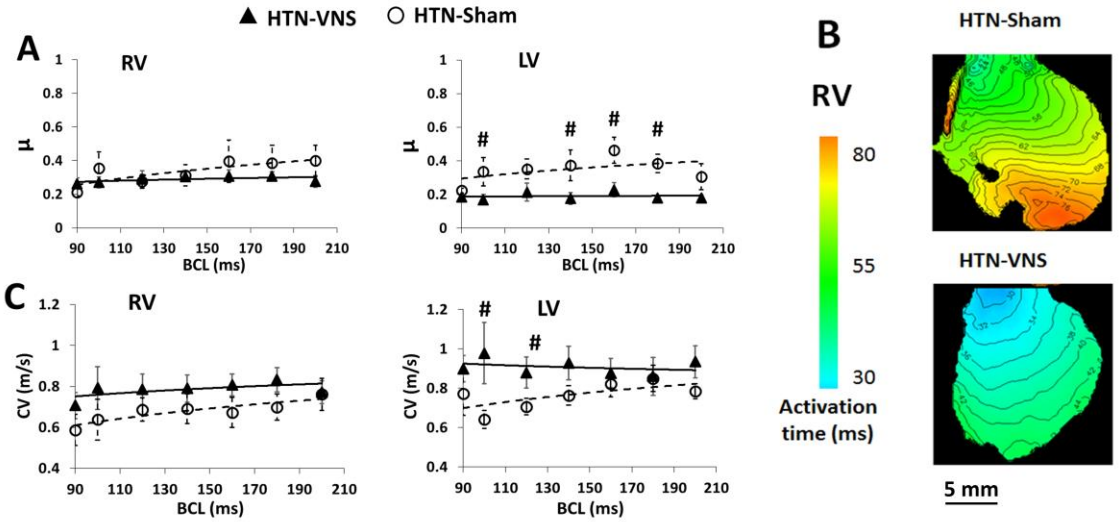

Figure 3.6 A) APD heterogeneity index, μ, and C) mean CV as a function of BCL for the RV and LV of VNS and Sham hearts. B) Representative examples of activation time maps calculated at BCL=180ms. # indicates statistical significance ($P < 0.05$) between VNS and Sham.

To investigate the effect of VNS on dynamical behavior of ex-vivo arrhythmias, optical mapping videos were analyzed from either spontaneously arrhythmias or from those induced at the end of the pacing protocol. In the optical mapping experiments, sustained VF was observed in all (6/6) Sham rats, while sustained VT, but not VF, was observed in four out of six VNS rat. None of the VNS rats developed VF, suggesting that VNS provided protection against the development of VF. The analysis of VT/VF dynamics is shown in Figure 3.7 panel A and B. Figure 3.7A shows a representative example of 2D DF maps for the RV of VNS and Sham rat hearts (top) with the single pixel traces (bottom) clearly indicating the presence of VT/VF. The DF_{max} and number of DF domains in the Sham and VNS rats are shown in Figure 3.7B. Note that the Sham rats not only had more DF domains but also had higher DF_{max} values than the VNS rats, indicating more complex dynamics of ex-vivo cardiac arrhythmias. Representative examples of phase movies during arrhythmias in VNS and Sham hearts are shown in Figure 3.7B.

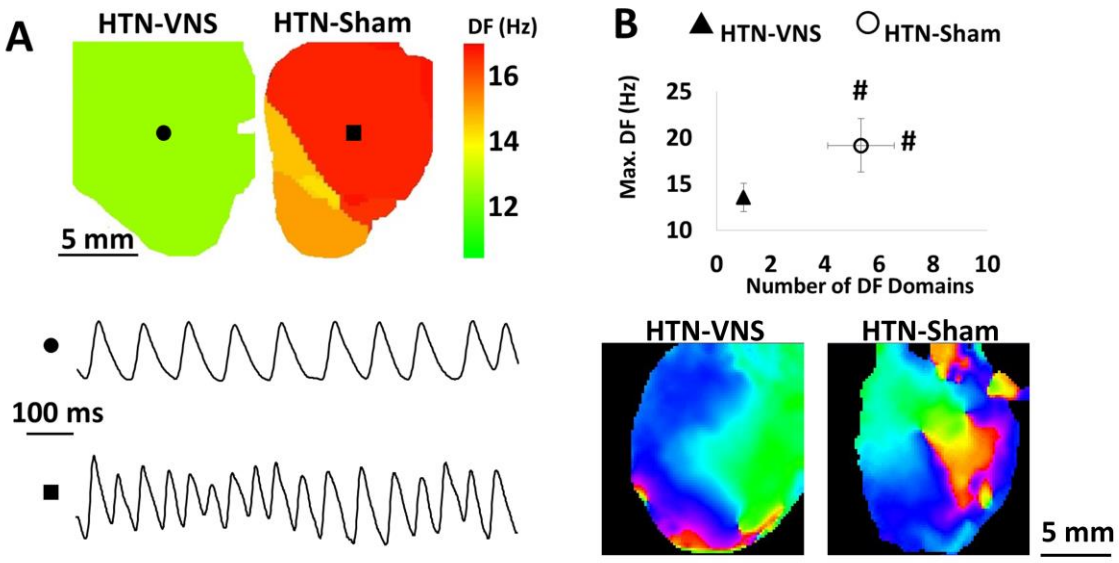

Figure 3.7 Dynamics of ex-vivo arrhythmias. A) Representative examples of 2D DF maps from the RV of VNS and Sham hearts (top) and single pixel sample traces of VT (●) and VF (■) (bottom). B) Maximum DF as a function of number of frequency domains from all arrhythmic episodes in VNS and Sham hearts. # indicates statistical significance ($P < 0.05$) between VNS and Sham. C) Snapshot of representative examples of phase movies during arrhythmias for VNS and Sham hearts.

Lastly, the HW/TL and the RV/LV wall thickness ratios were calculated at the end of the study. The results demonstrate that both parameters were similar in the VNS (HW/TL: 0.38 +/- 0.03; RV/LV: 0.32 +/- 0.01) and Sham (HW/TL: 0.42 +/- 0.01; RV/LV: 0.30 +/- 0.01, P = N/S) rats suggesting that four weeks of VNS therapy did not induce structural remodeling of the HTN hearts.

3.5 Discussion

Autonomic dysregulation is a feature of chronic HF and is characterized by a sustained abnormal elevation in sympathetic nerve activity and a withdrawal of parasympathetic nerve activity [129-131]. Autonomic imbalance, which is reflected in reduced HRV and reduced baroreflex sensitivity, is associated with worsening HF and increased risk of mortality [132, 133]. Modulation of parasympathetic activation with electrical stimulation is a potential therapy for HF, but has received limited attention due to its inherent complex cardiovascular effects [134-136]. However, recent clinical studies have demonstrated the salutary effects of parasympathetic stimulation in HF [72, 137].

In the present study, for the first, a hypertensive rat model was used to characterize the effect of VNS on BP and arrhythmia incidence, as well as the effects of VNS on the electrophysiological properties of the heart. The results confirm that VNS therapy modulates the balance of the ANS whether by promoting parasympathetic activity, decreasing sympathetic activity, or a combination of the two.

The major findings of this study are as follows: (1) 4 weeks of intermittent VNS attenuated the increase in MAP in VNS rats compared to Sham rats; (2) VNS reduced the number of in-vivo arrhythmic events, as well as the spatiotemporal complexity of ex-vivo arrhythmias in VNS rats compared to Sham rats; (3) VNS induced beneficial changes in the electrophysiological properties of the heart, including a reduction in APD during rapid drive pacing, μ, and S_{max}, and an increase in CV. Overall, these results provide further evidence for the therapeutic efficacy of VNS in HTN and HHD.

3.5.1 The Effect of VNS on Blood Pressure

Recent studies have shown that chronic electrical stimulation of the carotid sinus activates the baroreflex and reduces MAP by inhibiting central sympathetic outflow [138, 139]. This reduction of BP is substantial, and is currently being used as a clinical therapy for resistant HTN [140, 141].

The present study shows that chronic VNS also causes an attenuation of MAP elevation during the spontaneous development of chronic HTN, likely through similar mechanisms. In this study, the light-dark cycle for the rats has been accounted for. The rationale for the day-night separation is that the roles of the sympathetic and parasympathetic nervous system are different when the rats are active (during the night) and at rest (during the day). At rest, parasympathetic activity predominates over sympathetic tone [142]. Recently, it was demonstrated that the sympathetic and parasympathetic nervous systems are involved in diurnal variation in heart rate-corrected QT-intervals (QTc) in rats [143]. Specifically, the enhanced parasympathetic nervous activity during the night induces a slight but significant QTc prolongation. Our results show that VNS induced a more pronounced modulation of MAP during the daytime, when the rats are less active and sleeping, and suggest that VNS is more effective when parasympathetic nerve activity predominates and the sympathetic tone is reduced. This is an indirect indication that the parasympathetic nerve activity is impaired by HTN; and that VNS lowers MAP by enhancing parasympathetic nerve activity and restoring autonomic balance.

3.5.2 The Antiarrhythmic Effects of VNS

The antiarrhythmic effects of VNS in ischemic HF are shown in previous studies [144-146]. In this study, the results demonstrate that VNS also has antiarrhythmic effects in HHD. VNS therapy significantly reduced the incidence of in-vivo arrhythmias (tachycardia, bradycardia, and skipped beats) in hypertensive rats. In addition, the optical mapping results demonstrated that the complexity of the spontaneous and induced ex-vivo arrhythmias is significantly reduced in VNS rats compared to Sham rats, which is further evidence of the antiarrhythmic effects of VNS treatment in HHD.

Antiarrhythmic effects were associated with significant VNS-induced reduction in the APD and the slope of APD restitution in the RV, as well as the reduction in the spatial dispersion of APD and increase in CV in the LV during rapid drive pacing. The electrophysiological changes that occurred due to VNS in the LV are in contrast to those that were observed in most HF hearts. Reduction in CV and increase in μ have been shown to create an arrhythmic substrate that is able to promote the inception and preservation of reentrant arrhythmias [147, 148]. In HF, conduction slowing has been linked to a decrease in expression of gap-junction protein Connexin-43 [149]. Likewise, elevated Connexin-43 expression is correlated with faster conduction in the myocardium [150]. Short-term VNS therapy has been previously shown to preserve the expression of gap-junctional protein Connexin-43 over the course of minutes after cardiac injury [98]. Although, in this study, Connexin-43 expression in the LV was not directly measured, the results seem to agree with this finding. All of these electrophysiological changes are likely contributing to the antiarrhythmic effects of VNS.

The exact mechanisms underlying the antiarrhythmic effects of VNS are still not well understood. One possible mechanism may be due to the activation of the vagus nitric oxide (NO) pathway, since direct neural stimulation of the vagus nerve releases NO through a neuronal NO synthase mechanism in the ventricle. Brack et al. previously demonstrated the important role of NO in mediating the protective effects of VNS in the rabbit hearts [95, 101]. Another possible mechanisms may involve reactive oxygen species (ROS). It is known that during myocardial injury, there is an increase in ROS production and oscillation of the mitochondrial membrane potential, which plays an important role in the genesis of cardiac arrhythmias [151]. Shinlapawittayatorn et al. has demonstrated that VNS was able to stabilize cardiac mitochondrial membrane potential by protecting the depolarization of the mitochondrial membrane [126].

It is important to note that in this study, only a limited number of spontaneous arrhythmic episodes were evaluated, and therefore, arrhythmias were relatively scarce even in Sham rats.

Another approach, such as stressing the heart using programmed stimulation, might have led to stronger results.

3.5.3 Mechanistic Insights into Chronic VNS Therapy

At the cervical level, the vagus nerve contains a composite of myelinated A- and B-fibers, as well as unmyelinated C-fibers, which are the most numerous (approximately 65% to 80%) [152]. According to Woodbury et al. [153], activation of C-fibers requires higher stimulation amplitudes and longer pulse durations compared to the activation of the myelinated A- and B-fibers. For instance, Zagon et al. demonstrated that the myelinated vagal fibers were activated in anesthetized rats at 100 μA (at 30 Hz and a pulse width of 0.5 ms), while increasing current up to 200 μA activated the nonmylinated fibers [154]. The stimulation parameters that have been used in this study (pulse width of 0.5 ms and current of 1.0 mA) suggest that both myelinated and unmyelinated fibers are stimulated. Similar levels of stimulation will also engage the vagal motor fibers, especially the myelinated fibers, according to the study of Ben-Menatchem et al. [155]. Future studies are needed to determine whether the therapeutic mechanism of VNS predominately occurs through afferent or efferent neural pathways.

In addition, chronic VNS may also provide an anti-inflammatory effect through the cholinergic anti-inflammatory pathway. The neural signal that is sent from the efferent fibers in the vagus nerve can inhibit the release of cytokines and release the neurotransmitter acetylcholine. Cytokine-producing cells contains acetylcholine receptors which transduce signals resulting in the inhibition of cytokine synthesis. By decreasing the level of cytokine synthesis, the magnitude of the inflammatory response is dampened [108]. This effect was demonstrated by Zhang et al. by measuring the plasma C-reactive protein (CRP) levels [110]. Pacing-induced HF promotes systemic inflammation and was shown to have increased plasm CRP. VNS treatment significantly reduced the plasm CRP.

3.6 CONCLUSION

The results of this study clearly demonstrate that VNS is capable of attenuating the high MAP in the hypertensive rats and inducing antiarrhythmic effects, which provides evidence for VNS as an effective device-based therapy for HTN and HHD. The results also suggest that the therapeutic effects of VNS are associated with chronic treatment, rather than acute stimulation. Indeed, the beneficial effect of VNS on attenuating high MAP became significant only after four weeks of

chronic VNS therapy. Therefore, further evaluation of VNS as a clinical HTN therapy requires prolonged chronic stimulation.

This study demonstrates the beneficial effects of VNS on blood pressure and arrhythmias in a hypertensive rat model and investigates the effect of VNS on several electrophysiological parameters. Nevertheless, more comprehensive evaluation is required to reveal the mechanisms by which VNS affects different in-vivo and ex-vivo electrophysiological and structural characteristics of the rats. The current study raises a number of questions that can help in designing future experiments.

The results show that VNS affected the RV and LV in slightly different ways. Indeed, VNS reduced APD and S_{max} only in the RV, but increased CV and decreased APD spatial dispersion predominately in the LV. This suggests that different electrical remodeling of both ventricles takes place as a result of chronic HTN and VNS therapy. On the other hand, the data does not suggest any anatomical remodeling of either ventricles. These results are somewhat intriguing since the LV (but not the RV) contractile properties are expected to be the main determinant of MAP. It is unclear whether the RV/LV electrophysiological remodeling is accompanied by a remodeling of the corresponding extracellular matrix.

Chapter 4

Chronic low-level vagus nerve stimulation improves long-term survival in salt-sensitive hypertensive rats

4.1 INTRODUCTION

Chapter 4 presents the methods and results for a chronic survival study to evaluate the long-term efficacy of vagus nerve stimulation (VNS) as a therapy in a dahl salt-sensitive (DSS) hypertensive rat model. Methods for longitudinal data analyses of the cardiovascular, hemodynamics, and autonomic responses are presented and used to evaluate the progression of hypertension (HTN) and the role of VNS therapy. Ex-vivo studies are also described as a means to investigate the impact of VNS therapy on cardiac structural properties.

HTN most prominent risk factor for cardiovascular disease (CVD) [1, 156], and cardiovascular complications due to HTN result in over 9 million deaths annually [157]. The need to control the rise in blood pressure (BP) while also addressing the negative effects of complex co-morbidities makes the clinical management of HTN challenging. Currently, the majority of hypertensive patients are treated with antihypertensive drugs to control BP. However, many limitations exist, including resistant HTN, inability to tolerate therapy, and non-compliance with the medication regime [122, 158]. There is a need for novel treatment options for hypertensive patients to control BP while also addressing the adverse cardiac effects of HTN.

Recently, we proposed to specifically target the parasympathetic nervous system using VNS, and evaluated the efficacy of four weeks of VNS treatment for HTN and HTN-induced heart disease (HHD) in a rat model of HTN [159]. Our study and others have demonstrated the beneficial effects of chronic VNS in treating HTN, and its associated improvement of endothelial function and cardiac electrophysiological properties, leading to suppression of ventricular arrhythmias [60, 92, 125]. Antiarrhythmic effects have also been recently demonstrated by our lab in healthy hearts in the absence of sympathetic overdrive [160]. Further, acute VNS therapy has also shown a beneficial effect on BP and heart rate (HR) dynamics in hypertensive rats [62, 63, 161].

4.2 AIM

To date, there has been limited research evaluating the long-term effects of VNS on BP and associated cardiovascular complications in advanced-stage HTN in rats. The aim of this study is to investigate the effects of low-level, intermittent chronic VNS therapy on the long-term survival of hypertensive rats and to evaluate the impact of VNS therapy on BP control, HR dynamics, and structural cardiac properties.

4.3 METHODS

All experiments conform to the Guidelines for the Care and Use of Laboratory Animals (NIH publication No. 85-23, revised 1996) and the University of Minnesota guidelines for the care and use of animals. Prophylactic antibiotic (gentamicin sulphate; 10 mg/kg, i.m.) was given prior to each surgery. During the surgeries, rats were anaesthetized with isoflurane (5% for induction, 2% or 3.5% for maintenance) in oxygen (2 L/min for induction, 1 L/min for maintenance). The rat's body temperature was maintained at 37ºC on a temperature-controlled surgery table.

4.3.1 Experimental Design

Five week old male DSS rats (Charles River Laboratories, Wilmington, MA) were fed a high salt (8% NaCl) diet to induce HTN, and this diet was maintained for the duration of the study (see Figure 4.1A). Four weeks after initiating the high salt diet, the hypertensive rats were implanted with vagus nerve stimulators (Model 103, LivaNova USA, Inc., formerly Cyberonics Inc., Houston, TX) and physiological telemetry devices (HD S11, DSI Inc., St. Paul, MN) and randomly divided into two groups: VNS (n = 9; functional VNS stimulators) and Sham (n = 9; non-functional VNS stimulators). One Sham rat was excluded from analysis because of the delayed recovery from surgery, resulting in n=8 for Sham. At Week 6 (Baseline), the low-level VNS therapy was activated and applied for up to 8 weeks or until an endpoint (death or severe HTN-related events such as a stroke or hematoma) was reached. During VNS therapy, ECG and BP recordings were simultaneously captured through the DSI telemeters for both Sham and VNS rats. The event-free survival rate was calculated with respect to the start of VNS therapy at Week 6. A summary of the data analyses used, the time points selected, and the number of rats in each group can be found in Table 4.1.

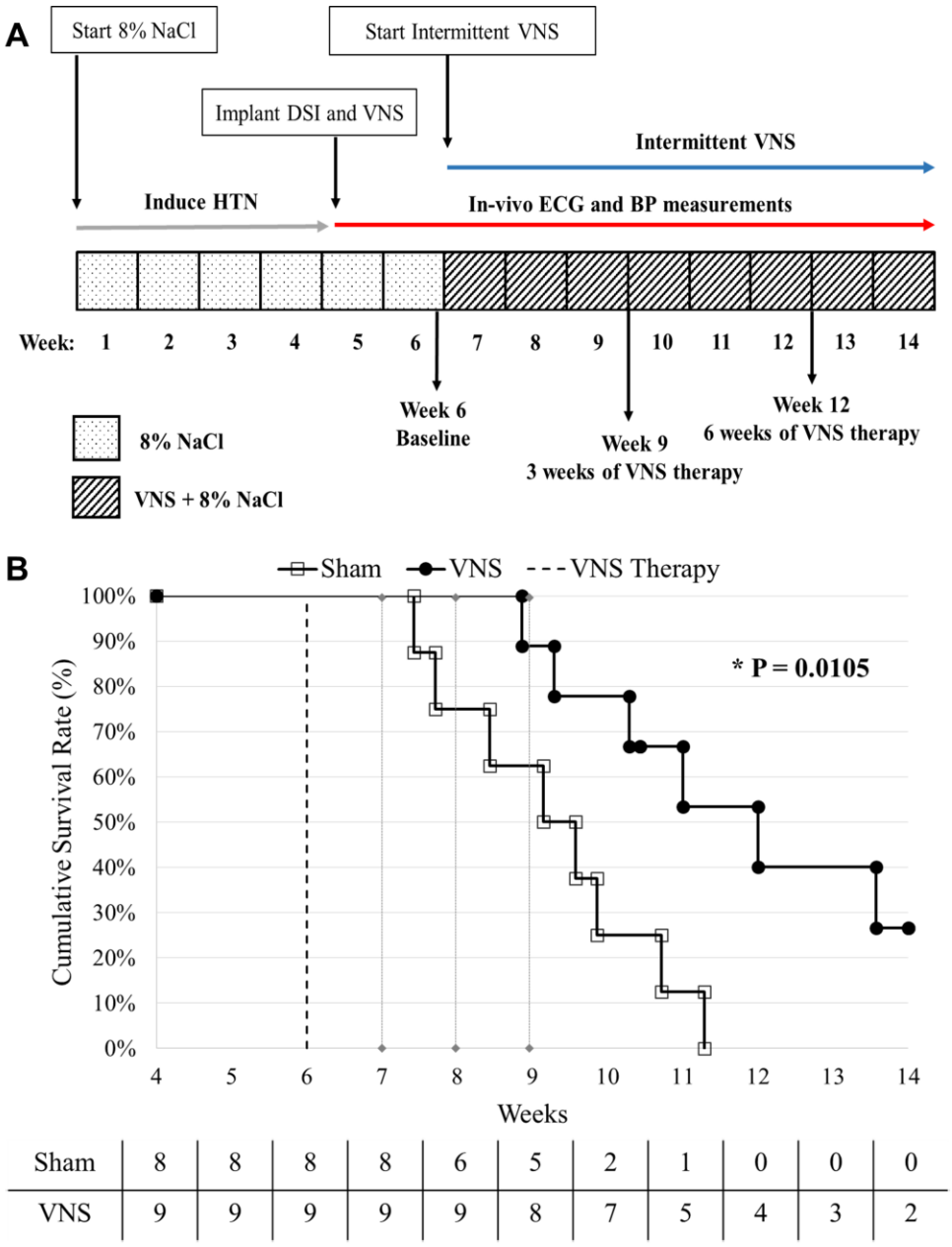

Figure 4.1 (A) Experimental design. HTN was induced using a high salt diet (8% NaCl). At Week 4, the rats were implanted with vagal nerve stimulators and DSI transmitters, and randomly divided into Sham (n = 8) and VNS (n=9) groups. VNS therapy was turned on at Week 6 and continuous BP and ECG was recorded until the end of the study. (B) Kaplan-Meier event-free survival curves for Sham and VNS rats are statistically different ($P < 0.05$). The dashed vertical line indicates the start of VNS therapy at Week 6. The number of rats remaining in each group is included along the x-axis.

Table 4.1 Summary of data analyses performed including time points and number of rats included in the analysis

	Time Point				
Analysis	Week 6	Week 7	Week 8	Week 9	Week 12
Acute VNS Response 4-h segment (***Day*** $_{4h}$ and ***Night*** $_{4h}$) VNS Rats Only*	VNS (n = 6)†			VNS (n = 6) †	VNS (n = 2) †
Longitudinal Analysis SBP, MAP, DBP, PP, HR, HRV 12-h segment (***Day*** $_{12h}$ and ***Night*** $_{12h}$)	Analysis uses all data from all rats and time points				
Circadian Rhythm 24-h segment	VNS (n = 9) Sham (n = 8)			VNS (n = 8) Sham (n = 5)	
BRS 4-h segment (***Day*** $_{4h}$ and ***Night*** $_{4h}$)	VNS (n = 9) Sham (n = 8)	VNS (n = 9) Sham (n = 8)	VNS (n = 9) Sham (n = 6)	VNS (n = 8) Sham (n = 5)	

* Only VNS rats with adequate ECG signal to identify stimulation intervals were used for analysis

† Data presented in Chapter 5 of this thesis

4.3.2 Vagus Nerve Stimulator Implantation

The VNS pulse generator and cuff electrodes were implanted as described previously [125, 126]. Briefly, the surgical regions on the back and the neck were shaved. Bipolar cuff electrodes were implanted through a small incision on the neck and placed around the right cervical vagus nerve and common carotid artery bundle. The pulse generator was implanted subcutaneously and positioned on the back of the rat. VNS was applied with a pulse frequency of 20 Hz, a pulse width of 500 μs, and an output current of 0.25 - 1.0 mA. The amplitude of the current was selected based on a stimulation level of sufficient strength to appear on the ECG but without causing an acute peak reduction in HR greater than 10% during the active phase of the stimulation cycle. Each VNS cycle consisted of an active phase, consisting of 14 seconds of full strength stimulation plus a 2-second ramp up and ramp down phase, followed by an inactive phase, 62 seconds in duration, resulting in a duty cycle of 22.5%.

4.3.3 DSI Telemeter Implantation

DSI transmitters were implanted as described previously [127]. Briefly, the chest and inner thigh were shaved and the transmitter pressure catheter was implanted through a small incision on

the inner left hind limb into the descending aorta via the left femoral artery. The two ECG leads were fixed subdermally on the chest muscle. After surgery, the rats were individually housed in cages where they were able to freely move about while receivers (model RPC1, DSI Inc.) connected to a computer via a Data Exchange Matrix (MX2, DSI Inc.) continuously collected data from each rat. The ECG and arterial BP data were collected at a sampling rate of 500 Hz throughout the study.

4.3.4 Data Analysis

4.3.4.1 Chronic Effects of VNS Therapy: Disease Progression

Simultaneous ECG and BP data acquired from the DSI telemeters were averaged over 12-hour Day_{12h} (7am-7pm) and $Night_{12h}$ (7pm-7am) intervals, defined by the light-dark cycle of the room. BP and HR measures, including systolic blood pressure (SBP), diastolic blood pressure (DBP), mean arterial pressure (MAP), pulse pressure (PP), HR, and heart rate variability (HRV), were calculated.

Baseline BP and HR parameters were quantified as the three-day average prior to the start of VNS therapy at Week 6. Individual values for Day_{12h} and $Night_{12h}$ intervals was compared to Baseline data to determine the relative change in BP (ΔSBP), HR (ΔHR), and HRV (ΔHRV) for each animal, as described previously [159]. The longitudinal data for Sham and VNS rats were individually fit with a linear regression to quantify the disease progression, and the slopes of the linear fits were averaged for Sham and VNS rats for comparison between groups.

Circadian rhythm analysis was performed at Baseline and at Week 9. A 24-hour continuous segment of data was divided into 1-hour intervals and fit with a cosinor function using the following equation

$$Y = MESOR + Amplitude * \cos(Frequency * X + Acrophase),$$

where X is the 1-hour average HR or BP from the Sham or VNS rats, *MESOR* is the mean value of the cosinor function, *Amplitude* is the difference between the peak value and the *MESOR*, and *Acrophase* is the phase shift. The *Frequency* was set to 0.2618 rad/hr, corresponding to a 24-hour period.

4.3.4.2 Baroreflex Sensitivity

The time domain baroreflex sensitivity (BRS) sequence method quantifies concordant changes in BP and HR. BRS analysis was analyzed from Week 6 to Week 9. The parameters for the BRS method were set to the following: a minimum sequence length of 16 consecutive beats, a minimum change in BP of 5 mmHg, and a R^2 value threshold of 0.85. Baroreflex sensitivity (BRS) was

quantified using a traditional sequence method for Day_{4h} and $Night_{4h}$ intervals to compare autonomic tone in the hypertensive rats [162].

4.3.4.3 Histology and Gross Morphology

After reaching an endpoint of the in-vivo protocol, excluding death, the heart was extracted through a midline incision and immediately submerged in cold cardioplegic solution. The hearts were weighed and normalized to tibia length (HW/TL) as a measure of hypertrophy [159], and were then preserved in 10% formalin solution for histology studies. Sham (n = 8) and VNS (n = 6) hearts were embedded in paraffin, cut into 5 μm thick cross-sectional slices, and stained with Masson's Trichrome. The stained heart slices were imaged using Nikon microscope (Model ECLIPSE Ni-E, Nikon Corporation, Tokyo, Japan) system at 4x magnification. NIS-Elements AR (version 4.51.01) software was used to scan each slide and export the images for post-processing.

4.3.5 Statistics

BP and HR data are presented as mean ± standard error. Cumulative event-free survival is presented using Kaplan-Meier curves, and the Log-Rank test was used to determine statistical significance. The acute effects of VNS at different time intervals were compared using repeated measures one-way ANOVA with Tukey's multiple comparisons correction. The linear regression slopes for the longitudinal BP and HR measures were compared between Sham and VNS rats using one-way ANOVA. The circadian rhythm parameters were compared between Sham and VNS rats and Week 6 and Week 9 time points using two-way ANOVA with Tukey's multiple comparisons correction. Finally, the structural effects were compared using simple linear regressions to compare structural measures as a function of survival for Sham and VNS rats. Statistical significance was determined at $P < 0.05$.

4.4 RESULTS

4.4.1 Baseline Parameters

Baseline ECG (HR, HRV) and BP (MAP, SBP, DBP and PP) parameters show no significant differences between Sham and VNS rats (see Table 4.2). Specifically, Baseline HR (Sham: 386 ± 5 bpm, VNS: 389 ± 5 bpm) and SBP (Sham: 192 ± 10 mmHg, VNS: 187 ± 8 mmHg) were similar between groups and are consistent with previously published parameters in hypertensive rats [159].

Table 4.2 Baseline parameters, presented as mean +/- standard error, for VNS (n=9) and Sham (n=8) rats calculated as a three day average prior to the start of therapy.

Baseline Parameter	Sham (n = 8)	VNS (n = 9)	P-value
HR (bpm)	386 ± 5	389 ± 5	0.52
HRV (%)	9.5 ± 0.6	9.8 ± 0.3	0.55
SBP (mmHg)	192 ± 10	187 ± 8	0.65
MAP (mmHg)	160 ± 9	155 ± 7	0.66
DBP (mmHg)	131 ± 9	128 ± 6	0.7
PP (mmHg)	61 ± 2	59 ± 3	0.63

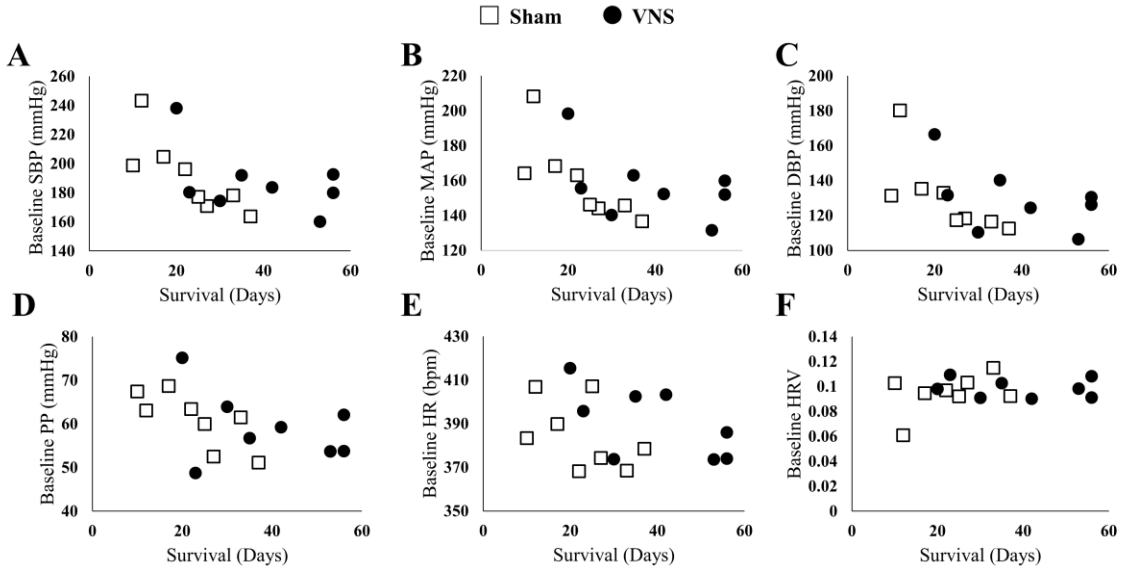

Figure 4.2 Baseline characteristics of Sham and VNS rats versus event-free survival times. Baseline SBP (A), MAP (B), DBP (C), PP (D), HR (E), and HRV (F) show no significant differences between groups demonstrating no significant influence on the differences observed in event-free survival times in Sham and VNS rats.

4.4.2 Event-Free Survival Assessment

Figure 4.1B shows the cumulative event-free survival rates of the Sham and VNS rats, with a significant improvement in survival of VNS rats ($P < 0.05$). The median survival improved by 78% in VNS rats with median survival times increasing from 23.5 (95% CI: 12 to 33) days for Sham rats to 42 (95% CI: 30 to 53) days for VNS rats. In addition, 2/9 VNS rats survived to the end of the study, whereas 0/8 Sham rats survived. Individual baseline parameters for Sham and VNS rats were plotted versus survival time, in days, to observe whether any baseline parameters factored into the survival times observed in the two groups (Figure 4.2). All parameters showed similar

ranges in both Sham and VNS rats at baseline, and did not contribute significantly to different observed in survival.

To better understand possible factors contributing to the prolonged survival of VNS rats, we further evaluated the effects of VNS therapy on (1) chronic disease progression, (2) autonomic tone, and (3) structural properties of the heart.

4.4.3 Impact of Chronic, Cyclic VNS on HTN Progression

HTN progression in the Sham and VNS rats was quantified by the relative change in SBP (ΔSBP) and HR (ΔHR) over time with respect to baseline values during the Day_{12h} and $Night_{12h}$ intervals. Figure 4.3A and 4.3B (left panels) shows that the progressive increase of ΔSBP due to HTN is attenuated in the VNS rats compared to the Sham rats, as is suggested by the growing separation in the ΔSBP curves over time. Indeed, the linear regression slopes in the Sham rats are significantly larger when compared to VNS rats during both the Day_{12h} (Sham: 14.6 ± 2.0 mmHg/week; VNS: 9.2 ± 2.3 mmHg/week; $P < 0.05$) and $Night_{12h}$ (Sham: 14.6 ± 1.7 mmHg/week; VNS: 8.8 ± 1.4 mmHg/week; $P < 0.05$) intervals.

The circadian rhythm was evaluated at Week 6 and Week 9 (Figure 4.3C and 4.3D, respectively). While similar circadian rhythm characteristic were observed for both Sham and VNS rats at Week 6, three weeks of VNS therapy resulted in a significantly increased average baseline (*MESOR*) value in Sham rats in comparison to the VNS rats (see * in Figure 4.3D), providing further evidence of an attenuation in the rise in SBP due to VNS.

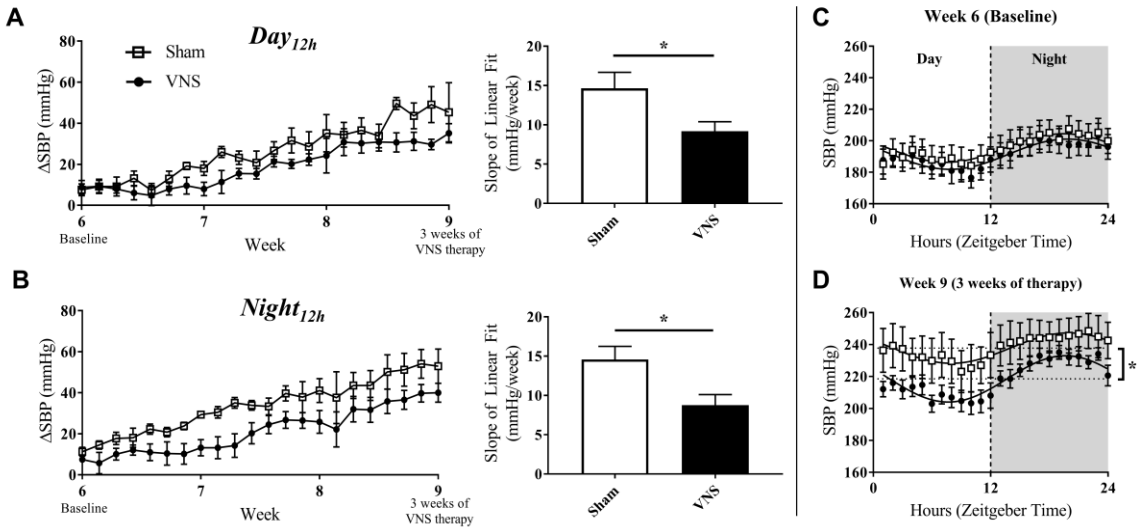

Figure 4.3 Relative changes in SBP (ΔSBP) as HTN progresses. ΔSBP as a function of time and slopes of the linear regressions are shown for Sham and VNS rats during the (A) Day_{12h} and (B) $Night_{12h}$ intervals. Circadian rhythm of SBP for Sham and VNS rats are shown for Week 6 (C) and Week 9 (D). * indicates statistical significance between Sham and VNS rats.

Longitudinal analyses were performed on additional BP measures including MAP, DBP, and PP, which are shown in Figures 4.4-4.6. The disease progression of MAP, shown in Figure 4.4 panel A and B for Day_{12h} and $Night_{12h}$ intervals respectively, shows an attenuation in ΔMAP for VNS rats in comparison to Sham rats. This attenuation, quantified by the slope of the linear regression, is significant during the $Night_{12h}$ interval (Sham: 13.1 ± 1.6 mmHg/week; VNS: 8.5 ± 1.1 mmHg/week; $P < 0.05$) but not the Day_{12h} interval (Sham: 13.7 ± 1.7 mmHg/week; VNS: 9.2 ± 1.1 mmHg/week; $P = 0.1029$). Circadian rhythm analysis at Week 6 and Week 9 are shown in panels C and D. There are no differences in circadian characteristics at baseline. However, after three weeks of therapy, there is a significant separation in the MESOR value, with Sham rats having a significantly higher MAP MESOR value than the VNS rats.

The progression of DBP from Week 6 to Week 9 during Day_{12h} and $Night_{12h}$ are shown in Figure 4.5, panel A and B. Although there is a separation in the ΔDBP, it is not significantly different between Sham and VNS rats during either the Day_{12h} or $Night_{12h}$ interval. The results of the circadian rhythm analysis are shown in panels C and D for Week 6 and Week 9 respectively. Again, there were no significantly differences in the circadian rhythm characteristics at baseline, and after three weeks of therapy there was a significant difference in the MESOR values between the Sham and VNS rats. The Sham rats had a significantly larger DBP MESOR value.

Figure 4.6 shows the progression of PP in the Sham and VNS rats over the first three weeks of

therapy. ΔPP showed similar results, with no significant differences in ΔPP between groups during either the Day_{12h} or $Night_{12h}$ interval. In addition, the circadian rhythm analysis produced similar results with no differences observed at Week 6 and a significant increase in the PP MESOR value for Sham rats compared to VNS rats at Week 9.

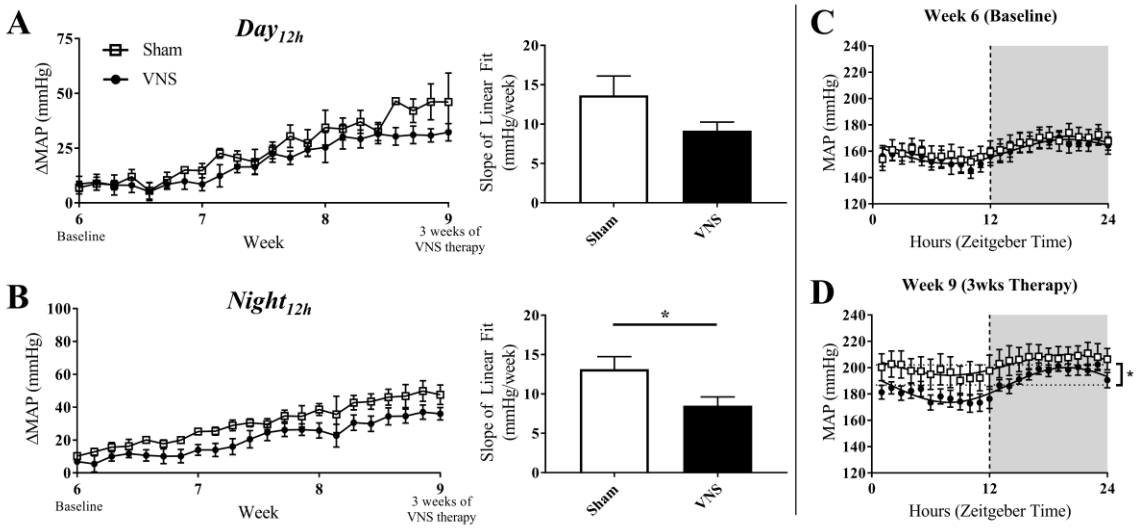

Figure 4.4 Relative changes in MAP (ΔMAP) as HTN progresses. ΔMAP as a function of time and slopes of the linear regressions are shown for Sham and VNS rats during the (A) Day_{12h} and (B) $Night_{12h}$ intervals. Circadian rhythm of SBP for Sham and VNS rats are shown for Week 6 (C) and Week 9 (D). * indicates statistical significance between Sham and VNS rats.

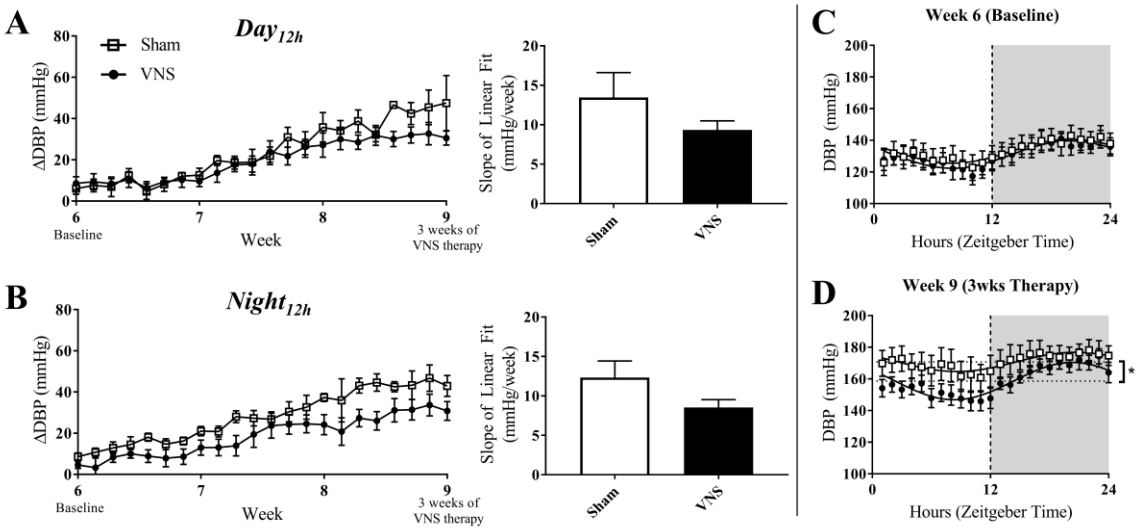

Figure 4.5 Relative changes in DBP (ΔDBP) as HTN progresses. ΔDBP as a function of time and slopes of the linear regressions are shown for Sham and VNS rats during the (A) Day_{12h} and (B)

$Night_{12h}$ intervals. Circadian rhythm of SBP for Sham and VNS rats are shown for Week 6 (C) and Week 9 (D). * indicates statistical significance between Sham and VNS rats.

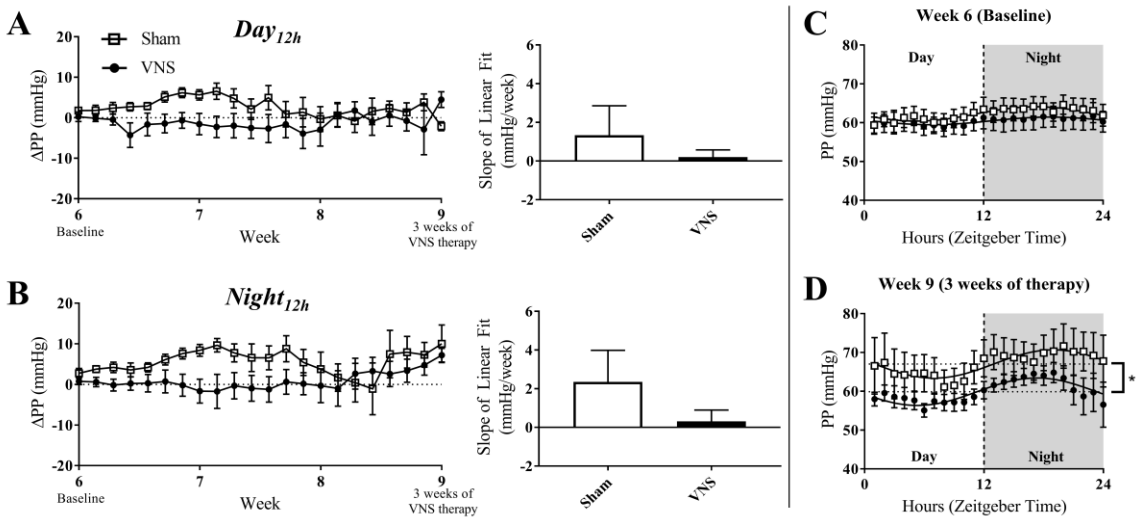

Figure 4.6 Relative changes in PP (ΔPP) as HTN progresses. ΔPP as a function of time and slopes of the linear regressions are shown for Sham and VNS rats during the (A) Day_{12h} and (B) $Night_{12h}$ intervals. Circadian rhythm of SBP for Sham and VNS rats are shown for Week 6 (C) and Week 9 (D). * indicates statistical significance between Sham and VNS rats.

Figure 4.7A and 4.7B (left panel) quantifies the relative change in HR over time during the Day_{12h} and $Night_{12h}$ intervals in the Sham and VNS rats. The slopes of the ΔHR linear regression, although greater in Sham rats, were not significantly different during either interval (Figures 4.7A and 9B, right panel). Circadian rhythm of HR showed no difference between Sham and VNS rats at Week 6 (Figure 4.7C), but after three weeks of VNS therapy, the *MESOR* value for Sham rats was significantly higher compared to VNS rats (see * in Figure 4.7D).

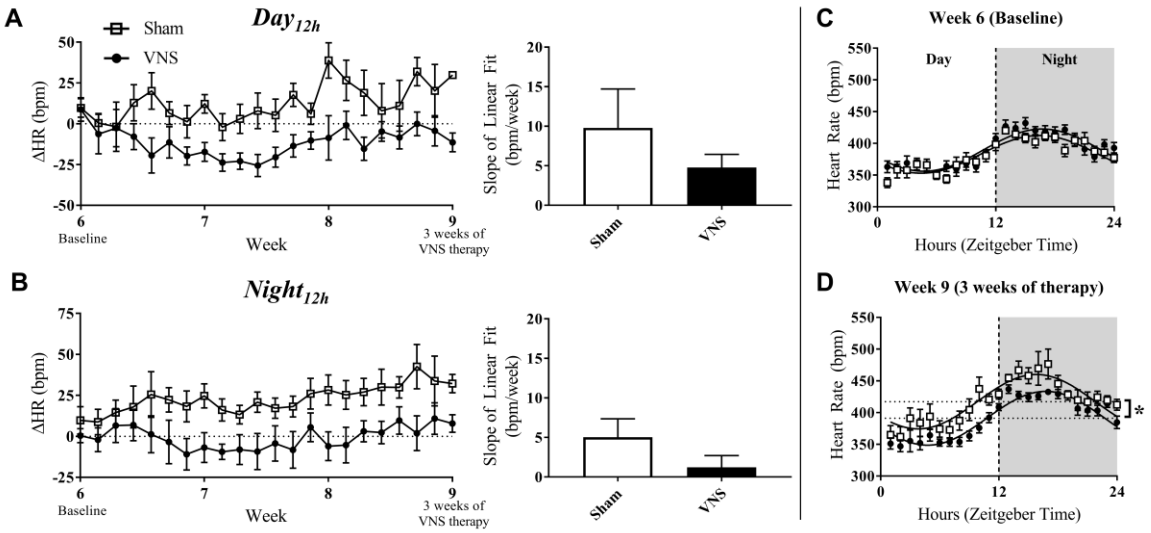

Figure 4.7 Relative changes in HR (ΔHR) as HTN progresses. ΔHR as a function of time and slopes of the linear regressions are shown for Sham and VNS rats during the (A) Day_{12h} interval and (B) $Night_{12h}$ intervals. Circadian rhythm analysis of HR for Sham and VNS rats are shown for Week 6 (C) and Week 9 (D). * indicates statistical significance between Sham and VNS rats.

4.4.4 Impact of VNS on Autonomic Regulatory Function

The effects of VNS on autonomic tone were evaluated through HRV and BRS measures and are presented in Figure 4.8. The relative change in HRV during Day_{12h} and $Night_{12h}$ intervals are shown for Sham and VNS rats in Figure 4.8A and 4.8B respectively. The results show that VNS significantly affects the dynamics of HRV over time. Specifically, ΔHRV was maintained or slightly increased in VNS rats as opposed to the Sham rats, which experienced negative ΔHRV as HTN progressed. Indeed, the slopes of the ΔHRV linear regression were significantly decreased over three weeks of therapy for Sham (Day_{12h}: -1.5 ± 0.3%; $Night_{12h}$: -0.8 ± 0.3 %) but not for VNS rats, where ΔHRV remained relatively stable over time (Day_{12h}: 0.01 ± 0.3%; $Night_{12h}$: 0.1 ± 0.2%). Finally, Figure 4.8C and 4.8D shows BRS values measured weekly from Week 6 to Week 9, showing significantly increased BRS values in VNS rats compared with Sham rats at Week 7 during both Day_{4h} and $Night_{4h}$ and at Week 8 during the $Night_{4h}$ interval. This acute increase in BRS for VNS treated rats was not present at Week 9, where BRS values were similar between VNS and Sham rats.

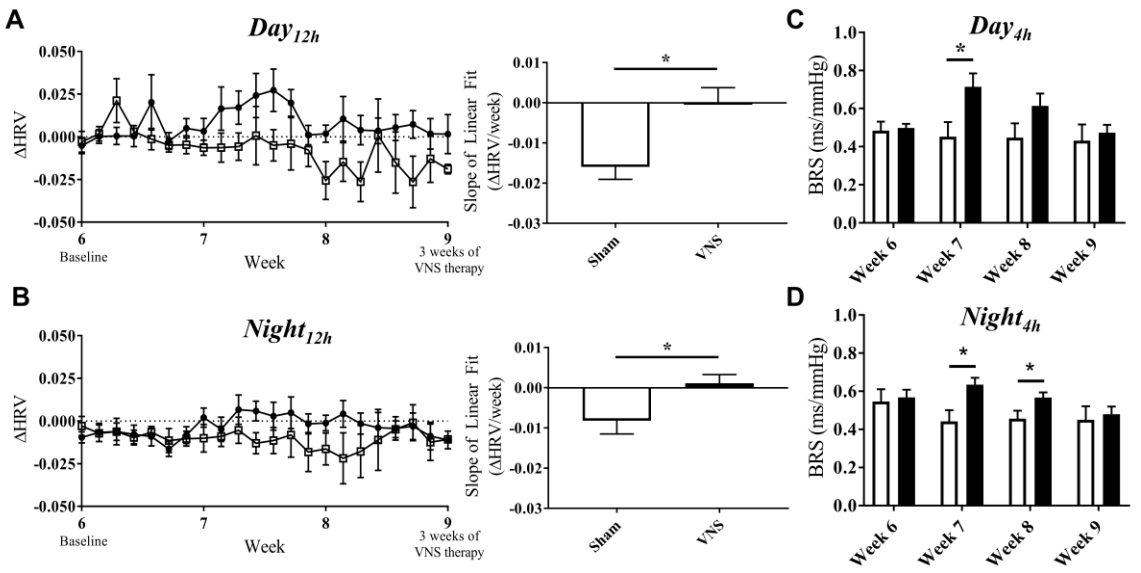

Figure 4.8 Relative changes in HRV (ΔHRV) as HTN progresses. ΔHRV as a function of time and slopes of the linear regressions are shown for Sham and VNS rats during the (A) Day_{12h} interval and (B) $Night_{12h}$ intervals. BRS was quantified during the Day_{4h} (C) and $Night_{4h}$ (D) intervals for Week 6 through Week 9. * indicates statistical significance between Sham and VNS rats.

4.4.5 Impact of VNS on Structural Changes in the Hypertensive Heart

The results of the gross morphology and histology studies are shown in Figure 4.9 as a function of survival along with the corresponding linear regression from Sham and VNS rats. Examples of stained cardiac cross-sections for Sham and VNS rats are shown in Figure 4.10. Figure 4.9A shows the relationship of HW/TL over time, which was significantly different between groups. Sham rats had a decrease in HW/TL (-0.0027 ± 0.0019 g/cm/day) while VNS rats exhibited an increase in HW/TL as a function of survival time (0.0038 ± 0.0013 g/cm/day; $P < 0.05$). In addition, HW/diameter (Figure 4.9B) showed a similar result with Sham rats having a decrease in HW/diameter over time (-0.0024 ± 0.0006 g/cm/day), while VNS rats showing an increase over time (0.0001 ± 0.0006 g/cm/day; $P < 0.05$). Although changes were observed in HW, individual thickness measures of the RV and LV free wall as well as septum showed no significant differences between treatment groups (Figure 4.9D-F). In addition, no changes were seen in diameter or body weight between Sham and VNS rats as a function of survival (Figure 4.10). Finally, chronic VNS therapy resulted in no changes in the percent of fibrosis in the cardiac cross-sections as seen in Figure 4.9C.

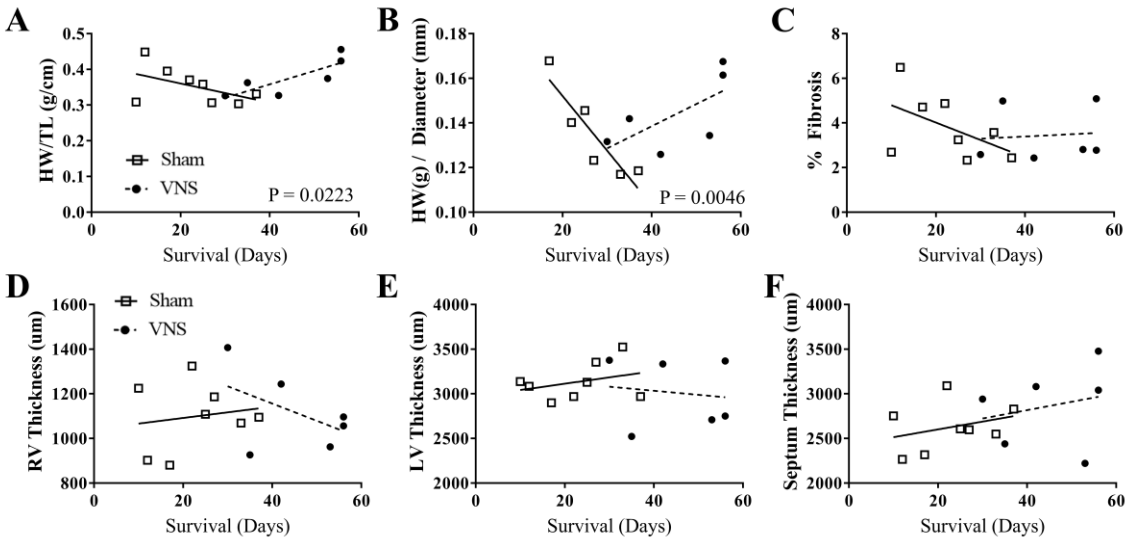

Figure 4.9 Gross morphology and histology studies. The effects of VNS on cardiac structural properties – (A) HW/TL, (B) HW/diameter, (C) percent fibrosis, (D) right ventricle (RV) and (E) left ventricle (LV) free wall thickness and (F) septum thickness – as a function of survival rate along with corresponding linear regression fits.

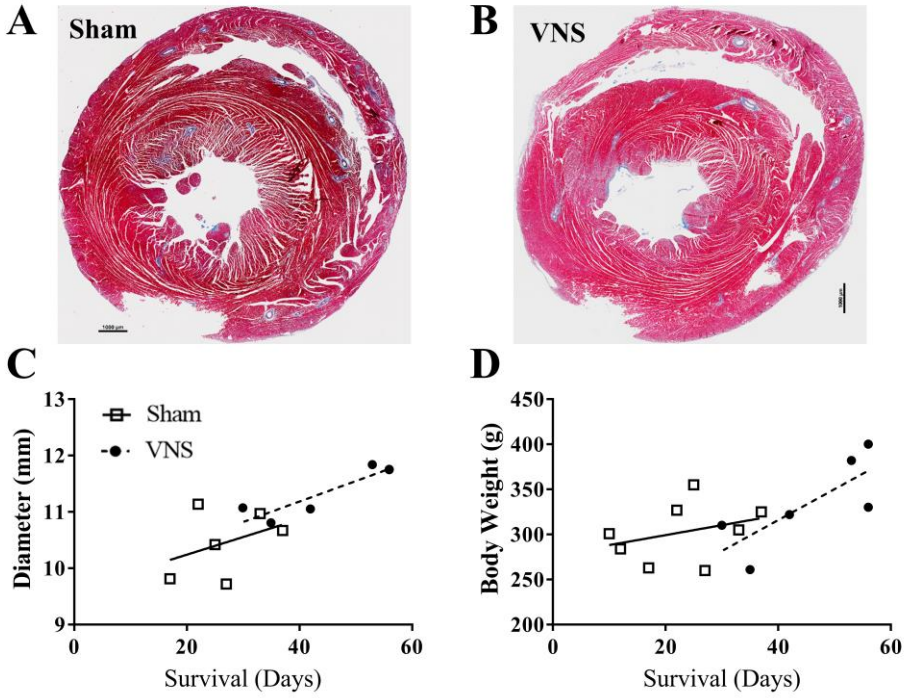

Figure 4.10 Examples of the cardiac cross sections from the Sham (A) and VNS (B) hearts stained with Masson's Trichrome. The cardiac fibrosis can be seen in blue around the vessels and within the interstitial space. (C) Cross section diameter and (D) body weight as a function of survival times with corresponding linear regressions for Sham and VNS rats.

4.5 DISCUSSION

The major finding of this study was a significant improvement in the long-term survival of hypertensive rats treated with VNS therapy, with median event-free survival increasing by 78% for VNS rats in comparison to Sham rats. This study further evaluated the effects of VNS various cardiovascular, hemodynamic, and structural cardiac properties that may contribute to prolonged survival of VNS rats with respect to Sham rats. Our results can be summarized as follows: (1) chronic VNS slowed the progression of HTN through and an attenuation in the rise of SBP, demonstrated in the linear regression analysis during the day and night intervals and the *MESOR* shift in circadian rhythm, (2) chronic VNS preserved autonomic balance as HTN progressed by maintaining elevated HRV and BRS measures in the VNS rats compared to Sham rats, and (3) VNS significantly altered cardiac structure increasing heart weight, but did not alter the amount of fibrosis in the hypertensive hearts.

4.5.1 Chronic Disease Progression

VNS therapy has been demonstrated to have beneficial long-term effects in hypertensive animal models. Our previous chronic study demonstrated the impact of low-level intermittent VNS on BP through a long-term effect resulting in a reduction in the spontaneous rise in BP after 4 weeks of therapy in hypertensive rats [159]. Here, a significant attenuation was observed after just three weeks of VNS therapy. This attenuation in rising SBP by Week 9 may play a role in the delay in the onset of adverse events in hypertensive rats.

The characteristics of BP control in Sham and VNS rats were further evaluated using cosinor analysis to compare circadian rhythms in SBP and HR, which are mediated by cyclic variations in autonomic activity [163]. Although there was a significant increase in the *MESOR* value for Sham in both HR and SBP, the amplitude and acrophase of the cosinor parameters were not significantly different. In addition, this abnormality in circadian rhythm is associated with an increased risk of cardiovascular risk and target organ injury [164]. Through stimulation of the parasympathetic nervous system, VNS may help maintain regular cyclic BP control.

4.5.2 Autonomic Regulatory Function

HRV is commonly used in clinical practice as a prognostic indicator of cardiovascular

conditions. In the case of HTN and heart failure (HF), autonomic dysfunction results in decreased HRV. It is postulated that stimulation of the parasympathetic nervous system, through right cervical VNS, has the potential to rebalance the autonomic nervous system (ANS) by direct increasing parasympathetic activity and reflexively reducing sympathetic activity. Indirect measures of autonomic balance, such as HRV and BRS, have been assessed in numerous studies showing a restoration of autonomic balance and improved prognostic indications for the VNS-treated group.[69, 165] Here, we demonstrate results consistent with those previously seen. VNS preserved HRV values from Week 6 through Week 9, while Sham rats experienced a large reduction in HRV during both the day and night intervals. Our results also showed an acute increase in BRS for several weeks, indicating improved BP and HR control. In HTN, chronic structural changes in the heart and vasculature alter the function of the arterial baroreceptors decreasing their sensitivity to fluctuations in BP, ultimately decreasing BRS [166]. Overall, the beneficial effects on HRV and BRS in the VNS rats may be mediated through balancing autonomic activation and altering structural changes in vasculature, which may ultimately contribute to the prolonged survival in VNS rats.

4.5.3 Structural Cardiac Effects

Our results demonstrate that VNS had a significant impact on hypertrophy with increased HW as survival times increased in hypertensive rats. In addition, opposite trends in LV and RV free wall thicknesses were observed, with VNS showing a reduction over time. However there is no change in the amount of fibrosis between Sham and VNS rats. Although, without sufficient overlap of Sham and VNS data at early and late time points in the survival curve, assessing the progression of structural changes in the treated and untreated heart is challenging. In addition, the increased survival of VNS rats means these rats were older and exposure to high-salt diet for a longer duration at the time the hearts were analyzed, which may influence the results observed in this study.

VNS may be altering the progression of cardiac remodeling in response to increasing BP levels. Previously, DSS rats have been shown to advance to later stages of HTN rapidly while on 8% NaCl with significant hypertrophy and LV dilation as early as 11 and 15 weeks of age, respectively [167]. With respect to our experimental design, those time points correspond to Week 6 and Week 10. VNS therapy may delay or alter the time course of HHD in these rats. Another important factor to consider is the advanced-stage of HTN in the rats in this study. Nguyen et al. demonstrated that even in the early stages of HTN, the heart undergoes structural and electrical remodeling [168]. The rats in this study had well established HTN at the beginning of VNS therapy and were

continued on a high salt diet for the remainder of the study. Intervening in the earlier stages of HTN may provide restorative or preventative structural cardiac effects. Further studies are necessary to fully understand the effects of VNS therapy on HHD in various stages of HTN.

Numerous other mechanism of VNS therapy have been evaluated in HTN and cardiovascular disease models which could be contributing to the improved survival, attenuation in the spontaneous rise in BP, and improved autonomic tone observed in this study. Additional mechanisms through which VNS has been hypothesized to provide therapeutic effects include anti-adrenergic effects, anti-inflammatory pathways, activation of nitric oxide release in the heart, and inhibition of the renin-angiotensin system. Suppressing central sympathetic outflow through activation of vagal nerve afferent fibers can lead to a reduction in sympathetic nervous system activity, resulting in reductions in HR, vascular resistance, and arterial BP. Several studies have demonstrated the ability of VNS to reduce systemic inflammation through the activation of the cholinergic anti-inflammatory pathway, reducing cytokine synthesis and the inflammatory response [69, 108]. Inflammation is associated with HTN, although the cause-and-effect relationship still remains unclear. It is hypothesized that inflammation can lead to endothelial dysfunction and increased oxidative stress, which promote the development and progression of HTN [107]. VNS has also been shown to directly activate the nitric oxide pathway producing nitric oxide in the ventricles, altering cardiac electrophysiology and decreasing arrhythmia susceptibility [101]. Another proposed mechanism of VNS is inhibition of the renin-angiotensin system through afferent vagal nerves, resulting in a reduction in renin in the kidneys and marked reduction in plasm angiotensin II levels [69, 114].

4.5.4 Limitations

This study has several limitations. First, there were nine and eight rats in the VNS and Sham groups, respectively, and they were in advanced stages of HTN by Week 6 when therapy was initiated for VNS rats. Further studies need to be conducted to evaluate the effects of VNS therapy in various stages of HTN to investigate the preventative and restorative potential of VNS in controlling BP and addressing adverse cardiovascular effects associated with HTN. Second, acute effects and autonomic evaluation through BRS measures was limited to four-hour data segments during day and night intervals. Future work will include quantifying these parameters over larger data segments to better understand the progression due to HTN as well as changes due to variation in autonomic tone based on time of day. In addition, the high salt diet (8% NaCl) produced an aggressive cardiovascular insult that resulted in the death of all Sham rats; further studies are

needed to evaluate the effects of slightly lower salt diet (e.g. 4%).

4.6 Conclusion

Overall, our results are consistent with previous studies that show potential for VNS to provide therapy for HTN and HTN-induced heart disease. This study shows a strong beneficial effect of VNS therapy on long-term survival, BP control, and autonomic tone. These results motivate additional studies to investigate the mechanism of VNS in treating HTN and determine optimal stimulation parameters for therapeutic effects.

Chapter 5

Acute cardiovascular and hemodynamic effects of vagus nerve stimulation in conscious hypertensive rats

5.1 Introduction

In this chapter I present the methods and result for evaluating the acute effects of vagus nerve stimulation (VNS) in hypertensive rats over the course of chronic therapy to evaluate two main questions: (1) what happens acutely in response to VNS and (2) does this effect persist over the course of therapy in our chronic study.

Several researchers have evaluated acute effects of VNS quantifying hemodynamic, autonomic, and inflammatory responses in various animal models. Specifically, acute VNS was shown to have anti-inflammatory effects and result in a significant reduction in heart rate (HR) in rats with pulmonary arterial hypertension (HTN) [169]. In addition, VNS has been demonstrated to reduce blood pressure (BP) acutely when targeting the aortic depressor nerve within the vagus nerve [62, 63]. However, the majority of studies were conducted with continuous VNS while the animal was under anesthesia. These experimental conditions raise two fundamental questions: (1) are the effects of VNS different when applied continuously versus intermittently, and (2) what are effects anesthesia and cold the effect of VNS either be diminished or exaggerated?

5.2 Aim

The aim of this study is to better understand the acute effects of low-level intermittent VNS in hypertensive rats through evaluation of cardiovascular and hemodynamic response while the rat is conscious. Here, changes in mean and variability measures of BP and HR are quantified to better understand physiological changes by acute activation of the vagus nerve.

5.3 Methods

All experiments were approved by the University of Minnesota Animal Care and Use Committee and were conducted in accordance with Institutional and NIH guidelines (NIH publication No. 85-23, revised 1996).

5.3.1 Experimental Model

HTN was induced in Dahl salt-sensitive (DSS) rats (n = 6, 5 weeks old, male) using high salt 8% NaCl diet (S10001, Research Diets, Inc., New Brunswick, NJ, USA), which was maintained for the entire duration of the study. After 5 weeks of high salt diet, the rats underwent surgery to implant physiological telemeters (HD-S11, Data Sciences Inc. (DSI)) and vagal nerve stimulators (Model 103, Cyberonics Inc.) as described previously [159]. Briefly, the telemetry device was placed in the abdomen of the rat with a pressure catheter inserted into the left femoral artery for continuous BP monitoring and two leads were placed subdermally on the chest wall of the rat for continuous ECG monitoring. The VNS stimulator was placed under the skin on the back of the rat, and a lead connected to the pulse generator was implanted through a midline incision on the neck. The bipolar cuff electrodes were then placed around the right cervical vagus nerve and carotid bundle. The rats were given at least one week to recover prior to the start of VNS therapy.

5.3.2 Vagus Nerve Stimulation

The low-level VNS was applied intermittently with a pulse frequency of 20 Hz, a pulse width of 500 us, and with an "On" and "Off" time of 14 and 66 seconds respectively. Each stimulation period has a 2-second ramp up and ramp down interval, which are added to the "On" period resulting in a 22.5% duty cycle (Figure 1, top panel). The amplitude of the VNS stimulation was set individually for each rats to influence HR by no more than 10%, resulting in current values of 0.25-0.75 mA. Rats were individually housed and free to move about their cages while being continuously monitored for the remainder of the study.

5.3.3 Data Analysis

BP and ECG traces were collected at a sampling rate of 500 Hz. Four-hour data segments were acquired for day (10am-2pm) and night (10pm-2am) intervals for each rat at Week 6 (Day 1 of VNS therapy), Week 9 (after 3 weeks of therapy), and Week 12 (after 6 weeks of therapy). Data was segmented into the following windows: "Pre," "VNS On," "Post 1," and "Post 2" (Figure 5.1). "Pre" was defined as the 7-second segment prior to VNS therapy. "VNS On" was defined as the 14 seconds during which VNS was applied, excluding the 2-second ramp up and ramp down intervals. "Post 1" and "Post 2" were defined as two consecutive 7-second segments immediately after VNS. For each data segment, the following values were calculated: systolic blood pressure (SBP), blood pressure

variability (BPV), HR and heart rate variability (HRV), and contractility, which was determined as the maximum slope of the derivative of the BP waveform (dP/dt_{max}). BPV was calculated as

$$BPV = \sigma_{BP} / BP,$$

where σ_{BP} and BP are the standard deviation and mean of the BP data, respectively, and BP was measured as the systolic BP peak value. HRV was calculated as

$$HRV = \sigma_{HR} / HR,$$

where σ_{HR} and HR are the standard deviation and mean of the HR data, respectively. Due to the noisy nature of the 2-lead ECG data, HR was derived using pulse interval calculated from the BP trace, as described in [170]. Data are presented as percent change relative to the "Pre" stimulation interval. All data analysis was performed using custom MATLAB code.

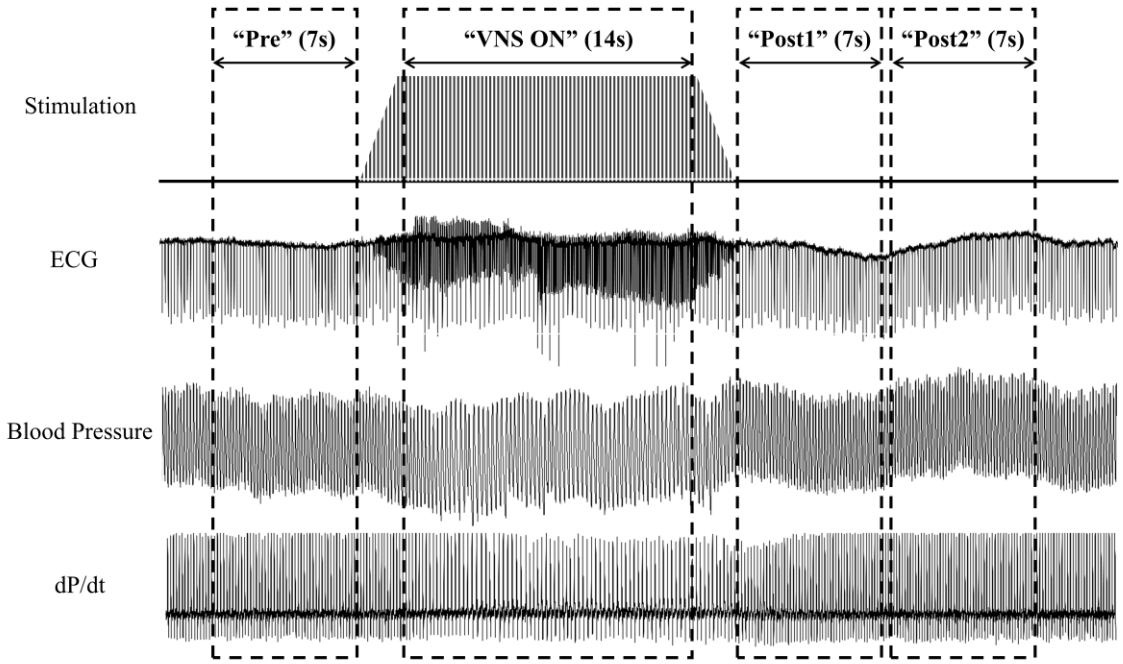

Figure 5.1 An example of the data segmentation into "Pre", "VNS On", "Post 1" and "Post 2" intervals for one episode of VNS in the rat. The top panel is the representative stimulation including the ramp up and ramp down periods. The second panel shows the recorded ECG trace with VNS artifacts visible during the "VNS On" segment. The third and fourth panels show the corresponding BP and BP derivative (dP/dt) traces, respectively.

5.3.4 Statistical Analysis

One-way ANOVA was used to compare values at each segment ("Pre," VNS On," "Post 1," and "Post 2"). Post hoc analysis was performed with Tukey's multiple comparison correction. Significance was determined at $P < 0.05$.

5.4 RESULTS

The custom MATLAB program was developed to analyze ECG and BP data traces for approximately 400 VNS episodes per rat (Figure 5.1) Day and night intervals were combined together to obtain average values for all measured parameters.

5.4.1 Week 6 Acute VNS Response

Mean HR derived from the BP waveform was calculated for each interval during Day 1 of VNS therapy and showed no significant changes before, during, or after VNS therapy (Figure 5.2). However, VNS significantly increased HRV during the "VNS On" interval when compared to the "Pre" interval. Nevertheless, the HRV decreased back to baseline levels immediately after VNS was turned off, so that both HRV during "Post 1" and "Post 2" have similar values as during the "Pre" interval (Figure 5.2B). Similarly, the mean SBP response of the VNS rats showed no significant changes before, during and after VNS therapy (Figure 5.2D). However, there was a significant increase in BPV during the "VNS On" period, which returned to "Pre" values immediately after VNS therapy is turned off (Figure 5.2E).

Contractility was assessed by quantifying the maximum rate of change of the pressure waveform (dP/dt_{max}). With increased vagus activity, contractility is known to decrease. However, during low-level VNS therapy in our study, no significant acute changes (less than 1% change) were observed in the intervals analyzed. Figure 5.2C shows no change in dP/dt_{max} during any intervals surrounding episodes of VNS therapy.

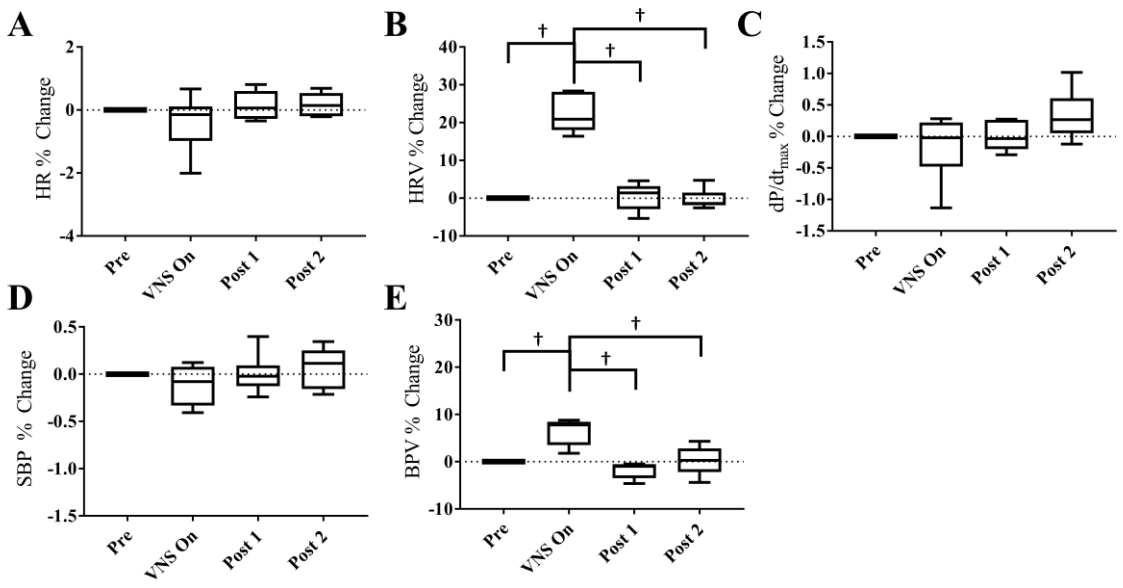

Figure 5.2 Acute (A) HR, (B) HRV, (C) Contractility (dP/dt_{max}), (D) SBP, and (E) BPV responses during VNS therapy in hypertensive rats (n = 6) for "Pre", "VNS On", "Post 1" and "Post 2" intervals at Week 6, the first day of VNS therapy. † indicates statistical significance in mean values between intervals

5.4.2 Week 9 Acute VNS Response

Figure 5.3 shows the percent change in HR, HRV, contractility, SBP, and BRS with respect to the "Pre" interval values. Both SBP and contractility slightly decrease during the "VNS On" interval, which is significantly lower with respect to the "Post 2" interval where a slight overshoot from pre-stimulation values was observed. In contrast, HRV and BPV were significantly increased during "VNS On" with respect to both pre- and post-stimulation values, and immediately returned to pre-stimulation values after the cessation of therapy. However, HR was not significantly affected by the low-level VNS therapy.

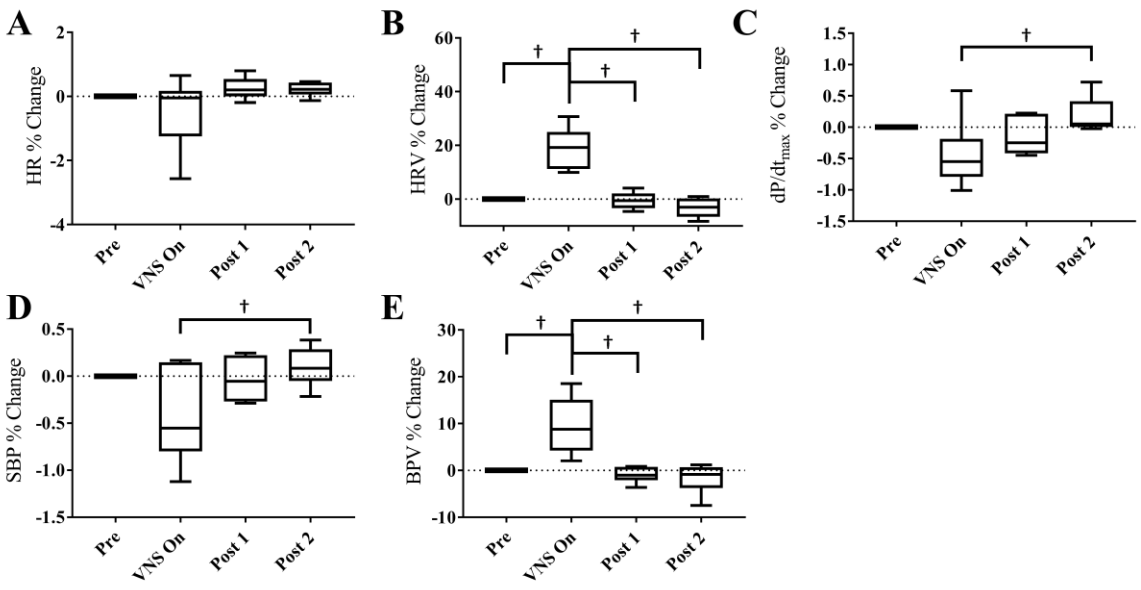

Figure 5.3 Acute (A) HR, (B) HRV, (C) Contractility (dP/dt_{max}), (D) SBP, and (E) BPV responses during VNS therapy in hypertensive rats (n = 6) for "Pre", "VNS On", "Post 1" and "Post 2" intervals at Week 9, after 3 weeks of VNS therapy. † indicates statistical significance in mean values between intervals.

5.4.3 Week 12 Acute VNS Response

At Week 12, the remaining VNS rats were evaluated for their acute cardiovascular and hemodynamic response to stimulation (Figure 5.4). No significant differences were observed in SBP, BPV, HR, or contractility values. However, HRV demonstrated a similar response to Week 6 and 9, with a significant increase in HRV during "VNS On" in comparison to the "Post 2" interval.

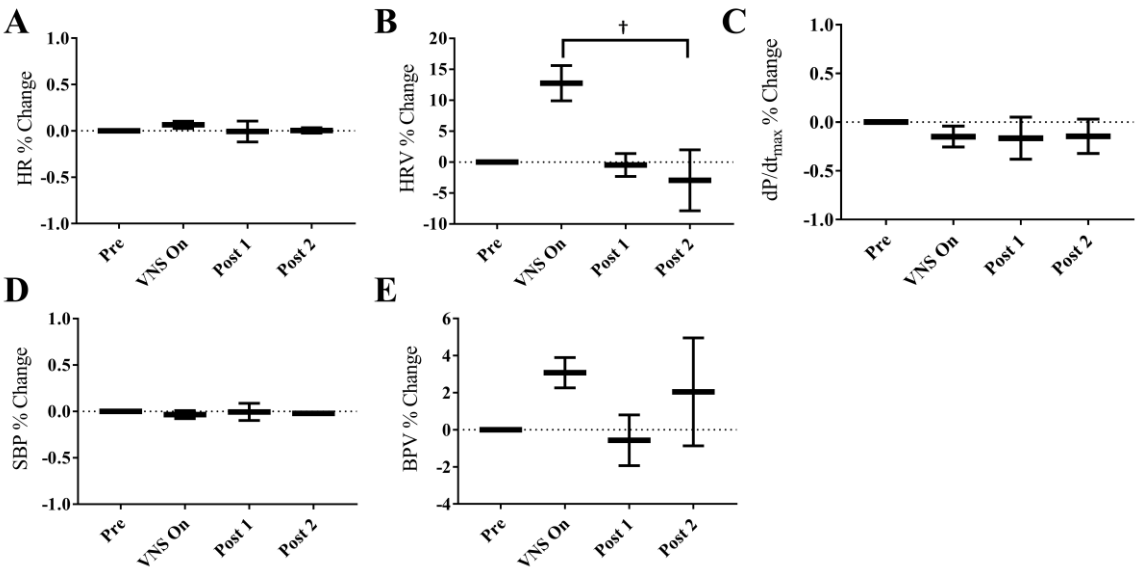

Figure 5.4 Acute (A) HR, (B) HRV, (C) Contractility (dP/dt_{max}), (D) SBP, and (E) BPV responses during VNS therapy in hypertensive rats (n = 2) for "Pre", "VNS On", "Post 1" and "Post 2" intervals at Week 12, after 6 weeks of VNS therapy. † indicates statistical significance in mean values between intervals.

5.5 DISCUSSION

This study evaluated the acute effects of low-level, intermittent VNS in conscious hypertensive rats. The major finding of this paper were the following: (1) no significant acute changes in HR were induced during the "VNS On" period, when compared to the "Pre" and "Post" intervals, (2) SBP and contractility were both significantly reduced during VNS compared to the "Post 2" interval only at Week 9, and (3) both HRV and BPV were significantly increased acutely during the "VNS On" period.

5.5.1 The Effect of VNS on Mean Cardiovascular and Hemodynamic Responses

During VNS, there were no significant acute changes in HR in the hypertensive rats. Indeed, in this study we used low-level VNS therapy that intentionally does not drastically alter either HR or BP. This effect can be controlled through the selection of stimulation parameters. Specifically, varying the amplitude has been shown to induce significantly different acute cardiovascular responses [58, 171]. The stimulation settings and subsequent effects depend on the goal of the therapy. Here, VNS was initially titrated to cause no more than a 10% drop in HR during day time stimulation to provide low-level therapy while reducing side effects. Therefore, the short therapy

duration in combination with the low-level stimulation likely led to no significant changes in mean HR during acute episodes of VNS therapy.

VNS only caused small changes in SBP during Week 9 (between "VNS On" and "Post 2" intervals), but otherwise caused no changes at Week 6 or Week 12. Previously, several studies have shown an acute decrease in BP du rot selective VNS therapy in anesthetized rats, which was accompanied by a reduction in mean HR [62, 63]. This reduction was smaller when applying non-selective VNS using the same stimulation parameters [62]. Here, intermittent VNS stimulation is applied non-selectively at a low level with a 22.5% duty cycle. Such a short therapy duration and low amplitude may not have time to elicit a significant change in the SBP measures with respect to pre-stimulation levels before stimulation is turned off. Also, in previous studies, the acute effects of VNS on SBP and HR have been demonstrated in healthy rats [61-63], while here, we have evaluated the effect of acute VNS in hypertensive rats. HTN has been associated with an imbalance in the autonomic nervous system (ANS) with increased sympathetic nerve activity and a decrease in parasympathetic nerve activity [7]. This imbalance in the ANS could lead to a different response to acute stimulation, which may require higher amplitude or longer duration for stimulation to elicit a response in the altered autonomic state.

5.5.2 The Effect of VNS on Variability in Cardiovascular and Hemodynamic Responses

The results of the acute stimulation show a strong positive effect on HRV. HRV is a common prognostic indicator used in the clinic to evaluate the cardiac condition of patients. In disease states, such as HTN and heart failure, the overactive sympathetic nervous system reduces the autonomic control of cardiac function, decreasing HRV. Increases in HRV indicate better autonomic balance, through either a suppression of the sympathetic activity or activation of the parasympathetic activity, and can be indicative of therapeutic efficacy. The acute changes in HRV observed here could have an additive effect, contributing to the long term beneficial effects of VNS therapy.

In addition to changes in HRV, acute changes in BPV were also observed in the hypertensive rats. Traditionally in the clinic, increases in BPV are associated with increased risk [172]. However, this effect on BPV observed here has been shown before, with variability in BP occurring in response to HRV induced through vagal activation [173]. This response observed in this study, returns to baseline values at the cessation of therapy.

5.5.3 The Effect of VNS on Contractility

The results show a small but significant change in contractility during stimulation. However, this effect is only observed at Week 9 in conjunction with the decrease in SBP. Week 6 and Week 12 measures had no differences in contractility between intervals. It is commonly known that enhanced parasympathetic activity has a negative inotropic effect on the heart. This effect has been recently demonstrated using various VNS parameters applied for 30 seconds in anesthetized sheep [171]. There are several key differences however that can explain this difference observed in this study including the species, disease state, and duration of stimulation. Short VNS duration in our study may result in a smaller cumulative effect on the contractility of the heart in the conscious hypertensive rats. Increasing duration or amplitude of stimulation may result in a measurable change in contractility along with changes in other cardiac parameters including HR.

5.5.4 The Effect of VNS over Time

VNS continued to show a strong acute effect on HRV even after three weeks of therapy, increasing HRV as stimulation was applied. In addition to changes in HRV, BPV was also significantly increased, but to a lesser extent. This result has been observed previously as BPV reflexively increases acutely in response to vagal activation [173, 174]. The acute change in HRV is evident of enhance parasympathetic activity or decreased sympathetic activity, and may contribute to chronic therapeutic effects of VNS. This effect on HRV was even seen at Week 12 indicating that VNS therapy still elicits the same cardiovascular response and suggests therapy remains efficacious even after six weeks.

5.5.5 Limitations

There are several limitations for the current data analysis. First, only 4-hour day and night segments were analyzed from each of the VNS-treated rats. Larger data segments may give more information about the acute changes and whether time of day and related autonomic balance affects the acute cardiovascular and hemodynamic response to VNS. Second, this study only evaluates the acute response to one set of VNS parameters. Future studies will investigate the effects of various intermittent VNS parameters on the cardiovascular and hemodynamic responses. Finally, further evaluation of HRV using spectral analyses can provide indication so sympathetic and parasympathetic tone.

5.6 CONCLUSION

Quantifying acute cardiovascular and hemodynamic changes due to VNS in conscious animals can help provide a better understanding of VNS therapy and physiological responses to acute parasympathetic activation. The small acute changes observed during intermittent VNS could be additive, leading to beneficial chronic changes in BP and HR control [159]. Evaluating the acute effects can help further the understanding of VNS in its application as a chronic therapy and assist in parameter selection and optimization for providing beneficial effects for treating HTN.

Chapter 6

Part 1 Conclusions

6.1 Conclusions

Hypertension (HTN) is an extremely prevalent condition which now affects almost half of the adults in the United States. Further, with the aging population, the number of patients with HTN is expected to continue to rise. Although numerous treatment options exist, including antihypertensive medications, there are still an alarming number of patients, approximately half of all hypertensive patients, who do not achieve target blood pressure (BP) levels and as a result face increased risk of cardiovascular disease (CVD) and end organ damage. Numerous clinical limitations contribute to this statistic including comorbidities, drug resistance, non-compliance, and intolerance. There is a significant clinical need to develop new therapies that can help overcome limitation associated with the current clinical approach to help improve patient outcomes.

The aim of Part 1 of this dissertation is to evaluate the potential of low-level, intermittent vagus nerve stimulation (VNS) applied to the right cervical vagus nerve to treat HTN and associated cardiovascular complications that can addresses limitations with current treatment approaches. Through direct activation of the parasympathetic nervous system, VNS provides a novel approach to target the imbalance in the autonomic nervous system (ANS), which is known to play a critical role in the pathogenesis of HTN. These studies investigated acute and chronic hemodynamic and cardiovascular responses of dahl salt-sensitive hypertensive rats treated with and without VNS therapy. Further, this dissertation aims to evaluate the electrophysiological and structural cardiac effects of VNS therapy.

The results of these studies demonstrate the potential for low-level, intermittent VNS to provide effective therapy for HTN and hypertension-induced heart disease (HHD). The initial chronic study evaluating the effects of four weeks of VNS therapy yielded promising results which led us to further evaluate VNS by extending therapy to quantify its impact on long-term survival. The results from both studies revealed numerous beneficial effects in hypertensive dahl salt-sensitive rats including improved long-term survival, blood pressure control, preserved autonomic tone, and beneficial electrophysiological cardiac remodeling.

VNS shows a progressive effect on BP resulting in a significant attenuation in the rise in spontaneous BP, suggesting chronic therapy is necessary to have a measurable effect. In addition, the impact observed on BP suggests a predominately afferent signaling driven effect modulating

the systemic balance of sympathetic and parasympathetic activity. The modulation of the ANS was demonstrated through both acute and chronic studies showing VNS acutely increasing heart rate variability (HRV) during stimulation, and confirmed through the preservation of HRV as HTN continued to progress in dahl salt-sensitive rats.

VNS therapy demonstrated cardioprotective effects in HHD. Beneficial results have been hypothesized to be due to a reduction in heart rate (HR), lowering the metabolic demand of the heart. Here, the low-level VNS therapy does not significantly alter HR, with initial stimulation titrated to affect the HR by no more than 10%. However, beneficial cardiac electrophysiological effects were still evident, consistent with the anti-arrhythmic effects previous demonstrated in other cardiovascular disease models. Specifically, VNS reduced action potential duration (APD), maximum slope of the APD restitution curve, APD spatial dispersion, and the complexity of ex-vivo induced ventricular arrhythmias. This suggests the role of both afferent and efferent stimulation in the cardioprotective effects demonstrated in this model.

Overall, VNS shows promise as a novel therapy for HTN and HHD that can address limitations associated with current treatment approaches. Specifically, VNS targets the imbalance in the ANS inherent in HTN and can possibly provide an effective alternative to patients with resistance HTN. In addition, as a device-based therapy, patients and physicians may have less concern with compliance. Therapy can also be titrated to limit or avoid undesirable side effects, with advances in therapy continuing to improve targeted stimulation. Finally, VNS provides a multifaceted therapy providing the primary effect of BP control, likely mediated through predominately afferent signaling, as well addressing secondary cardiovascular effects, mediated through a combination of afferent and efferent stimulation.

6.2 Future Work

The positive results demonstrated here motivate further evaluation of VNS as a therapy for HTN. Future studies include modifying the severity of HTN and the stage in which therapy is initiated. Lowering the percentage of the high salt diet fed to the dahl salt-sensitive rat will slow the progression HTN and allow for longer in-vivo evaluation of VNS on hemodynamic and cardiovascular parameters and its impact on the pathophysiology of HTN. Additional studies can be performed to investigate the impact of VNS therapy initiated at varying points in the disease. Specifically, can VNS initiated at lower BP levels when HTN is first established, prevent the rise in BP and subsequent cardiac remodeling? Conversely, can VNS therapy initiated at a later stage of

HTN, at a lower salt intake and thus slower progression, lead to a reversal in the rise in BP levels and reversal in adverse cardiac remodeling?

Additional studies are needed to determine the appropriate stimulation parameters and paradigms to optimize therapy for HTN and HHD. There are numerous variables that can be set for VNS therapy including current amplitude, pulse width, frequency, duty cycle, selective or non-selective, right- or left-sided stimulation, invasive or non-invasive, and stimulation site (i.e. the cervical or auricular branch). Across VNS research, disease states and stimulation parameters have widely varied, leading to variable results, which begs the question: which stimulation parameters are optimal for achieving the dual effect on BP and cardiovascular function? Acute and chronic studies are needed to expand on our knowledge and understanding of the mechanisms of VNS therapy. Acute studies can provide a means to evaluate a large parameters space to quantify hemodynamic and cardiovascular responses and can be then used to inform chronic studies evaluating efficacy of VNS in hypertensive models. Furthering our understanding of VNS parameters and associated mechanisms can help improve the efficacy of VNS therapy and tailor its application to specific disease states and individual patients.

Part 2

Investigating novel mapping techniques to identify rotors in cardiac arrhythmias

OBJECTIVE

The objective of Part 2 of my dissertation is to evaluate the accuracy and robustness of novel mapping techniques – multiscale frequency, kurtosis, Shannon entropy, and multiscale entropy – to identify regions of rotors and provide translation to clinical applications in intracardiac mapping. These techniques are validated using ex-vivo optical mapping studies where electrical activity can be directly visualized and clinical limitations such as shortened time series duration and reduced spatial resolution can be simulated. The ability of these novel techniques in identifying rotors to outperform a clinically available mapping approach, dominant frequency, is demonstrated using optical mapping movies of cardiac arrhythmias with stationary and meandering rotors. In addition, the consistent identification under simulated clinical limitations further highlights the potential for these techniques to be translated to clinical use where improved signal processing techniques can help further our understanding of the generation and maintenance of atrial fibrillation and ultimately improve ablation procedure success rates and terminate the arrhythmia.

Chapter 7

Background

7.1 Atrial Fibrillation

Atrial fibrillation (AF) is characterized by unorganized electrical activity in the atrium resulting in inefficient contractions and reduced cardiac output (Figure 7.1). AF is further categorized into patients with paroxysmal, persistent, and long-standing AF. Paroxysmal AF refers to episodes of AF that are able to terminate on their own, lasting less than seven days. In contrast, persistent AF persists for more than 7 days at a time and usually requires treatment to return to normal sinus rhythm. Long-standing AF is defined as AF occurring continuously for more than 12 months [175]. AF is the most common cardiac arrhythmia; with high incidence affecting between 2.7 and 6.1 million individuals in the United States alone and over 30 million people worldwide [2, 176]. In addition, AF is a prognostic indicator for stroke, heart failure, and even death [176]. Further, AF and its complications pose a large burden on the U.S. health care system, accounting for over $6.6 billion each year [177, 178]. Many patients could benefit from targeted treatments to reduce the occurrence of these arrhythmias and the accompanying risk factors.

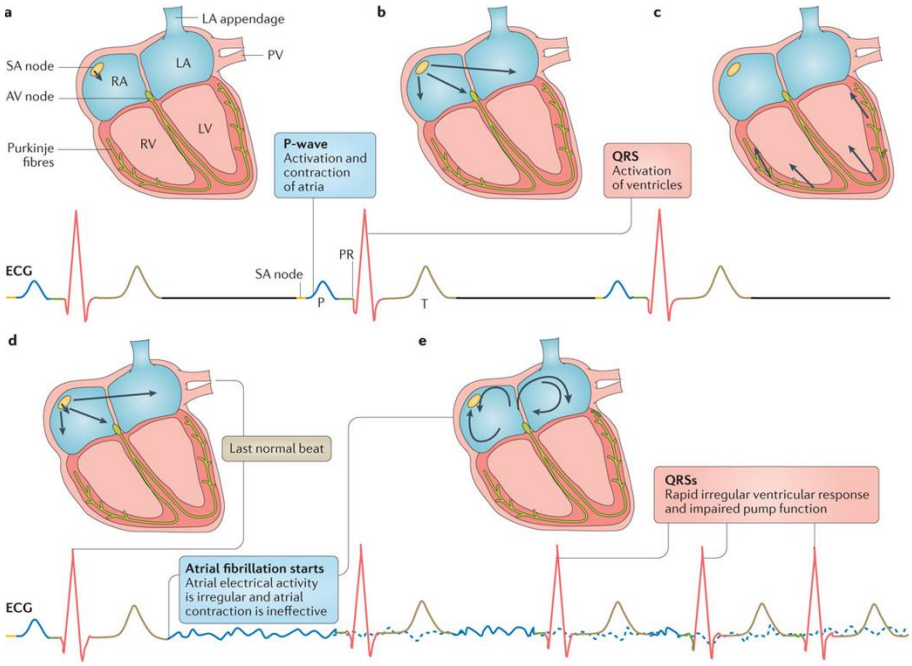

Figure 7. 1 Electrical activity in the heart during normal sinus rhythm (A-C) and AF (D-E). Adapted from Lip et al. 2016 [179].

7.2 Current Treatment Approaches

The continuing challenges in fully understanding the etiology of AF makes currently available treatments suboptimal with regards to using pharmacological, percutaneous and surgical interventional approaches.

7.2.1 Pharmacotherapy

Antiarrhythmic drugs are the first line of treatment for patients with AF, with the goal of maintaining normal sinus rhythm and preventing AF-related complications. Acute management of AF uses pharmacological agents to restore normal sinus rhythm or reduce rapid ventricular rates [180]. Long-term management, however, focuses more on managing symptoms of AF, such as thromboembolism, and improving quality of life [181]. However, pharmacological treatment for AF has major limitations in that this approach does not always provide adequate means of control and can lead to intolerable side effects, such as organ toxicity and bleeding [175, 182]. New pharmacotherapy approaches are needed for acute and chronic management of AF. Further research in understanding the pathophysiology of AF can lead to better medication options with improved efficacy and safety profiles [182].

7.2.2 Ablation

There is a growing interest in catheter ablation therapy to terminate AF by targeting specific regions in the atrium including the triggers and substrates responsible for initiating and maintaining AF. Recently, ablation procedures attempt to isolate triggers responsible for the initiation of AF. In the case of paroxysmal AF, the pulmonary veins are targeted as they are often the source of ectopic beats, triggering episodes of AF. A depiction of pulmonary vein isolation (PVI) is shown in Figure 2.2. For paroxysmal AF, the PVI procedure is successful in terminating AF in ≥ 70% of patients [4]. However, in patients with persistent or long-standing AF, this PVI procedure only results in a success rate of 20-30% after a single procedure and 51% for repeat procedures [5, 6, 183]. Ablation procedures in non-paroxysmal AF have had limited success as the underlying mechanisms are not fully understood. Recently, rotor-based ablation strategies have been demonstrated to outperform PVI ablation alone [15-17], but more research is needed to develop techniques that can accurately identify and target rotors and further evaluate whether rotors are suitable targets for ablation.

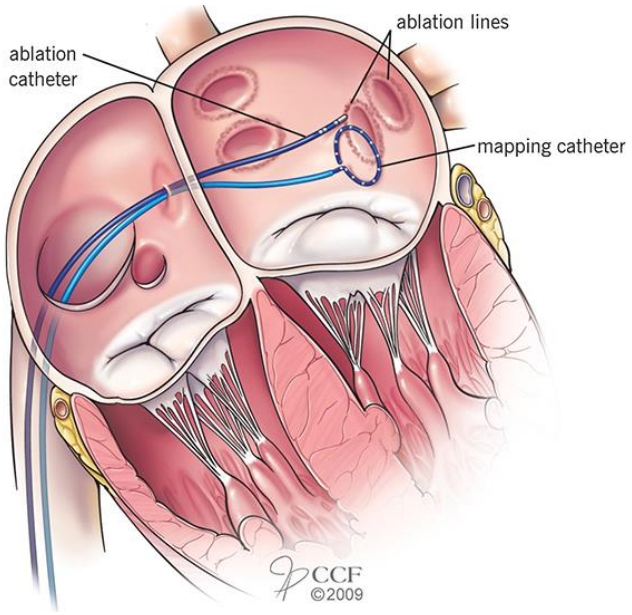

Figure 7.2 Depiction of the pulmonary vein isolation ablation procedure using mapping and ablation catheters to electrically isolate the pulmonary veins. Adapted from Chowdhury et al. 2009 [184].

The remainder of this chapter will focus on using ablation to target drivers of AF to terminate the arrhythmia. Current electrophysiology mapping techniques are described below as well as novel techniques being developed to overcome limitations of the current clinical approaches to more accurately identify the substrate maintaining AF.

7.3 Drivers of Atrial Fibrillation

For AF to persist in the heart, there needs to be both a trigger and a substrate. The trigger, such as an ectopic beat or premature atrial contraction (Figure 7.3, left panel), initiates the arrhythmia, while the substrate is responsible for maintaining the arrhythmia [185-187]. Cardiac arrhythmias, like AF, may be mediated by a variety of mechanisms, ranging from focal automaticity to macroreentry to more complex states where organized activity may be difficult or even impossible to define. In AF, the characteristic finding is global disorganization of activity in the associated chamber [188], and multiple hypotheses have been proposed since the 1950s regarding the pathophysiology underlying both the initiation and maintenance of the arrhythmia. Defining the mechanisms of arrhythmia maintenance, however, is more difficult as there are likely multiple mechanisms responsible for AF. In addition, as the duration of AF increases, as seen in patients with non-paroxysmal AF, the atria undergo electrical and structural remodeling leading to more complex mechanism responsible for the maintenance of the arrhythmia. Currently the two leading hypotheses for the maintenance of AF are (1) multiple wavelet theory and (2) functional reentry (i.e. rotors) which are shown in Figure 7.3.

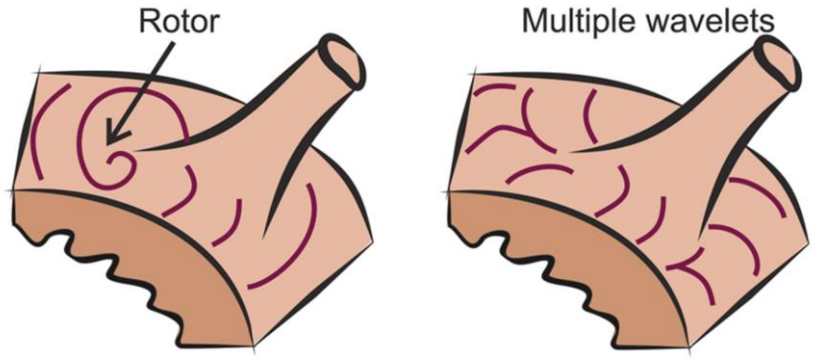

Figure 7. 3 Diagrams of the current hypotheses in AF initiation and maintenance – ectopic beat (left), rotors or functional reentry (middle), and multiple wavelets (right). Adapted from Guillem, 2016 [189].

7.3.1 Multiple Wavelet Reentry

Multiple wavelet theory was first defined by Moe et al. in 1959 and states that AF is maintained by a critical number of independent wavelets in a heterogeneous medium defined by the atrial size, mass, conduction velocity and refractory period [190, 191]. The wavelets randomly propagate and collide resulting in chaotic, fibrillatory conduction [186, 190]. Originally, it was hypothesized that the critical number of wavelets necessary to maintain the arrhythmia was more than 20 wavelets. Allessie later provided evidence that fewer, only 4 to 6, independent wavelets could maintain the arrhythmia [192, 193]. Currently, the multiple wavelet theory is accepted by most clinical electrophysiologists because of the results of the maze ablation procedure, which compartmentalized the atrial tissue to terminate AF. By removing the ability for multiple randomly propagating wavelets to exist in the atria, the arrhythmia was terminated, providing evidence for the multiple wavelet theory [192, 194].

7.3.2 Rotors

Another proposed mechanism of AF maintenance is spatially localized focal sources, or rotors [189], which was proposed as the driver of AF in the 1970s and later demonstrated experimentally in 1990 by Davidenko et al. [195, 196]. Rotors are an organized source of functional re-entry. The electrical activity at the core of the rotor rotates around the singularity point which is excitable but not yet excited tissue [197]. These rotors can remain stationary or can meander and drift through the atrium which contributes to irregularities in electrical recordings [198]. The trajectory of these meandering rotors can be complex and depend on the electrical and structural properties of the tissues nearby. Rotors have definitive characteristics such as extreme wavefront curvature at the core, an excitable and precessing core and a highly variable reentrant wavelength, with an often-undetectable excitable gap [199]. Precession of rotors may contribute towards global disorganization evident in AF, and indeed they are the source of fibrillatory wavefronts that control surrounding tissues passively thereby both initiating and maintaining AF [188, 200]. Due to rotor movement, locating these active sites for ablation presents significant challenges that necessitate more robust algorithms for mapping [189]. There is still significant debate around the theory of rotors. However, numerous optical mapping studies have demonstrated the existence of rotors [190, 201, 202]. These findings have led to the development of multiple methods aiming to use electrogram data to reproduce these optical mapping results and, in turn, determine potential critical ablation targets for treating AF [188, 197, 203, 204]. However, clinical studies have not been

reproducible, thus calling into question the ability to identify rotors using traditional electrogram approaches.

7.4 Electrophysiological Mapping for Ablation Procedures

Rotors provide a target for ablation therapy and terminating AF [197, 203, 204]. However, the current challenge is in accurately locating and ablating the regions in the atrium where the rotors exist. Currently, clinical electrophysiology studies are performed to record intracardiac electrograms from the endocardial surface of the atria. The electrical activity is captured using various mapping catheters placed in key regions of the atria in order to interpolate and reconstruct activity throughout the atria. These signals are then integrated and analyzed using an electroanatomical mapping systems such as the CARTO System (Biosense Webster, Diamond Bar, CA), EnSite Navx (Abbott, Chicago, IL), and RHYTHMIA HDx (Boston Scientific, Marlborough, MA). These systems provide physicians with real-time 3D anatomical views of the atria while positioning the catheter in various regions of the atria. Signal processing techniques can then be used in real-time or offline to generate 3D maps of the substrate from the unipolar or bipolar electrogram recordings to identity regions of interest for ablation. However, there are numerous clinical limitations associated with intracardiac mapping which makes the identification of rotors or other target regions maintaining AF difficult to identify.

Challenges in rotor identification stem from clinical limitations of electrophysiological studies including short electrograms recordings, low spatial resolution, and the presence of meandering rotors. Despite advances in cardiac mapping technologies, clinical intracardiac mapping can only capture a limited number of simultaneously recorded electrograms. During these procedures, the number of spatial locations that are able to be mapped are limited, resulting in non-uniform atrial recordings and a low spatial resolution. Also, while maneuvering the recording catheters within the atrium, poor contact of the electrode to the atrial tissue may not provide sufficient signal strength to identify atrial substrates. Finally, in addition to limitations to capturing adequate electrograms, the presence of meandering rotors can increase the complexity of rotor identification. Meandering rotors may only briefly be captured through intracardiac mapping. In combination with the duration and spatial limitations, meandering rotors prove challenging to accurately identify and locate.

Several techniques have previously been developed to analyze intracardiac electrograms to characterize rotors. These techniques include dominant frequency (DF) [205-208], local activation time (LAT) using isochronal maps [208, 209], complex fractionated atrial electrogram (CFAE)

mapping [208, 210, 211], and phase analysis using phase singularity evaluation [200, 208, 212], which have been evaluated in experimental and clinical applications, but have had varying success due to numerous limitations.

7.4.1 Local Activation Time

Local activation time maps visualize the timing of the excitation wavefront at multiple locations in the atrial tissue. The map generated is based on tissue conductions and repolarization times determined from the morphology of extracellular potentials [213]. In these activation maps, isochrones are lines used to depict simultaneous activation in the atria with propagation of the wavefront moving perpendicular to the isochrones [213]. This method is fairly simple to implement on high-amplitude, high-quality intracardiac electrograms which allows for automatic annotation of electrogram morphology to generate activation maps similar to those shown in Figure 7.4 [214]. However, this technique has several key limitations such as poor spatial resolution and susceptibility to noise. Inaccurate activation times can results from low-amplitude signals, external noise, and sufficient fragmentation requiring the signal to be annotated manually [214].

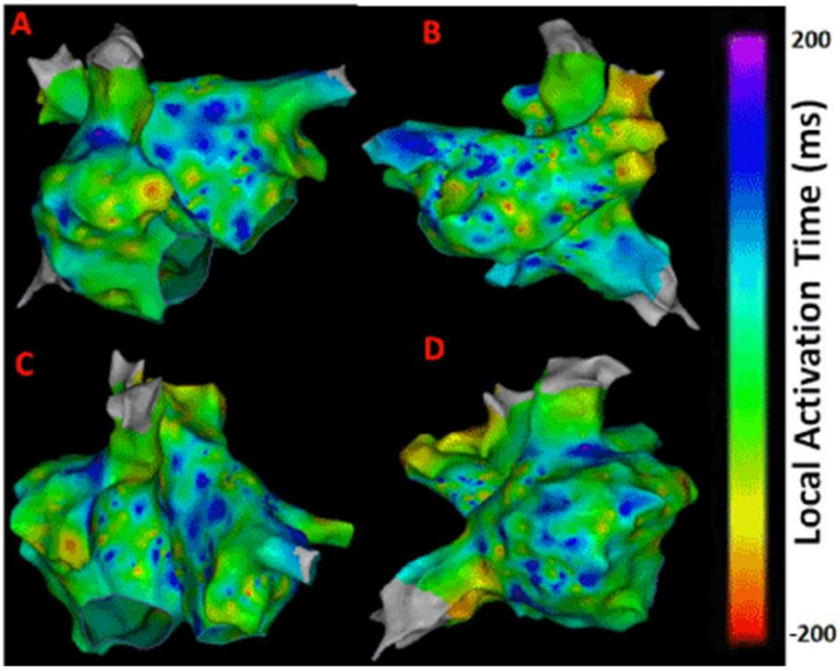

Figure 7.4 Example of LAT maps from a patient with persistent AF showing multiple views of the atria. Adapted from Arunachalam et al. 2017 [215].

7.4.2 Dominant Frequency

One approach that has been previously studied using optical mapping is dominant frequency (DF) analysis [205, 206]. DF, the peak frequency in the time series spectrum, has been used to identify focal sources in fibrillatory activity. The high frequency regions, indicating rapid and periodic activation, are believed to represent likely substrate responsible for the maintenance of AF [216]. An example of a DF map from a patient with persistent AF is shown in Figure 7.5. DF can easily be calculated using electrical recordings from the atrium, requiring only activation information. Mandapati et al. identified sources with the maximum DF in isolated sheep hearts using optical mapping and bipolar electrode recordings. Their results demonstrated that by using DF alone, discrete sites of high frequency periodic activity can rapidly be identified [206]. Expanding DF analysis to clinical data, Sanders et al. used this technique to identify regions of high frequency activity, and guide catheter ablation procedures in humans. In this study, patients with paroxysmal AF had an 89% success rate. However, for the 13 patients with persistent AF, the arrhythmia was not terminated [205]. The DF approach alone may not be suitable to provide accurate rotor localization due to several limitations including temporal instability, artifacts can significantly distort DF maps, and the rotor core cannot be specifically identified [217].

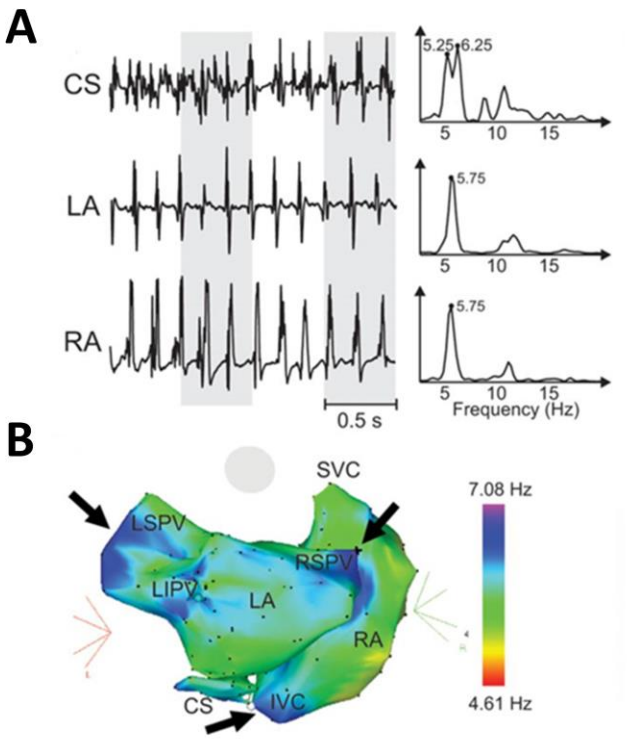

Figure 7.5 Example of DF mapping in a patient with persistent AF. (A) Recorded electrograms along with the corresponding power spectra. (B) DF map with arrows pointing to regions of high frequency. CS indicates coronary sinus; IVC, inferior vena cava; LA, left atrial; LIPV, left inferior pulmonary vein; LSPV, left superior pulmonary vein; RA, right atrial; RSPV, right superior pulmonary vein. Adapted from Guillem et al. 2013 [218].

7.4.3 Complex Fractionated Atrial Electrograms

In AF, rapid electrical activity emanating from the rotor propagate out into the periphery and become fractionated as the wavefront interacts with anatomical and functional inhomogeneity in the tissue. CFAE quantifies the fractionation occurring in the wavefront and identifies reentrant activity by having at least one of the following criteria: continuous electrical activity, at least two deflection, cycle length less than 120 ms, and an amplitude less than 0.05mV [210, 219, 220]. The electrograms can be classified into 4 types: C0 (non-fractionated), C1 (fractionated with periodic activity), C2 (both fractionated and non-fractionated periodic activity), and C3 (high frequency and continuous atrial activity) shown in Figure 7.6.

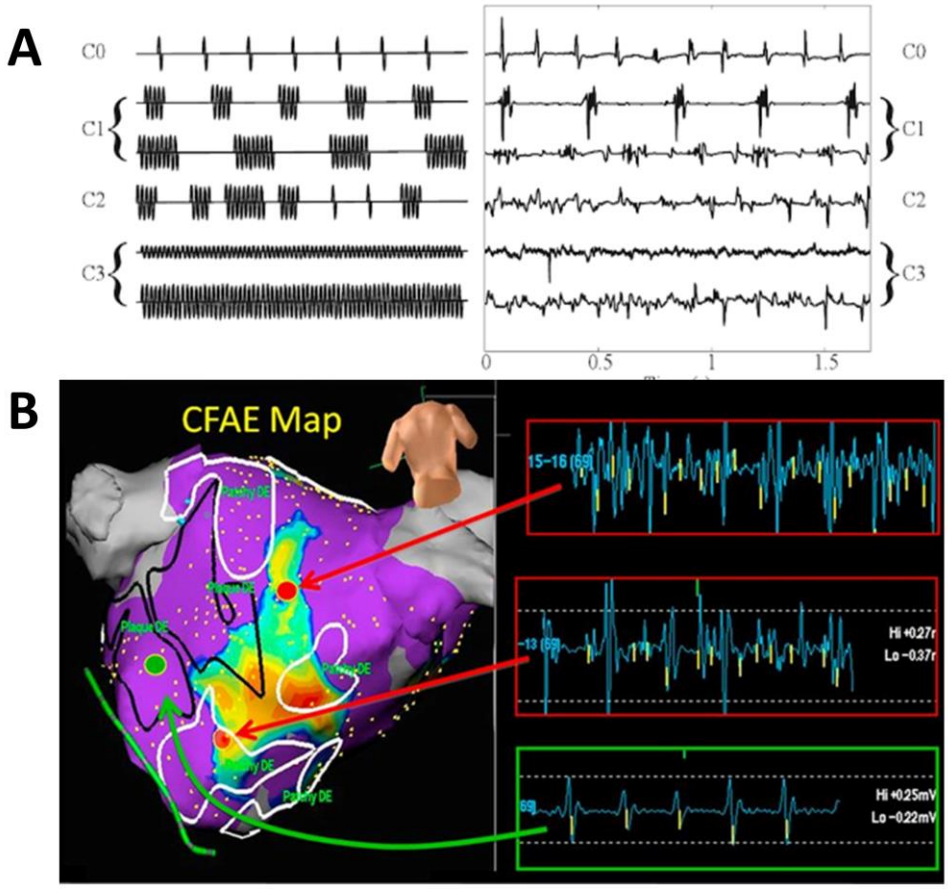

Figure 7.6 (A) Schematics (left) and corresponding recorded atrial signals (right) of the four common types of CFAEs. Adapted from Schilling, 2012 [221]. (B) An example of CFAE mapping in a patient with persistent AF along with atrial recordings of various typtes of CFAEs captured in the atria. Adapted from Jadidi et al. 2013 [222].

Early high-density cardiac mapping studies demonstrated the electrogram fractionation in AF [223, 224], which lead to clinical investigations whether PVI with CFAE ablation would outperform PVI alone. The Substrate and Trigger Ablation for Reduction of AF (STAR-AF) II Trial enrolled 100 patients with high-burden paroxysmal or persistent AF and randomized to PVI alone or PVI with CFAE ablation. However this study failed to demonstrated added benefit with the CFAE ablation [225]. These results have brought into question the validity of the CFAE approach in identifying regions of atria substrate maintaining AF. Further, numerous key limitations of CFAE mapping exist including low reproducibility, low specificity of the active regions, and high occurrence of identifying passive regions, which are not actively contributing the maintenance of AF [219, 224].

7.4.4 Phase Analysis

Phase analysis mapping provides insights into the spatiotemporal organization of fibrillation [226]. Phase maps are created by calculating the instantaneous phase of the electrogram using the Hilbert transform. This transformation into the phase domain allows for the signal to be depicted from $-\pi$ to $+\pi$ revealing patterns in fibrillatory activation as shown in Figure 7.7 [226, 227]. Specifically, the point at which the phases converge, called singularity points, are of specific interest as they may identify functional or anatomical rotational activity. Traditionally phase mapping is performed with high-spatial resolution in ex-vivo optical mapping experiments in animals using voltage-sensitive dyes. However, this approach is not feasible in the clinical due to the toxicity of the voltage sensitive dyes. Instead, intracardiac mapping using basket catheters and recently non-invasive body surface electrodes has been used to capture electrical activity and derive phase in human AF as demonstrated in Figure 7.7 [209, 228]. Although this technique offers the advantage of temporal and spatial resolution to visualize the sources of fibrillatory activity, there are several limitations with implementing this technique in the clinic. First, unipolar electrograms, representing a summation of local activity, are not optimal for calculating localized activation patterns. In addition, this technique can result in misleading phase calculations if the T-waves are captured. Finally, the results are dependent on having a high spatial resolution, and often times the number of electrodes and spacing in clinical studies are inadequate and require interpolation to generate phase maps [226].

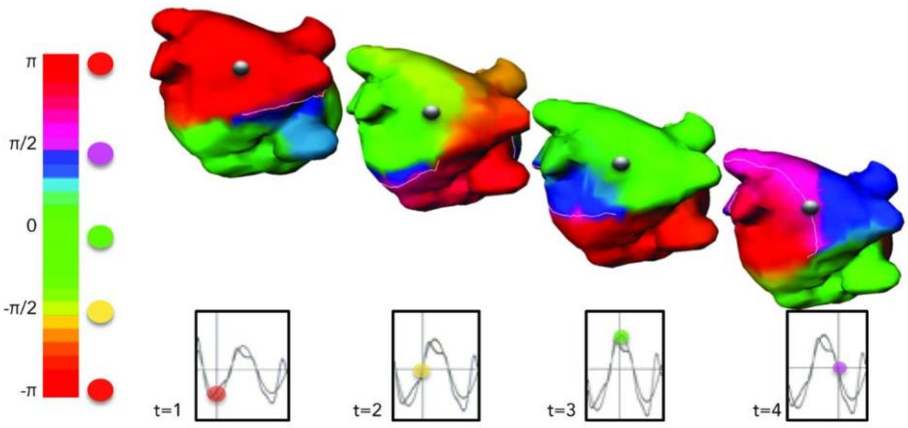

Figure 7. 7 Example of a phase map derived from body surface electrodes. Adapted from Sohal et al. 2015 [219].

Many recent advances have been made in quantitative intraprocedural signal analysis to guide the selection of ablation targets [208]. However, there is no solid evidence that any of these approaches can successfully identify rotor core zones or pivot point locations to terminate AF based on ablation at those identified sites, and no significant improvements in ablation outcomes were observed [225, 229].

7.5 Novel Mapping Techniques

There is a clear need for robust spatio-temporal techniques that can consistently identify rotors or areas of abnormal electrical activity using unique electrical characteristics of the pivot point that can be applied to clinical intracardiac mapping. This can be accomplished through the development of techniques that are validated using high resolution optical mapping studies and numerical simulations where clinical limitations such as decreased electrograms duration and reduced spatial resolution can be simulated.

Recently, several new signal analysis approaches have been developed – Shannon entropy (SE) [230, 231], multi-scale frequency (MSF) [232], kurtosis (Kt) [233], and multi-scale entropy (MSE) [234] – to identify the pivot points of rotors in the case when rotors can be easily visualized using optical mapping techniques. These proposed techniques utilize different cardiac signal characteristics, other than local activation, to uncover the intrinsic complexity of the electrical activity in the rotors, which are not taken into account in current mapping methods.

7.5.1 Multiscale Frequency

MSF estimation is a novel approach that incorporates various physiological frequencies present in the heart, and is not limited to single frequency analysis as with DF maps. This technique uses a robust algorithm to estimate instantaneous frequency using eight log-Gabor filters. Each of the eight filters are one octave apart and designed with a bandwidth of $2\sqrt{2}$. The center frequencies of these filters can be chosen to span the appropriate physiological range for heart rate. The remaining frequency components are combined to calculate a wide range local MSF estimate, ρ, using the weighted summation of eight log-Gabor filter pairs. MSF is calculated as follows:

$$\rho = \rho_o \left[\sum_{i=1}^{N-1} q_i \right]^{-1} \sum_{i=1}^{N-1} 2^{i+0.5} q_{i+1}$$

Where q_i is the output of the i[th] log-Gabor filter and ρ_o is the center frequency of the first log-Gabor filter. Due to the chaotic nature of the rotor and presence of additional underlying frequencies, the MSF value is expected to be different at the core of the rotor when compared to the periphery [232].

7.5.2 Shannon Entropy

SE is a statistical measure of expected information content based on the distribution amplitude of values in a histogram. The voltage signals at each spatial location/pixel is binned according to its voltage intensity into a histogram. The relative probability density, ρ, is defined as the number of counts in an intensity bin divided by the total count in all bin. SE is calculated as follows:

$$SE = \sum_{i=0}^{N-1} p_i \log_2 p_i$$

Where N is the number of amplitude bins, and p is the probability of any sample falling within a particular amplitude bin. At the core of the rotor, the interference of wavefronts and the presences of several physiological frequencies could lead to a reduction in the amplitude of the voltage signal, therefore creating a narrower distribution of voltage intensities. The narrower distribution corresponds to a higher certainty and lower SE at the core of the rotor. In the periphery, there is less interference as the wave propagates through, leading to a broader distribution in voltage intensities and therefore a higher SE value [230].

7.5.3 Kurtosis

Kt is a higher order statistical measure, the 4[th] central moment, dealing with non-Gaussian or possible nonlinear processes. Kt is a measure of peakedness of a probability density function of a real-valued random variable. For each voltage trace at each pixel, the intensities are binned to create a voltage histogram which can then be used to determine the peakedness of the probability density function. Distributions with a narrower distribution and higher peak will have a higher Kt value in comparison to those with a broad distribution and minimal peak. The 4[th] central moment is calculated as follows:

$$Kt\big(x(t)\big) = E\left\{\left(\frac{x(t) - E\{x(t)\}}{\sigma_x}\right)^4\right\}$$

Where E is the expected value or mean of the time signal x(t), and σ_x is the variance. Due to the expected narrow distribution at the core of the rotors, the core is expected to be identifiable with a high kurtosis value with respect to the periphery [233].

7.5.4 Multiscale Entropy

MSE approach employs a sample entropy algorithm over multiple time scales to fully capture the intrinsic complexity of non-stationary time series data. This method uses a nearest neighbor moving average kernel to better capture the complexity of a non-stationary time series data. This approach contains "memory" by accounting for previous and future time series values while computing the nearest neighbor average. A time scale factor, τ, represents the time scaling in the forward and reverse directions. For this analysis, the nearest neighbor moving-averaged time series is calculated using τ = 3. Using the moving-averaged time series, the number of matched vectors within the timer series were calculated for vector lengths of m and m+1. For this analysis, m = 2. Two samples were considered to match if the distance between the vectors is less than r, where r is chosen to be 0.2 times the standard deviation of the raw time series. MSE is calculated as the sample entropy of the total number of matched template vectors as shown below:

$$MSE = -\ln\left(\frac{n(m+1,r)}{n(m,r)}\right)$$

Where n(m+1,r) is the total number of matched vectors of length m+1, and n(m,r) is the total number of matched vectors of length m [234].

Chapter 8

Novel quantitative analytical approaches for rotor identification and associated implications for mapping

8.1 INTRODUCTION

Chapter 8 presents the results of the validation study demonstrating the potential of four novel mapping techniques – multiscale frequency (MSF), kurtosis (Kt), Shannon entropy (SE), and multiscale entropy (MSE) – to identify stationary and meandering rotors in ventricular arrhythmias captured in ex-vivo optical mapping studies in a rabbit heart. The study presented in this chapter evaluates the performance and robustness of MSF, Kt, SE, and MSE techniques with respect to several clinical limitations: decreased time duration and reduced spatial resolution. In addition, Chapter 8 discusses the clinical implications and translation of these techniques.

Cardiac arrhythmias may be mediated by a variety of mechanisms, ranging from focal automaticity to macroreentry to more complex states where organized activity may be difficult or even impossible to define. In certain arrhythmias, including atrial fibrillation (AF) and ventricular fibrillation (VF), the characteristic finding is global disorganization of activity in the associated chamber [188]. In the case of AF, for example, multiple hypotheses have been proposed since the 1950s regarding the pathophysiology underlying both the initiation and maintenance of the arrhythmia. One mechanism that has been of particular interest is rotors, or regions of functional reentry, as have been demonstrated using optical mapping ex-vivo studies [190]. These findings have led to the development of multiple methods aiming to use electrogram data to reproduce these optical mapping results and, in turn, determine potential critical ablation targets for treating AF [188, 197, 203, 204]. However, clinical studies have not been reproducible, thus calling into question the ability to identify rotors using traditional electrogram approaches; and whether these area, if identified, truly reflect ablation targets.

While the study of rotors has largely been focused on the treatment and understanding of AF, investigators have suggested that functional reentry may be relevant in some ventricular arrhythmias. Previous work has demonstrated that the underlying mechanism for certain experimental examples of ventricular tachycardia (VT) and VF in structurally normal hearts may in fact be functional reentry [235-238]. In addition, transitions between monomorphic VT, polymorphic VT, and VF may be subtended by shifts in the core size of isolated rotors during a

given arrhythmia [237, 239]. Thus, functional reentry likely subtends ventricular arrhythmogenesis in clinical examples of monomorphic VT. Therefore methods to define rotors using an electrogram-guided approach may have clinical relevance for the treatment of ventricular arrhythmias as well.

Several techniques have previously been developed to analyze intracardiac electrograms to characterize rotors. These techniques include dominant frequency (DF) [205-208], local activation time using isochronal maps [208, 209], complex fractionated electrogram mean index mapping [208, 210, 211], and phase analysis using phase singularity evaluation [200, 208, 212]. However, none of these techniques were successfully implemented in clinical settings due to various limitations [230]. Thus, there is a clear need for robust spatial-temporal techniques that can consistently identify rotors.

Recently, several new signal analysis approaches have been developed – SE [230, 231], MSF [232], Kt [233], and MSE [234] – to identify the pivot points of rotors in the case when rotors can be easily visualized using optical mapping techniques. These proposed techniques utilize different cardiac signal characteristics, other than local activation, to uncover the intrinsic complexity of the electrical activity in the rotors, which are not taken into account in current mapping methods. However, applications of experimental data regarding the relevance of rotors has been challenging, in part, due to several clinical limitations associated with intracardiac mapping including short duration electrogram recordings, low spatial resolution, and the presence of meandering rotors.

8.2 AIM

In this paper, we seek to determine whether our recently developed techniques, including MSF, SE, Kt, and MSE, can be used to successfully identify rotors in arrhythmia episodes captured using optical mapping data and show potential for translation to clinical intracardiac electrograms identifying targets for ablation. Specifically, we seek to overcome the following challenge: (1) limitations in attaining simultaneous data from spatially distant locations; (2) electrogram data, which looks at local activation, fundamentally looks at different information than optical mapping, which looks at both depolarization and repolarization; and (3) temporal variability in the geographic location of rotors making interpretation of individual electrograms obtained at different points in time difficult to interpret. Our results may help characterize the utility of different signal processing approaches to defined regions of organized activity in more complex arrhythmias.

8.3 METHODS

Optical mapping studies were performed on two isolated rabbit hearts as described previously [240, 241]. All procedures were approved by the University of Minnesota Animal Care and Use Committee and were conducted in accordance with Institutional and NIH guidelines. Episodes of ventricular tachycardia were induced using burst pacing, and two examples of rotors were used: (1) a single stationary rotor and (2) figure-of-8 reentry with one stationary and one meandering rotor. Movies were captured for a duration of 3 seconds at a rate of 600 frames per second with 64 x 64 pixel resolution using voltage-sensitive dye and 12-bit CCD cameras. In each frame, the background fluorescence was subtracted and spatial (3 x 3 pixels) and temporal (5 frames) conical convolution filters were used to increase the signal-to-noise ratio.

The phase movies were generated using the Hilbert transform, which calculates instantaneous phase allowing for the visualization of the depolarized and repolarized tissue. Gray et al. demonstrated that phase movies allow for the clear identification of the pivot point as the location at which all phases meet (phase singularity). Phase movies serve as a gold standard for locating the rotor in the examples presented [134]. Using phase maps, the singularity points were traced frame by frame to obtain a final pixel map representing the "true" location of the rotor pivot point. This map was used as a comparison for the identification of the pivot points for the five approaches described in Table 8.1. Specifically, DF and MSF were determined in the frequency domain. SE and Kt characterize the voltage intensities at each pixel. In addition, the time-series morphology and complexity were quantified using MSE. All analysis was performed using a custom-written MATLAB (Mathworks, Inc., Natick, MA) program.

Table 8.1 Summary of signal processing techniques

Table I. Summary of signal processing techniques

Method	Equation	Variable Definition	Description	References
Dominant Frequency (DF)	$DF = \underset{f}{\text{argmax}}(X(f))$	X(f): spectrum of the voltage intensity time series	Calculates the peak frequency in the signal spectrum (0-30 Hz) of the voltage intensity time series.	11-14
Multiscale Frequency (MSF)	$MSF = \rho_o \left[\sum_{i=1}^{N-1} q_i\right]^{-1} \sum_{i=1}^{N-1} 2^{i+0.5} q_{i+1}$	ρ: local MSF estimate q_i: output of the ith log-Gabor filter ρ_o: center frequency of the first log-Gabor filter	Calculates the instantaneous frequency using the signal spectrum (0-30 Hz) of the voltage intensity time series	24
Shannon Entropy (SE)	$SE = \sum_{i=0}^{N-1} p_i \log_2 p_i$	N: number of amplitude bins ρ: probability of any sample falling within a particular amplitude bin	Quantifies the uncertainty in the voltage intensity distribution	20, 23
Kurtosis (Kt)	$Kt = E\left\{\left(\frac{x(t) - E\{x(t)\}}{\sigma_x}\right)^4\right\}$	E: expected value x(t): voltage intensity time series σ_x: variance of the voltage intensity time serie	Quantifies the 'peakedness' of the voltage intensity distribution	25
Multiscale Entropy (MSE)	$MSE = -\log\left(\frac{A}{B}\right)$	A: number of matched vector pairs of length m+1 from the moving average time series B: number of matched vector pairs of length m from the moving average time series	Calculates the moving average of the voltage intensity time series and quantifies the regularity and repetitiveness of the data	26

8.3.1 Rotor Identification and Quantification

Receiver operating characteristic (ROC) curves were constructed for all techniques using corresponding 2D maps generated from the original 3 second, 64 x 64 pixel movies. Specifically, the corresponding MSF, SE, Kt, and MSE values for each 2D map ranged from 1% to 99%, and the optimal point on each ROC curve, corresponding to the highest sensitivity and specificity, was identified as demonstrated in Figure 8.1. These points were used to define individual thresholds for the identification of rotor pivot points for each technique.

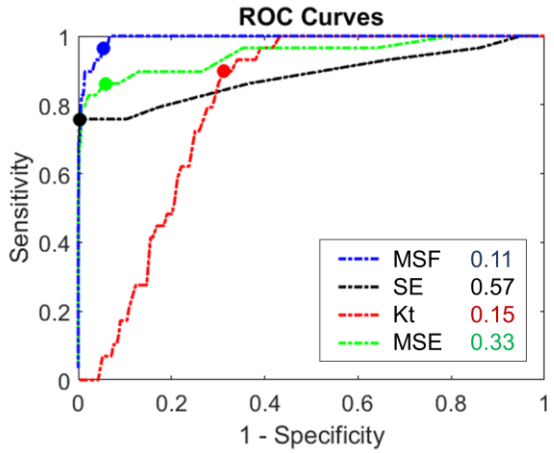

Figure 8.1 Receiver operator characteristic curves for the MSF, SE, Kt, and MSE techniques with the identification threshold varying from 0.01 to 0.99. The circles on each curve indicates the identification threshold for the 3-second duration time series for each mapping technique.

The pixels in the 2D maps corresponding to the pivot point of the rotor were determined based on the individual thresholds for each MSF, SE, Kt, and MSE techniques, and compared with the "true" rotor location, to calculate the accuracy of each technique. Specifically, the number of pixels, as well as their location, were identified to determine the number of true positive (TP), true negatives (TN), false positives (FP), and false negatives (FN). From this data, accuracy was calculated as:

$$Accuracy = \frac{TP + TN}{TP + TN + FP + FN}$$

The accuracy of each approach was calculated for various time series durations (3 seconds, 2 seconds, 1 second, and 0.5 seconds) and spatial resolutions (64 x 64, 32 x 32, 16 x 16, and 8 x 8 pixels) using the sliding window analysis. To determine the effect of decreased time series duration on the accuracy, the duration of the original optical mapping movies were decreased from 3 seconds down to 2, 1 and 0.5 seconds using a 0.5 second sliding window (Figure 8.2) which resulted in 3 2-second times series, 5 1-second time series, and 6 0.5-second time series. The figure below depicts how the analysis was performed. In addition this analysis approach was also applied to the spatial resolution data with the 64x64 pixel data. Uniformly removing pixels from the original video to decrease spatial resolution resulted in 4-32x32 pixel movies, 16-16x16 pixel movies, and 64-8x8 pixel movies. A similar process was then used to calculate optimal thresholds and optimal accuracies for each technique, which were defined separately for each reduced time series duration and spatial resolution.

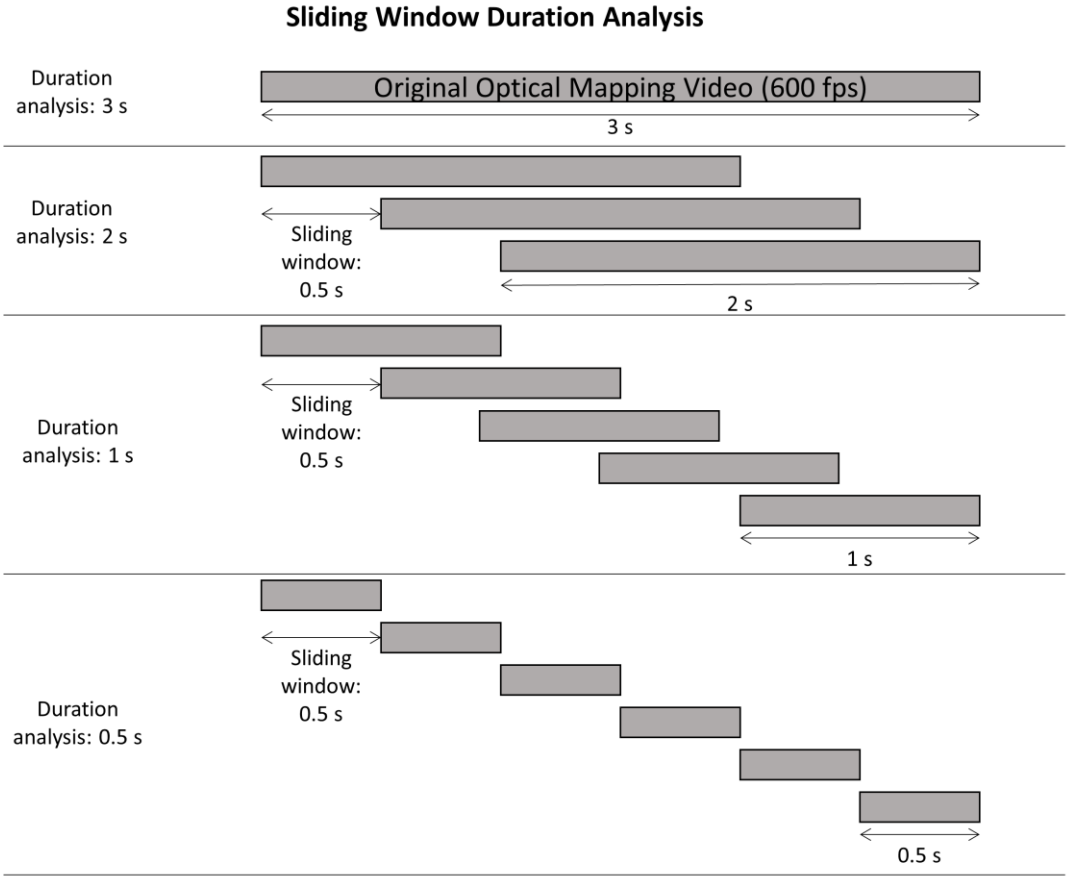

Figure 8.2 Schematic of the sliding window duration analysis for the simulated clinical limitation or reduced time series. A sliding window of 0.5 seconds was applied to the data to get multiple time series of 2, 1 and 0.5 second durations.

8.4 RESULTS

8.4.1 Identification of the Pivot Point in a Single Stationary Rotor

A snapshot of the phase movie from a single stationary rotor is shown in Figure 8.3A, where different colors represent different phases of an action potential, and the singularity point is seen where all phases converge [234]. Figure 3B shows the "true" location of the pivot point identified from the phase movie. Representative examples of times series, power spectrums, and voltage intensity distributions are shown in Figure 3D for the core and periphery of the rotor (pixels '1' and '2' from Figure 8.3A).

Figure 8.3C shows a corresponding 2D DF map calculated for a rotor showing a single DF = 7.8 Hz. Note that the DF approach cannot distinguish between the pivot point and periphery despite the clear differences in the time series data (Figure 8.3D).

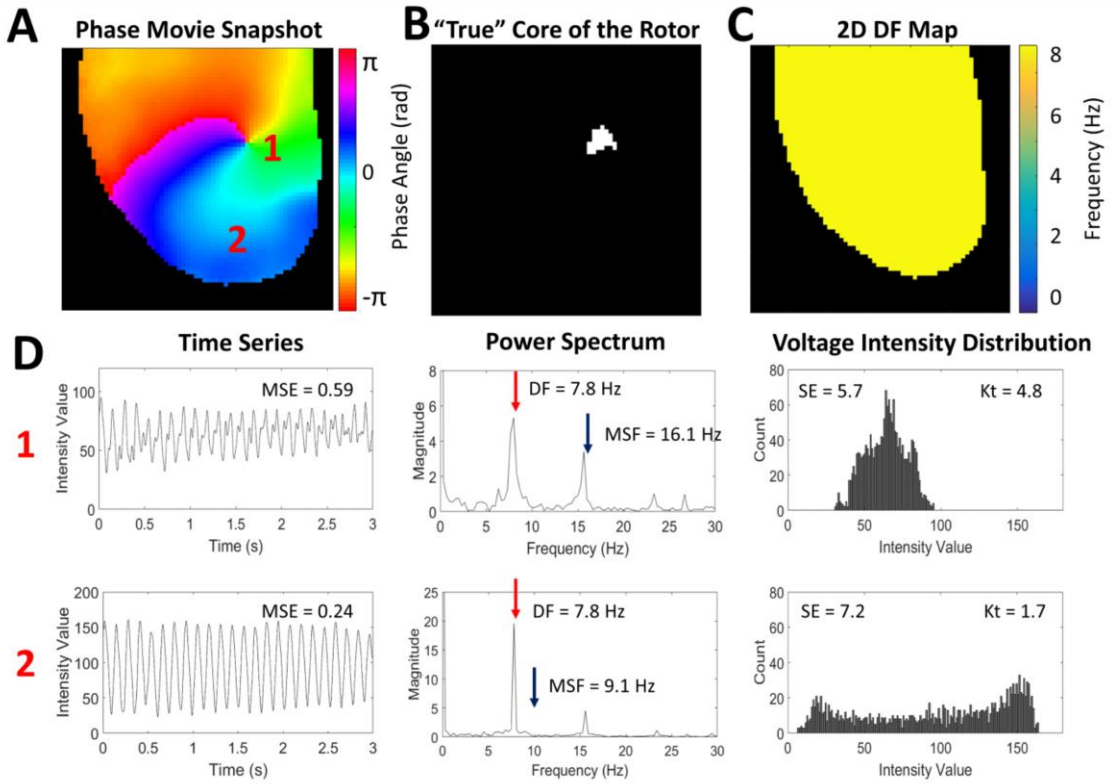

Figure 8.3 An example of a single stationary rotor from optical mapping of a rabbit heart. (A) Snapshot of the phase movie of the single stationary rotor with the depolarizing wave front shown in red. The pivot point and periphery of the rotor are identified by '1' and '2' respectively. (B) Pixel map showing the "true" location of the pivot point identified from the phase movie. (C) 2D DF map generated from the single stationary rotor showing a single DF of 7.8 Hz. (D) Representative examples of the time series, power spectrums, and voltage intensity distributions from the pivot point (location '1') and periphery (location '2') of the rotor demonstrating differences in signal characteristics.

The 2D maps from MSF, SE, Kt, and MSE for the original stationary rotor (64 x 64 pixels, 3 seconds) are shown in Figure 8.4A. Note that each of these techniques can clearly identify the core of the rotor, which is clearly associated with maximum (for the MSF, Kt, and MSE) or minimum (for SE) values when compared with the periphery of the rotor.

The ability of these new approaches to identify the core of the rotor can be explained using the properties of the signal at the core and periphery (Figure 8.3D). The MSF approach accounts for various underlying physiological frequencies that are present at the core but not in the periphery.

This results in a higher MSF value at the pivot point (16.1 Hz) in comparison to the periphery (9 Hz). The SE approach is based on the broadness of the distribution of voltage intensities at each pixel location. As is shown in Figure 8.3D, the pivot point of the rotor has a narrower distribution (SE = 5.7) than the periphery (SE = 7.2). The Kt approach uses the same data, but assesses the "peakedness" of the distribution. The narrow distribution at the core resulted in the more peaked distribution (Kt = 4.8) in comparison to the periphery (Kt = 1.7). The final approach, MSE, quantifies the complexity of the time series data. Regular voltage traces in the periphery result in a low MSE = 0.24, while at the core of the rotor MSE = 0.59 due to the irregularity in the voltage time series.

8.4.1.1 Pivot Point Identification for Shorter Duration of Time Series

Figure 8.4B evaluates the performance of MSF, SE, Kt and MSE approaches to identify the pivot point of the stationary rotor for progressively shortened durations of optical mapping data. A duration of 0.5 seconds was the shortest duration considered, which captures approximately 4 local activation-repolarization cycle. The results are shown as 3D contour plots to highlight the magnitude of the peak identifying the rotor as well as artifacts in the periphery and its relation to the times series duration. The x and y coordinates correspond to the (64 x 64) spatial resolution, and the z coordinate corresponds to different MSF, SE, Kt, and MSE values. As the duration of the data decreases from 3 seconds down to 2, 1 and 0.5 seconds, the amplitude identifying the stationary peak is reduced. However, the pivot point of the rotor is still distinguishable for all four approaches. Note that the SE and MSE approaches are associated with the presence of artifacts around the border, which may affect the performance of the approaches as the duration decreases further.

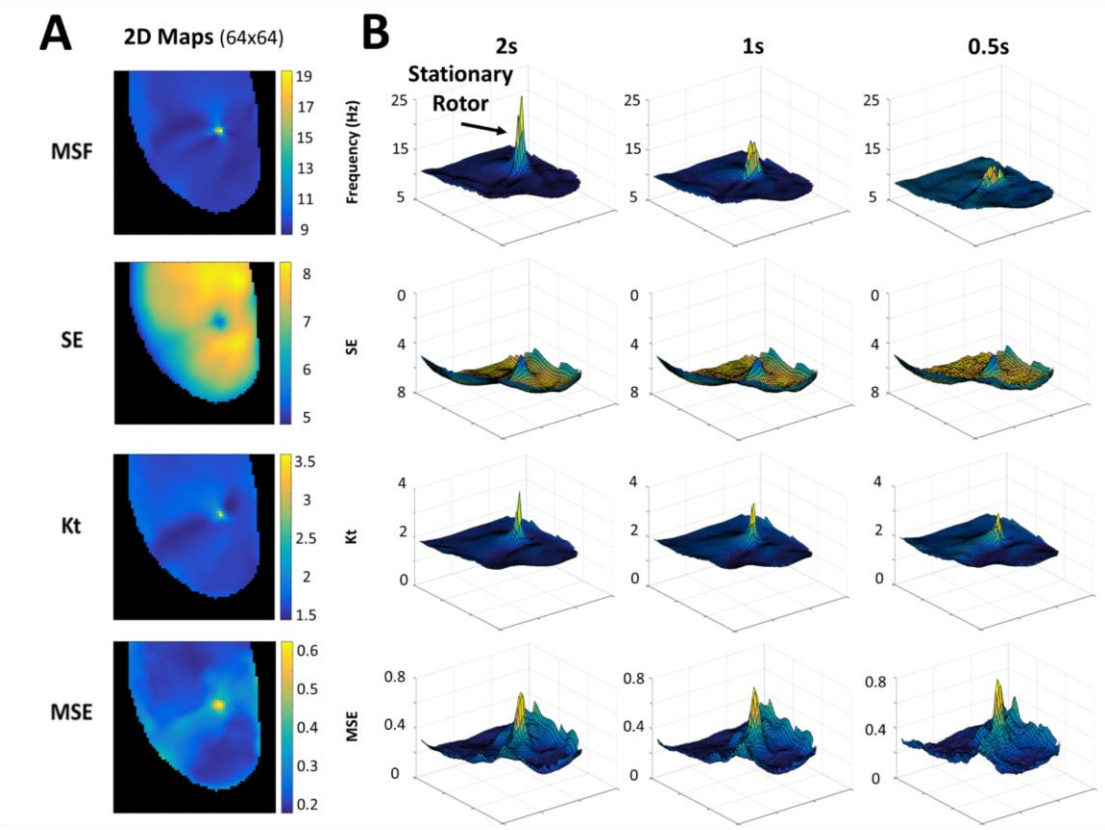

Figure 8.4 (A) 2D maps calculated for the 3 sec optical mapping video of the single stationary rotor using MSF, SE, Kt, and MSE approaches. (B) 3D contour plots demonstrate the ability of the techniques to identify the pivot point of the rotor for reduced arrhythmia durations of 2 sec, 1 sec, and 0.5 sec. The x and y coordinates correspond to (64x64) spatial resolution, and the z coordinate corresponds to the MSF, SE, Kt, and MSE values.

8.4.1.2 Pivot Point Identification for Reduced Spatial Resolution

Figure 8.5 evaluates the ability of the MSF, SE, Kt, and MSE approaches to identify the pivot point of the stationary rotor for progressively reduced spatial resolutions. As can be seen from Figure 8.5, all four techniques are able to correctly identify the pivot point of the stationary rotor.

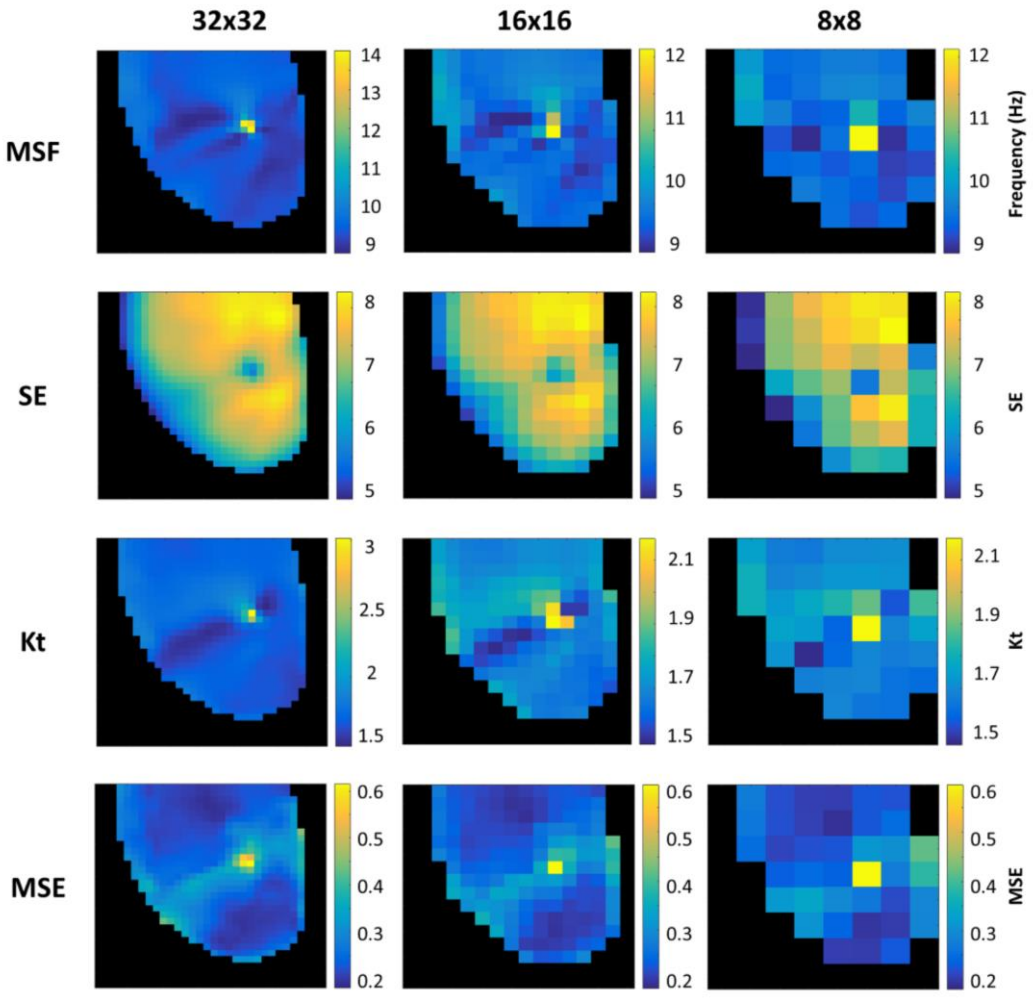

Figure 8.5 2D maps from MSF, SE, Kt, and MSE identifying the single stationary rotor for reduced spatial resolutions of 32x32 (left), 16x16 (middle), and 8x8 pixels (right).

To quantify the results presented in Figures 8.4 and 8.5, the location associated with the pivot point was identified for the MSF, SE, Kt, and MSE approaches and compared with the true pivot point location. Figure 8.6 quantitatively compares the performance of the mapping techniques in the identification of the pivot point of the rotor for reduced time series duration (Panel A) and spatial resolution (Panel B). The top panels show the accuracy of each technique using the individual threshold values that were determined for the original 3 second time series with 64 x 64 spatial resolution. These results show stable accuracy for the entropy approaches, SE and MSE. However, both MSF and Kt techniques have a large reduction in accuracy as the duration decreases. The individual thresholds for each technique were then optimized for each duration and spatial resolution to calculate optimal thresholds (middle panels) as well as corresponding optimal

accuracy for each technique (bottom panels). The results in Figure 8.6 show that optimal accuracy improves the ability all techniques to identify the pivot points of the rotor both for reduced durations (2, 1, and 0.5 seconds) and spatial resolutions (32 x 32, 16 x 16, 8 x8 pixels). The MSF, Kt, and MSE had similarly high accuracies (greater than 90%) even as duration and spatial resolution decreased. However, the performance of SE was significantly lower with an accuracy less than 70%.

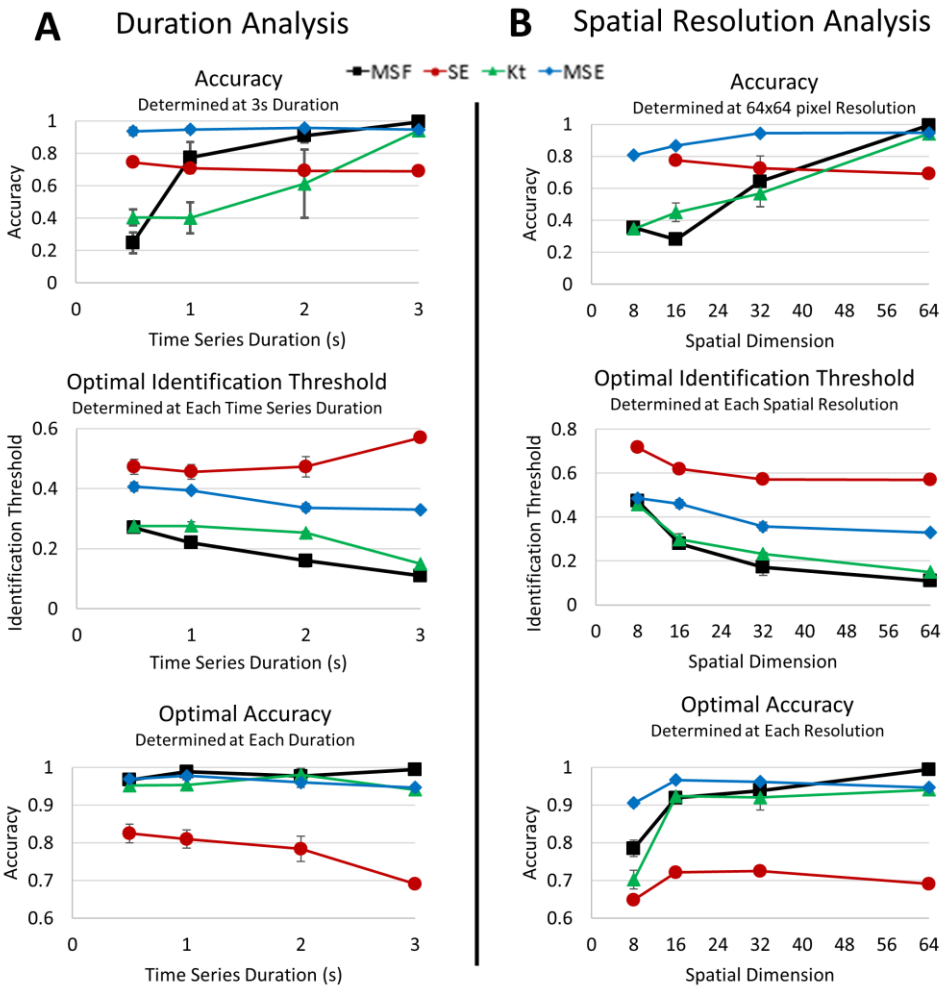

Figure 8.6 Accuracy of each technique to identify the stationary rotor from Figure 8.1A for reduced duration (A) and spatial resolution analysis (B). The top panels show accuracy calculated using the individual thresholds determined for the original 3s duration time series and 64x64 spatial resolution. Similar results are shown for the analysis using optimal thresholds (middle panel) and optimal accuracies (bottom panel).

8.4.2 Identification of Multiple Pivot Points in a Figure-of-8 Reentry

A snapshot of the phase movie from a figure-of-8 reentry is shown in Figure 8.7A. Figure 8.7B shows the location of the singularity points ("true" location of the pivot points) identified from the phase movie. The red line indicates where the map was divided between meandering and stationary rotors. The top rotor, labeled '1,' meanders while the bottom rotor remains stationary. Figure 8.7D shows representative filtered time series, power spectrums, and voltage intensity distributions from the pivot point of the meandering rotor and the periphery (pixels '1' and '2' respectively from 8.7A).

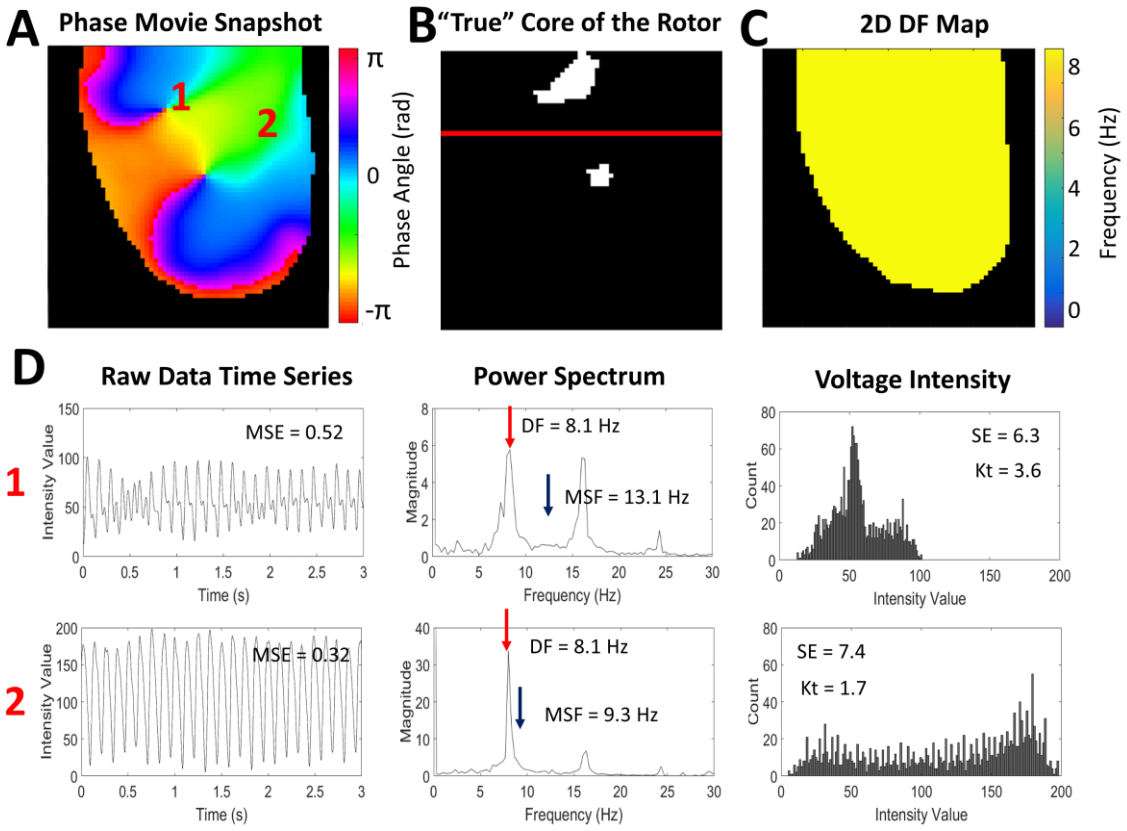

Figure 8.7 An example of multiple pivot points in a figure-of-8 reentry from optical mapping of a rabbit heart. (A) Snapshot of the phase movie for the figure-of-8 reentry, with the depolarizing wave front shown in red. The pivot point of the meandering rotor and periphery of the rotor are identified by '1' and '2' respectively. (B) Pixel map showing the "true" location of the pivot points of the meandering and stationary rotors identified from the phase movie. The red line indicates where the map was divided between meandering and stationary rotors. (C) 2D DF map from the figure-of-8 reentry showing a single DF of 8.1 Hz. (D) Representative examples of the time series, power spectrums, and voltage intensity distributions from the pivot point of the meandering rotor (location '1') and the periphery (location '2') of the rotors.

Figure 8.7C shows the corresponding 2D DF map calculated for the figure-of-8 reentry with a single DF = 8.1 Hz, which is unable to distinguish between the pivot points and the periphery in the figure-of-8 reentry. The 2D distributions of MSF, SE, Kt and MSE for the original figure-of-8 reentry movie from Figure 8.7A (64 x 64 pixels, 3 seconds) are shown in Figure 8.8A. Each of the techniques is able to identify the meandering and stationary rotor separately from the periphery.

8.4.2.1 Pivot Point Identification for Shorter Duration of Time Series

The 3D contour plots in Figure 8.8B demonstrate the ability of MSF, SE, Kt and MSE to identify both the meandering and stationary rotors as the duration of the optical mapping movie is decreased. Similar to the stationary rotor example presented in Figure 8.4, the location of the pivot points can still be identified, but the peak becomes less prominent as the duration decreases. Note that the SE and MSE result in increased artifacts as the duration decreases, which strongly impacts the accuracy of the rotor identification for the SE and MSE approaches. From the 3D contour plots presented, both the MSF and Kt approaches provided clear identification of both rotors with minimal artifacts, even at an acquisition duration of 0.5 seconds.

8.4.2.2 Pivot Point Identification for Reduced Spatial Resolution

Figure 8.9 evaluates the ability of each technique to accurately identify multiple rotors under the simulated clinical limitation of reduced spatial resolution. As the spatial resolution decreases, the meandering rotor can still be identified. However, the stationary rotor can no longer be identified in the 8 x 8 pixel resolution (Figure 8.9, right panel). For this analysis, multiple pixels from the 8 x 8 analysis were recorded directly from the region of the meandering rotor, while no pixels were captured directly from the location of the stationary rotor.

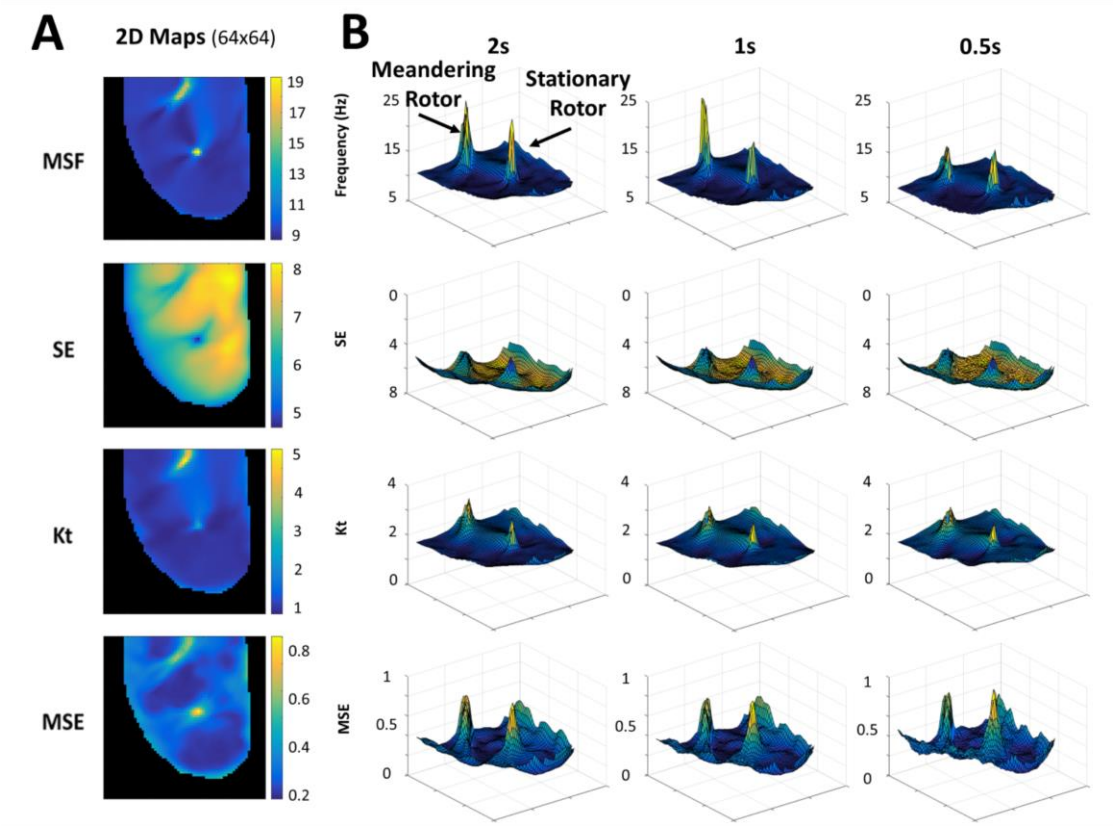

Figure 8.8 (A) 2D maps calculated for the 3 sec optical mapping video of figure-of-8 reentry using MSF, SE, Kt, and MSE approaches. (B) 3D contour plots demonstrate the ability of each technique to identify multiple pivot points, the meandering and stationary rotors, for reduced arrhythmia durations of 2 sec, 1 sec, and 0.5 sec. The x and y coordinates correspond to (64x64) spatial resolution, and the z coordinate corresponds to the MSF, SE, Kt, and MSE values.

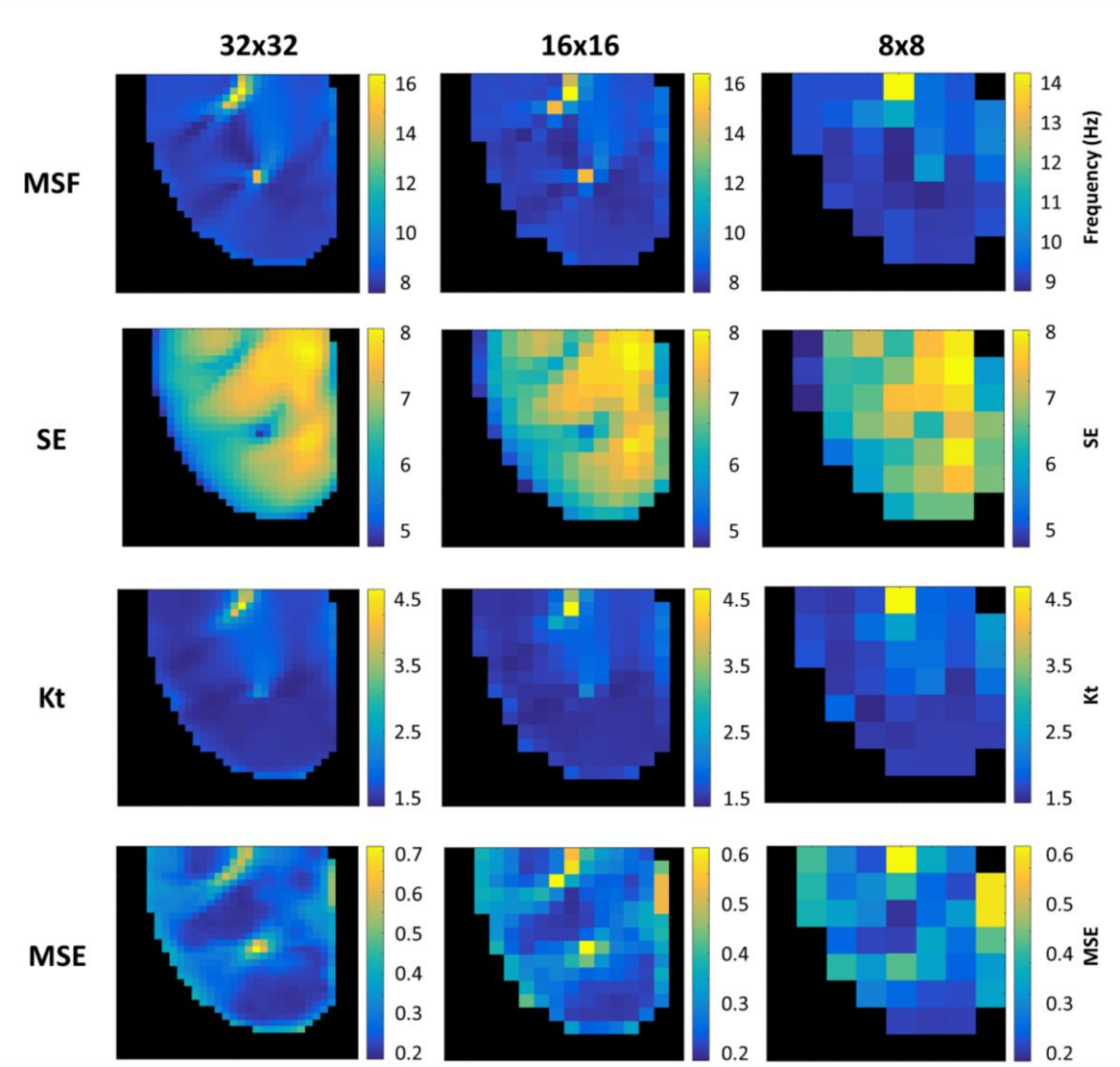

Figure 8.9 2D maps from MSF, SE, Kt, and MSE identifying the meandering and stationary rotors in the figure-of-8 reentry for reduced spatial resolutions of 32x32 (left), 16x16 (middle), and 8x8 pixels (right).

To quantitatively compare the results presented in Figures 8.8 and 8.9, the location of the pivot points for each approach were compared to the "true" location derived from the phase map. Figure 8.10 presents the optimal accuracy of each approach for a reduced time series (Figure 8.10A) and spatial resolution (Figure 8.10B) in which optimized thresholds were used for each time series duration and each spatial resolution. The results are presented as two rotors combined (Figure 8.10, top panels) and then split into separate analysis for the meandering (Figure 8.10, middle panels) and stationary (Figure 8.10, bottom panels) rotor. The MSF, Kt, and MSE approaches all resulted

in high accuracies for identifying the pivot point of the rotors together and individually. High accuracies were maintained under simulated clinical limitations down to 16 x 16 pixels. However, the results of SE were significantly reduced, with the lowest accuracies less than 60% as the spatial resolution decreased.

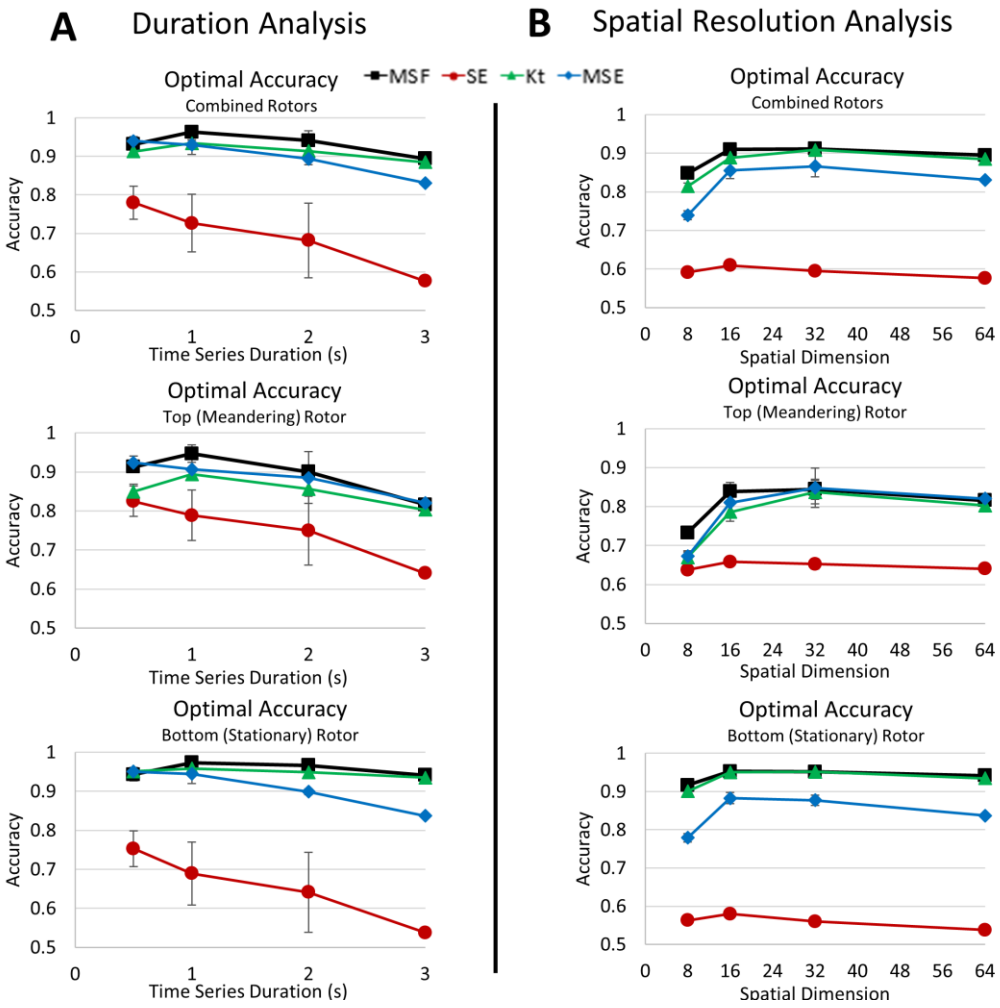

Figure 8.10 Optimal accuracy of each technique to identify the figure-of-8 from Figure 8.7A for reduced duration (A) and spatial resolution analysis (B). The optimal accuracies are shown for the combined rotors (top panel), the top, meandering rotor (middle panel), and the bottom, stationary rotor (bottom panel).

8.5 Discussion

This study evaluated the robustness of the newly developed signal processing techniques to identify the pivot points of the rotors from optical mapping-based experiments. We also simulated

several clinical limitations, specifically reduced spatial resolution and acquisition duration. We used a simplified ventricular arrhythmia model in an ex-vivo heart to demonstrate the potential utility of these techniques in identifying stationary and meandering rotors. The major findings of the manuscript are the following:

(1) MSF, Kt, and MSE were able to identify the rotor pivot point regardless of

(i) progressively reduced acquisition time;

(ii) decreased spatial resolution;

(iii) the presence of meandering rotors;

(2) MSE provided the highest accuracy for the signal stationary rotor;

(3) the MSF approach had the highest accuracy overall for identifying both the stationary and meandering rotors in the figure-of-8 reentry;

(4) the performance of SE approach was clearly diminished due to the large artifacts which reduced accuracy.

The critical value of the results is that these approaches do not rely on repolarization information to pinpoint the rotor and its critical elements. Thus, it is possible that these mathematical approaches may be applied to clinically acquired electrogram data, which may be acquired over short time periods or with limited spatial density. Proving that data reflecting depolarization alone can be used to pinpoint rotor elements is a critical step in proving whether rotors can be accurately identified in clinical, human models of arrhythmia using currently available catheters and electrogram acquisition software.

8.5.1 Efficacy of Each Technique

In examples of both a single rotor and figure-of-8 reentry, the DF map resulted in a single frequency throughout the heart, making the pivot point of the rotor and its periphery indistinguishable. The MSF approach expands upon this frequency approach, which accounts for the chaotic nature at the rotor pivot point by incorporating underlying physiological frequencies in addition to the DF. This approach gave the most accurate localization of the pivot point in the event of both stationary and meandering rotors in the figure-of-8 reentry example. In addition, MSF maintained high accuracy even as the time series duration decreased.

Both SE and Kt indices are based on the voltage intensity distribution and rely on the morphology of the electrical recordings, which significantly changes at the pivot point when compared to the periphery. This difference is reflected in the narrowing of the histogram at the pivot point of the rotor with a corresponding increase in the “peakedness” of the signal. The Kt

maps correctly identified the rotors in both examples, irrespective of time series duration and spatial resolution. However, the SE approach resulted in low contrast between the rotor and periphery reducing its accuracy.

The MSE approach, which relies on the complexity of the electrical signal, was able to consistently differentiate the pivot point from the periphery. In the instance of a single rotor, the accuracy was the highest of the four techniques presented. In the presence of multiple rotors, MSE was able to identify both rotors, however, with a lower accuracy than the MSF approach.

The next steps in this study will include characterizing the accuracy of these techniques in more complex experimental examples. Preliminary results shows the trajectory of the meandering rotor from a numerical simulation, which can be clearly identified using the MSF and MSE techniques. Figure 8.11 presents the analysis of a numerical simulation showing substantial meandering of a rotor in simulated human tissue (25mm x 25mm). The rotor trajectory for this example is shown in the upper right hand corner of the figure. The DF map below does not clearly identify the location of the rotor or its trajectory. The SE map shows the region through which the rotor traverses, but does not clearly show the trajectory and identifies a large portion of the periphery as part of the rotor. Finally the MSF, Kt, and MSE map show the most accurate rotor trajectories, with parts of the rotor path discernable in the final 2D maps. In addition, applying a variety of techniques to clinical examples of ventricular or atrial arrhythmias will assist in determining the reproducibility of the localization of specific rotors. Whether a single technique or combination of processing techniques using depolarization data from intracardiac electrograms may consistently and accurately characterize the location and critical components of rotors remains to be seen, though this work provides some further data on novel processing techniques that may facilitate these results.

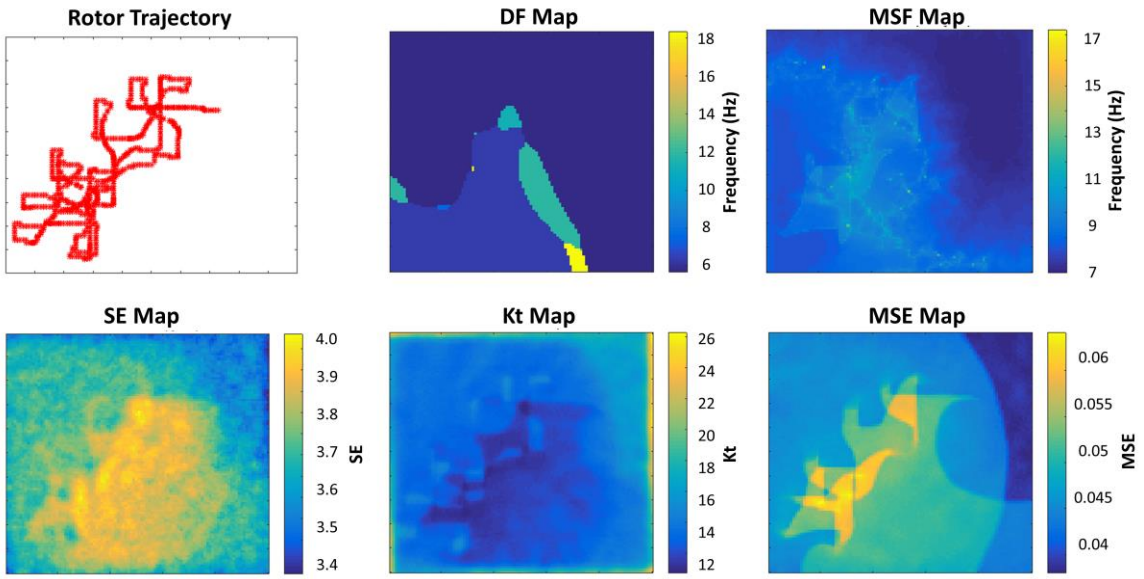

Figure 8.11 2D maps calculated for a meandering rotor in a numerical simulation of human atrial tissue demonstrating the identification of the pivot point of the rotor using DF, MSF, SE, Kt, and MSE techniques.

8.5.2 Clinical Translation

Theories about the "cause and maintenance" of AF and, in turn, identifying optimal ablation targets continue to be an area of active debate. The theory regarding the relevance of rotors dates back to Gordon Moe [190], who noted the presence of organized regions of fundamental reentry may mediate AF (as contrasted with the multiple random wavelet and other hypotheses of the time). He also stated that it is unlikely that any one of these theories of how AF occurs is unlikely to stand alone. In fact, AF is likely a reflection of a variety of pathophysiologic processes – with the manifestation of AF on ECG (as an apparently random activity within the atria) being a complex process that may be subserved by any one of a number of pathophysiologic processes that may co-exist in the same individual or be the primary mediator in a given individual. Thus, the scientific process to demonstrate that (1) a rotor exists; (2) these rotors play a principal role in AF propagation; and (3) that ablating these rotors actually has relevance to "curing" AF is inherently complex, particularly if it is possible for multiple mechanisms to co-exist or for the mechanism to vary between patients with inherently different substrates.

That being said, invasive treatment of AF in humans still has major gaps. While true that data of additive approaches beyond pulmonary vein isolation (PVI) (e.g., linear lines, rotor ablation, complex fractionated electrogram ablation, autonomic ganglia ablation) have not consistently

shown benefit, debates continue to abound regarding patient selection and decision making on individualized approaches to the appropriate lesion set. Additionally, in many cases of AF, the best cases outcomes after multiple ablations in certain patients (e.g., persistent AF) continues to be in the 50-60% range.

The principal question is, thus, whether currently available techniques that are used to make sense of the signals acquired during AF are sufficient to define "relevant substrate" or whether we should accept that all patients in whom PVI is ineffective must be subject to a lifetime of incurable AF, or whether a more "random" approach to treatment (e.g., empiric lines), or an approach that relies on targeting signals purely based on current methods of signal processing should be used.

It is our belief that identifying better ways of processing the acquired signals during intracardiac mapping may help in further critically understanding relevant arrhythmic substrate to AF pathogenesis in individuals. Our findings demonstrate difference between various signal processing techniques in accurately and consistently defining seemingly organized zones of activity. In addition, current clinically available approaches may have limitations, such as with the DF approach, which points to the fact that the lack of success of additive approaches to AF ablation beyond PVI may be limited not simply due to "futility" of such approaches but also to lack of tools to adequately define the relevant areas.

We further agree that any ablation, as much as it has the capacity to eliminate arrhythmia, also has the potential to create substrate for arrhythmia. This paper does not seek to say that these rotor zones will ultimately be the sites to target for ablation – instead they may represent zones of critical activity that may be targeted by other mechanisms or point to utility of specific types of antiarrhythmic medications based on their mechanism of action due to the presence of such rotors in specific individuals.

Here, we have evaluated the potential utility of alternative signal processing approaches defining critical areas responsible for arrhythmia propagation. The use of less complex arrhythmia examples highlights the differences in the mathematical approaches presented here and showing potential to be further expanded to progressively more complex examples. Future work includes applying these approaches to (1) optically mapped examples of AF and VF and (2) comprehensively mapped clinical human examples of AF.

8.5.3 Limitations

This study is characterized by several limitations. First, these analyses were performed using data acquired through optical mapping in an experimental animal model of ventricular arrhythmia.

Thus, applicability of these analyses to intracardiac electrograms, which have variable filtering and localization methodologies, is unclear. In addition to the general limitations that are associated with obtaining the pivot point of the rotor is the dependence of the exact measurement locations in identifying the source of the arrhythmia. The optical mapping data has a high spatial resolution, and therefore the core of the rotor can be identified with a high accuracy. In simulating a reduction in spatial resolution, the results demonstrated that when measurements were not taken from the core, the rotor may not be identified. In the 8 x 8 pixel analysis of the figure-of-8 reentry example, the 2D mapping techniques were unable to identify the stationary rotor as there were no direct measurements taken from within the core.

Another limitation of this study is the complexity of the arrhythmias analyzed. The optical mapping examples presented are on the lower end of complexity with uniform propagation through the tissue. In the presence of multiple wavebreaks, as occurs during AF, there will be additional complexity and irregularity in the electrical signals recorded which could affect the overall sensitivity and specificity of the mapping techniques presented. In addition, the data obtained from analysis of ventricular arrhythmias may not be directly applicable to atrial arrhythmias due to different atrial wall thickness and fundamental electrophysiological differences between these chambers. Finally, our examples of point acquisition during optical mapping are uniform. However, during intracardiac mapping, the points obtained may be affected by catheter orientation relative to the underlying myocardium, randomly distributed with clustering of points in specific areas, and include far field data from other structures. Thus, validation of these data when considering these increasing orders of complexity remains to be studied.

8.6 Conclusion

These results motivate further validation using intracardiac electrograms to determine if these approaches can identify pivot points in a clinical setting. It also highlights the potential utility of more experimental data in identifying which single technique or combination of techniques is necessary to accurately characterize rotors in various arrhythmia states. More accurate rotor localization could offer improved method of characterizing arrhythmias and, in turn, offer a means by which to more accurately study whether or not rotor ablation is a viable and effective treatment.

Chapter 9

Part 2 Conclusions

9.1 Conclusions

Atrial fibrillation (AF) impacts 33.5 million people worldwide with diagnoses each year continuing to rise. Patients are often treated with pharmacological agents for the short-term management, to return the patient to normal sinus rhythm, and long-term management, to reduce AF-associated risks when the arrhythmia is unable to be controlled. Another treatment options for patients is catheter ablation to isolate the pulmonary veins, a region of increased ectopic activity and a possible source of the arrhythmia. For some patients, namely those with paroxysmal AF, this approach is relatively successful, terminating AF in approximately 7 out of 10 patients. However, for those with persistent AF or long-standing AF, this treatment approach has suboptimal success, with only 2 in 10 ablation procedures terminating the arrhythmia.

One of the largest hurdles to appropriately targeting and subsequently terminating the arrhythmia in catheter ablation procedures is the lack of understanding of the spatial organization of AF. Multiple theories exists to explain the initiation and maintenance of arrhythmia, however the complex progression of AF and the large patient variability present significant challenges to clinically mapping the electrical activity in the atria. Numerous mapping techniques have been evaluated clinically to guide ablation procedures, but have not significantly improved patient outcomes. There is a clinical need for more accurate and robust mapping techniques to help enhance our understanding of the underlying spatial organization of the arrhythmia and to guide ablation procedures and ultimately improve outcomes.

Here, we have evaluated the potential utility of alternative signal processing approaches defining critical areas responsible for arrhythmia propagation. Optical mapping studies were used to validate new signal processing techniques – multiscale frequency (MSF), kurtosis (Kt), Shannon entropy (SE), and multiscale entropy (MSE) – to identify regions of abnormal electrical activity. These studies allow for the visualization of electrical activity, both activation and recovery, in the heart through the use of voltage sensitive dye [242, 243], and allow for accurate localization of pivot point of rotors in episodes of fibrillation, providing a good platform for validating mapping techniques [201, 206].

Our findings reveal differences between various novel signal processing techniques in accurately and consistently identifying rotors or regions of functional reentry. These results demonstrate that MSF, Kt, and MSE accurately identified both stationary and meandering rotors, and these techniques remained accurate under simulated clinical limitations: shortened electrogram duration and decreased spatial resolution. In addition, the results demonstrate the limitations of the clinically available dominant frequency approach, which points to the fact that the lack of success of additive approaches to AF ablation beyond pulmonary vein isolation may be limited not simply due to "futility" of such approaches but also to lack of tools to adequately define the relevant areas. More accurate rotor localization could offer improved method of characterizing arrhythmias and, in turn, offer a means by which to more accurately study whether or not rotor ablation is a viable and effective treatment.

The use of less complex arrhythmia examples from optical mapping studies highlights the differences in the mathematical approaches presented here and allows for validation of rotor identification. Further, the examples presented show potential to be further expanded to progressively more complex examples in simulated arrhythmias and clinical intracardiac electrograms. These results also highlight the potential utility of more experimental data in identifying which single technique or combination of techniques is necessary to accurately characterize rotors in various arrhythmia states.

9.2 Future Work

Further research in this area is necessary to translate and validate these techniques for clinical studies where unipolar and bipolar intracardiac electrograms are used to evaluate and guide ablation for AF patients. First, future work will apply these novel techniques to more complex arrhythmias in experimental and simulated cardiac arrhythmia examples. Converting transmembrane voltage signals to equivalent unipolar and bipolar electrogram recordings can provide an indication of whether the techniques will be effective in identifying rotors in a different representation of the cardiac electrical signal. In addition, further research may reveal that a combination of mapping techniques provides more accurate rotor localization compared to a single mapping technique alone. These studies will allow for further validation of these techniques prior to implementation in a clinical setting.

Once validated, future studies will apply these techniques to recorded intracardiac electrograms recorded in patients with paroxysmal and non-paroxysmal AF both before and after ablation to

evaluate whether the new mapping techniques could successfully predict arrhythmia termination based on pre- and post-ablation recordings. With successful implementation of these novel mapping techniques, the ultimate goal is to integrate these techniques with current mapping system to evaluate arrhythmias in real-time and guide ablation therapy to improve the percentage of patients who are arrhythmia free after ablation procedures.

Bibliography

[1] N. R. F. Collaboration, "Worldwide trends in blood pressure from 1975 to 2015: a pooled analysis of 1479 population-based measurement studies with 19· 1 million participants," *The Lancet,* vol. 389, no. 10064, pp. 37-55, 2017.

[2] S. S. Chugh *et al.*, "Worldwide epidemiology of atrial fibrillation: a Global Burden of Disease 2010 Study," *Circulation,* 113.005119, 2013.

[3] P. K. Whelton *et al.*, "2017 ACC/AHA/AAPA/ABC/ACPM/AGS/APhA/ASH/ASPC/NMA/PCNA guideline for the prevention, detection, evaluation, and management of high blood pressure in adults: a report of the American College of Cardiology/American Heart Association Task Force on Clinical Practice Guidelines," *Hypertension,* vol. 71, no. 6, pp. e13-e115, 2018.

[4] S. Dixit, D. Lin, D. S. Frankel, and F. E. Marchlinski, "Catheter ablation for persistent atrial fibrillation: antral pulmonary vein isolation and elimination of nonpulmonary vein triggers are sufficient," *Circ-Arrhythmia Elec,* vol. 5, no. 6, pp. 1216-1223, 2012.

[5] G. Fassini *et al.*, "Left mitral isthmus ablation associated with PV isolation: long-term results of a prospective randomized study," *J Cardiov Electr,* vol. 16, no. 11, pp. 1150-1156, 2005.

[6] S. Willems *et al.*, "Substrate modification combined with pulmonary vein isolation improves outcome of catheter ablation in patients with persistent atrial fibrillation: a prospective randomized comparison," *Eur Heart J,* vol. 27, no. 23, pp. 2871-2878, 2006.

[7] G. Mancia and G. Grassi, "The autonomic nervous system and hypertension," *Circ Res,* vol. 114, no. 11, pp. 1804-1814, 2014.

[8] A. C. Carlsson *et al.*, "Association Between Circulating Endostatin, Hypertension Duration, and Hypertensive Target-Organ DamageNovelty and Significance," *Hypertension,* vol. 62, no. 6, pp. 1146-1151, 2013.

[9] Q. Nguyen, J. Dominguez, L. Nguyen, and N. Gullapalli, "Hypertension management: an update," *American Health & Drug Benefits,* vol. 3, no. 1, p. 47, 2010.

[10] S. J. Shah and R. S. Stafford, "Current Trends of Hypertension Treatment in the United States," *Am J Hypertens,* vol. 30, no. 10, pp. 1008-1014, 2017.

[11] S. K. Nadar, M. H. Tayebjee, F. Messerli, and G. Y. Lip, "Target organ damage in hypertension: pathophysiology and implications for drug therapy," *Curr Pharm Design,* vol. 12, no. 13, pp. 1581-1592, 2006.

[12] P. Greenland *et al.*, "Major risk factors as antecedents of fatal and nonfatal coronary heart disease events," *JAMA,* vol. 290, no. 7, pp. 891-897, 2003.

[13] P. Muntner, J. He, L. Hamm, C. Loria, and P. K. Whelton, "Renal insufficiency and subsequent death resulting from cardiovascular disease in the United States," *J Am Soc Nephrol,* vol. 13, no. 3, pp. 745-753, 2002.

[14] M. H. Drazner, "The progression of hypertensive heart disease," *Circulation,* vol. 123, no. 3, pp. 327-334, 2011.

[15] B. C. Berk, K. Fujiwara, and S. Lehoux, "ECM remodeling in hypertensive heart disease," *J Clin Invest,* vol. 117, no. 3, pp. 568-575, 2007.

[16] C. W. Yancy *et al.*, "2016 ACC/AHA/HFSA focused update on new pharmacological therapy for heart failure: an update of the 2013 ACCF/AHA guideline for the management of heart failure: a report of the American College of Cardiology/American Heart Association Task Force on Clinical Practice Guidelines and the Heart Failure Society of America," *J Card Fail,* vol. 22, no. 9, pp. 659-669, 2016.

[17] R. S. Vasan and D. Levy, "The role of hypertension in the pathogenesis of heart failure: a clinical mechanistic overview," *Archives of Internal Medicine,* vol. 156, no. 16, pp. 1789-1796, 1996.

[18] G. Bakris and M. Sorrentino, "Redefining Hypertension—Assessing the New Blood-Pressure Guidelines," *New Engl J Med,* 2018.

[19] M. Kallistratos, L. Poulimenos, and A. Manolis, "Arterial hypertension: benefits and limitations of treatment," *E-Journal Cardiol. Practice,* vol. 11, no. 13, p. 28, 2015.

[20] S. Oparil and R. E. Schmieder, "New approaches in the treatment of hypertension," *Circ Res,* vol. 116, no. 6, pp. 1074-1095, 2015.

[21] D. A. Calhoun *et al.*, "Resistant hypertension: diagnosis, evaluation, and treatment," *Circulation,* vol. 117, no. 25, pp. e510-e526, 2008.

[22] G. Mazzaglia *et al.*, "Patterns of persistence with antihypertensive medications in newly diagnosed hypertensive patients in Italy: a retrospective cohort study in primary care," *J Hypertens,* vol. 23, no. 11, pp. 2093-2100, 2005.

[23] B. L. Van Wijk, O. H. Klungel, E. R. Heerdink, and A. de Boer, "Rate and determinants of 10-year persistence with antihypertensive drugs," *J Hypertens,* vol. 23, no. 11, pp. 2101-2107, 2005.

[24] E. R. Carthy, "Autonomic dysfunction in essential hypertension: a systematic review," *Annals of Medicine and Surgery,* vol. 3, no. 1, pp. 2-7, 2014.

[25] C. Tsioufis *et al.*, "Pathophysiology of resistant hypertension: the role of sympathetic nervous system," *International Journal of Hypertension,* vol. 2011, 2011.

[26] R. Klabunde, *Cardiovascular Physiology Concepts*. Lippincott Williams & Wilkins, 2011.

[27] T. A. Fischell *et al.*, "Transcatheter alcohol-mediated perivascular renal denervation with the peregrine system: first-in-human experience," *JACC-Cardiovasc Inte,* vol. 9, no. 6, pp. 589-598, 2016.

[28] H. Mussalo *et al.*, "Baroreflex sensitivity in essential and secondary hypertension," *Clin Auton Res,* vol. 12, no. 6, pp. 465-471, 2002.

[29] O. Ormezzano, J.-L. Cracowski, J.-L. Quesada, H. Pierre, J.-M. Mallion, and J.-P. Baguet, "EVAluation of the prognostic value of BARoreflex sensitivity in hypertensive patients: the EVABAR study," *J Hypertens,* vol. 26, no. 7, pp. 1373-1378, 2008.

[30] A. Yoruk, J. D. Bisognano, and J. P. Gassler, "Baroreceptor stimulation for resistant hypertension," *Am J Hypertens,* vol. 29, no. 12, pp. 1319-1324, 2016.

[31] I. J. Scheffers *et al.*, "Novel baroreflex activation therapy in resistant hypertension: results of a European multi-center feasibility study," *J Am Coll Cardiol,* vol. 56, no. 15, pp. 1254-1258, 2010.

[32] J. D. Bisognano *et al.*, "Baroreflex activation therapy lowers blood pressure in patients with resistant hypertension: results from the double-blind, randomized, placebo-controlled rheos pivotal trial," *J Am Coll Cardiol,* vol. 58, no. 7, pp. 765-773, 2011.

[33] U. C. Hoppe *et al.*, "Minimally invasive system for baroreflex activation therapy chronically lowers blood pressure with pacemaker-like safety profile: results from the Barostim neo trial," *J Am Soc Hypertens,* vol. 6, no. 4, pp. 270-276, 2012.

[34] J. W. Osborn and J. D. Foss, "Renal Nerves and Long-Term Control of Arterial Pressure," *Compr Physiol,* 2017.

[35] G. F. Dibona and U. C. Kopp, "Neural control of renal function," *Physiol Rev,* vol. 77, no. 1, pp. 75-197, 1997.

[36] J. W. Osborn and C. T. Banek, "Catheter-Based Renal Nerve Ablation as a Novel Hypertension Therapy: Lost, and Then Found, in Translation," *Hypertension,* vol. 71, no. 3, pp. 383-388, 2018.

[37] U. C. Kopp, "Role of renal sensory nerves in physiological and pathophysiological conditions," *Am J Physiol-Reg I,* vol. 308, no. 2, pp. R79-R95, 2014.

[38] A. Stella and A. Zanchetti, "Functional role of renal afferents," *Physiol Rev,* vol. 71, no. 3, pp. 659-682, 1991.

[39] L. C. Booth, C. N. May, and S. T. Yao, "The role of the renal afferent and efferent nerve fibers in heart failure," *Front Physiol,* vol. 6, p. 270, 2015.

[40] H. Krum *et al.*, "Catheter-based renal sympathetic denervation for resistant hypertension: a multicentre safety and proof-of-principle cohort study," *The Lancet,* vol. 373, no. 9671, pp. 1275-1281, 2009.

[41] H. Krum *et al.*, "Percutaneous renal denervation in patients with treatment-resistant hypertension: final 3-year report of the Symplicity HTN-1 study," *The Lancet,* vol. 383, no. 9917, pp. 622-629, 2014.

[42] S. H.-. Investigators, "Renal sympathetic denervation in patients with treatment-resistant hypertension (The Symplicity HTN-2 Trial): a randomised controlled trial," *The Lancet,* vol. 376, no. 9756, pp. 1903-1909, 2010.

[43] D. E. Kandzari *et al.*, "Catheter-based renal denervation for resistant hypertension: rationale and design of the SYMPLICITY HTN-3 Trial," *Clin Cardiol,* vol. 35, no. 9, pp. 528-535, 2012.

[44] M. Esler, "Illusions of truths in the Symplicity HTN-3 trial: generic design strengths but neuroscience failings," *J Am Soc Hypertens,* vol. 8, no. 8, pp. 593-598, 2014.

[45] D. E. Kandzari *et al.*, "Predictors of blood pressure response in the SYMPLICITY HTN-3 trial," *Eur Heart J,* vol. 36, no. 4, pp. 219-227, 2014.

[46] R. R. Townsend *et al.*, "Catheter-based renal denervation in patients with uncontrolled hypertension in the absence of antihypertensive medications (SPYRAL HTN-OFF MED): a randomised, sham-controlled, proof-of-concept trial," *The Lancet,* vol. 390, no. 10108, pp. 2160-2170, 2017.

[47] D. E. Kandzari *et al.*, "The SPYRAL HTN Global Clinical Trial Program: Rationale and design for studies of renal denervation in the absence (SPYRAL HTN OFF-MED) and presence (SPYRAL HTN ON-MED) of antihypertensive medications," *Am Heart J,* vol. 171, no. 1, pp. 82-91, 2016.

[48] H. C. Patel, C. Hayward, and C. Di Mario, "SYMPLICITY HTN 3: The death knell for renal denervation in hypertension?," *Global Cardiology Science and Practice,* p. 15, 2014.

[49] H.-R. Berthoud and W. L. Neuhuber, "Functional and chemical anatomy of the afferent vagal system," *Auton Neurosci-Basic,* vol. 85, no. 1, pp. 1-17, 2000.

[50] J. Nolte and J. Sundsten, "Cranial nerves and their nuclei," *The Human Brain: an Introduction to its Functional Anatomy (5th edition),* Mosby, Philadelphia, p. 303, 2002.

[51] M. A. Patestas and L. P. Gartner, *A textbook of neuroanatomy*. John Wiley & Sons, 2016.

[52] F. H. Netter, "Atlas of human anatomy," 2016.

[53] H. D. Schultz, "Cardiac vagal chemosensory afferents," *Ann Ny Acad Sci,* vol. 940, no. 1, pp. 59-73, 2001.

[54] J. Hall, "Nervous regulation of the circulation and rapid control of arterial pressure," *Guyton and Hall Textbook of Medical Physiology,* vol. 12, pp. 201-211, 2011.

[55] H. Yuan and S. D. Silberstein, "Vagus nerve and vagus nerve stimulation, a comprehensive review: part I," *Headache: The Journal of Head and Face Pain,* vol. 56, no. 1, pp. 71-78, 2016.

[56] S. Gilman and S. W. Newman, *Manter and Gatz's Essentials of Clinical Neuroanatomy and Neurophysiology*. FA Davis, 1996.

[57] J. L. Ardell and W. C. Randall, "Selective vagal innervation of sinoatrial and atrioventricular nodes in canine heart," *American Journal of Physiology-Heart and Circulatory Physiology,* vol. 251, no. 4, pp. H764-H773, 1986.

[58] H. M. Stauss, "Differential hemodynamic and respiratory responses to right and left cervical vagal nerve stimulation in rats," *Physiological Reports,* vol. 5, no. 7, p. e13244, 2017.

[59] M. Durand, A. Mota, A. Barale, J. Castania, R. Fazan Jr, and H. Salgado, "Time course of the hemodynamic responses to aortic depressor nerve stimulation in conscious spontaneously hypertensive rats," *Brazilian Journal of Medical and Biological Research,* vol. 45, no. 5, pp. 444-449, 2012.

[60] M. W. Chapleau, D. L. Rotella, J. J. Reho, K. Rahmouni, and H. M. Stauss, "Chronic vagal nerve stimulation prevents high-salt diet-induced endothelial dysfunction and aortic stiffening in stroke-prone spontaneously hypertensive rats," *Am J Physiol-Heart C,* vol. 311, no. 1, pp. H276-H285, 2016.

[61] M. Gierthmuehlen, T. Stieglitz, J. Zentner, and D. T. Plachta, "Haemodynamic responses to selective vagal nerve stimulation under enalapril medication in rats," *PloS one,* vol. 11, no. 1, p. e0147045, 2016.

[62] D. T. Plachta *et al.*, "Blood pressure control with selective vagal nerve stimulation and minimal side effects," *J Neural Eng,* vol. 11, no. 3, p. 036011, 2014.

[63] D. T. Plachta, J. Zentner, D. Aguirre, O. Cota, T. Stieglitz, and M. Gierthmuehlen, "Effect of Cardiac-Cycle-Synchronized Selective Vagal Stimulation on Heart Rate and Blood Pressure in Rats," *Adv Ther,* vol. 33, no. 7, pp. 1246-1261, 2016.

[64] M. Gierthmuehlen, D. Aguirre, O. Cota, J. Zentner, T. Stieglitz, and D. T. Plachta, "Influence of Clonidine on Antihypertensive Selective Afferent Vagal Nerve Stimulation in Rats," *Neuromodulation: Technology at the Neural Interface,* vol. 19, no. 6, pp. 597-606, 2016.

[65] J. F. Nonidez, "The aortic (depressor) nerve and its associated epithelioid body, the glomus aorticum," *Dev Dynam,* vol. 57, no. 2, pp. 259-301, 1935.

[66] M. T. La Rovere *et al.*, "Baroreflex sensitivity and heart rate variability in the identification of patients at risk for life-threatening arrhythmias: implications for clinical trials," *Circulation,* vol. 103, no. 16, pp. 2072-2077, 2001.

[67] A. K. Schuster, J. E. Fischer, J. F. Thayer, D. Mauss, and M. N. Jarczok, "Decreased heart rate variability correlates to increased cardiovascular risk," *Int J Cardiol,* vol. 203, pp. 728-730, 2016.

[68] W. Zhou, A. Mahajan, K. Yamamoto, K. Yamakawa, and A. Mahajan, "Effect of vagal nerve stimulation on heart rate variability in a porcine model (1169.17)," *The FASEB Journal,* vol. 28, no. 1 Supplement, p. 1169.17, 2014.

[69] Y. Zhang *et al.*, "Chronic Vagus Nerve Stimulation Improves Autonomic Control and Attenuates Systemic Inflammation and Heart Failure Progression in a Canine High-Rate Pacing ModelCLINICAL PERSPECTIVE," *Circ-Heart Fail,* vol. 2, no. 6, pp. 692-699, 2009.

[70] I. Libbus, B. D. Nearing, B. Amurthur, B. H. KenKnight, and R. L. Verrier, "Quantitative evaluation of heartbeat interval time series using Poincaré analysis reveals distinct patterns of heart rate dynamics during cycles of vagus nerve stimulation in patients with heart failure," *J Electrocardiol,* vol. 50, no. 6, pp. 898-903, 2017.

[71] S. Akselrod, D. Gordon, F. A. Ubel, D. C. Shannon, A. Berger, and R. J. Cohen, "Power spectrum analysis of heart rate fluctuation: a quantitative probe of beat-to-beat cardiovascular control," *Science,* vol. 213, no. 4504, pp. 220-222, 1981.

[72] R. K. Premchand *et al.*, "Autonomic Regulation Therapy via Left or Right Cervical Vagus Nerve Stimulation in Patients With Chronic Heart Failure: Results of the ANTHEM-HF Trial," *J Card Fail,* vol. 20, no. 11, pp. 808-816, Nov 2014.

[73] F. Shaffer and J. Ginsberg, "An overview of heart rate variability metrics and norms," *Frontiers in Public Health,* vol. 5, p. 258, 2017.

[74] J. L. Ardell *et al.*, "Vagus nerve stimulation normalizes autonomic neural processing and reduces cardiac hypertrophy in a canine model of preserved ejection fraction heart failure," ed: *Am Heart Assoc,* 2016.

[75] J. J. Hamann *et al.*, "Vagus nerve stimulation improves left ventricular function in a canine model of chronic heart failure," *EurJ Heart Fail,* vol. 15, no. 12, pp. 1319-1326, 2013.

[76] Y. Zhang, I. Ilsar, H. N. Sabbah, T. B. David, and T. N. Mazgalev, "Relationship between right cervical vagus nerve stimulation and atrial fibrillation inducibility: therapeutic intensities do not increase arrhythmogenesis," *Heart Rhythm,* vol. 6, no. 2, pp. 244-250, 2009.

[77] K. Lemola *et al.*, "Pulmonary vein region ablation in experimental vagal atrial fibrillation: role of pulmonary veins versus autonomic ganglia," *Circulation,* vol. 117, no. 4, pp. 470-477, 2008.

[78] P. Schauerte *et al.*, "Catheter ablation of cardiac autonomic nerves for prevention of vagal atrial fibrillation," *Circulation,* vol. 102, no. 22, pp. 2774-2780, 2000.

[79] Y. Zhang and T. N. Mazgalev, "Arrhythmias and vagus nerve stimulation," *Heart Fail Rev,* vol. 16, no. 2, pp. 147-161, 2011.

[80] Y. Sha *et al.*, "Low-Level Right Vagal Stimulation: Anticholinergic and Antiadrenergic Effects," *J Cardiovasc Electr,* vol. 22, no. 10, pp. 1147-1153, 2011.

[81] X. Sheng *et al.*, "Prevention and reversal of atrial fibrillation inducibility and autonomic remodeling by low-level vagosympathetic nerve stimulation," *J Am Coll Cardiol,* vol. 57, no. 5, pp. 563-571, 2011.

[82] L. Yu *et al.*, "Low-level vagosympathetic nerve stimulation inhibits atrial fibrillation inducibility: direct evidence by neural recordings from intrinsic cardiac ganglia," *J Cardiovasc Electr,* vol. 22, no. 4, pp. 455-463, 2011.

[83] S. Stavrakis *et al.*, "Low-level transcutaneous electrical vagus nerve stimulation suppresses atrial fibrillation," *J Am Coll Cardiol,* vol. 65, no. 9, pp. 867-875, 2015.

[84] S. Stavrakis *et al.*, "Low-level vagus nerve stimulation suppresses post-operative atrial fibrillation and inflammation: a randomized study," *JACC-Clin Electrophysiol,* vol. 3, no. 9, pp. 929-938, 2017.

[85] S. Salavatian *et al.*, "Vagal stimulation targets select populations of intrinsic cardiac neurons to control neurally induced atrial fibrillation," *Am J Physiol-Heart C,* vol. 311, no. 5, pp. H1311-H1320, 2016.

[86] S. Ansari, K. Chaudhri, and K. Al Moutaery, "Vagus nerve stimulation: indications and limitations," in *Operative Neuromodulation*: Springer, 2007, pp. 281-286.

[87] A. H. Milby, C. H. Halpern, and G. H. Baltuch, "Vagus nerve stimulation for epilepsy and depression," *Neurotherapeutics,* vol. 5, no. 1, pp. 75-85, 2008.

[88] P. J. Schwartz *et al.*, "Long term vagal stimulation in patients with advanced heart failure First experience in man," *Eur J Heart Fail,* vol. 10, no. 9, pp. 884-891, 2008.

[89] E. Ben-Menachem, "Vagus nerve stimulation, side effects, and long-term safety," *J Clin Neuro,* vol. 18, no. 5, pp. 415-418, 2001.

[90] W. A. Huang, K. Shivkumar, and M. Vaseghi, "Device-based autonomic modulation in arrhythmia patients: the role of vagal nerve stimulation," *Current Treatment Options in Cardiovascular Medicine,* vol. 17, no. 5, p. 22, 2015.

[91] G. A. Ng, "Vagal modulation of cardiac ventricular arrhythmia," *Exp Physiol,* vol. 99, no. 2, pp. 295-299, 2014.

[92] J. Huang *et al.*, "Vagus nerve stimulation reverses ventricular electrophysiological changes induced by hypersympathetic nerve activity," *Exp Physiol,* vol. 100, no. 3, pp. 239-248, 2015.

[93] K. Yamakawa *et al.*, "Electrophysiological effects of right and left vagal nerve stimulation on the ventricular myocardium," *Am J Physiol-Heart C*, vol. 307, no. 5, pp. H722-H731, 2014.

[94] J. B. Martins and D. P. Zipes, "Effects of sympathetic and vagal nerves on recovery properties of the endocardium and epicardium of the canine left ventricle," *Circ Res*, vol. 46, no. 1, pp. 100-110, 1980.

[95] K. E. Brack, V. H. Patel, J. H. Coote, and G. A. Ng, "Nitric oxide mediates the vagal protective effect on ventricular fibrillation via effects on action potential duration restitution in the rabbit heart," *J Physiol-London*, vol. 583, no. 2, pp. 695-704, Sep 1 2007.

[96] K. E. Brack, J. H. Coote, and G. A. Ng, "Vagus nerve stimulation protects against ventricular fibrillation independent of muscarinic receptor activation," *Cardiovasc Res*, vol. 91, no. 3, pp. 437-446, Aug 1 2011.

[97] C. Zheng, M. Li, M. Inagaki, T. Kawada, K. Sunagawa, and M. Sugimachi, "Vagal stimulation markedly suppresses arrhythmias in conscious rats with chronic heart failure after myocardial infarction," in *Engineering in Medicine and Biology Society, 2005. IEEE-EMBS 2005. 27th Annual International Conference of the*, 2006, pp. 7072-7075: IEEE.

[98] M. Ando *et al.*, "Efferent vagal nerve stimulation protects heart against ischemia-induced arrhythmias by preserving connexin43 protein," *Circulation*, vol. 112, no. 2, pp. 164-170, Jul 12 2005.

[99] W. Wu and Z. Lu, "Loss of anti-arrhythmic effect of vagal nerve stimulation on ischemia-induced ventricular tachyarrhythmia in aged rats," *The Tohoku Journal of Experimental Medicine*, vol. 223, no. 1, pp. 27-33, 2011.

[100] R. G. Katare *et al.*, "Vagal nerve stimulation prevents reperfusion injury through inhibition of opening of mitochondrial permeability transition pore independent of the bradycardiac effect," *The Journal of Thoracic and Cardiovascular Surgery*, vol. 137, no. 1, pp. 223-231, 2009.

[101] K. E. Brack, V. H. Patel, R. Mantravardi, J. H. Coote, and G. A. Ng, "Direct evidence of nitric oxide release from neuronal nitric oxide synthase activation in the left ventricle as a result of cervical vagus nerve stimulation," *J Physiol-London*, vol. 587, no. 12, pp. 3045-3054, Jun 15 2009.

[102] P. J. Marvar, H. Lob, A. Vinh, F. Zarreen, and D. G. Harrison, "The central nervous system and inflammation in hypertension," *Curr Opin Pharmacol*, vol. 11, no. 2, pp. 156-161, 2011.

[103] L. E. Bautista, J. E. Atwood, P. G. O'malley, and A. J. Taylor, "Association between C-reactive protein and hypertension in healthy middle-aged men and women," *Coronary Artery Dis*, vol. 15, no. 6, pp. 331-336, 2004.

[104] D. L. Mann, "Inflammatory mediators and the failing heart: past, present, and the foreseeable future," *Circ Res,* vol. 91, no. 11, pp. 988-998, 2002.

[105] G. J. Blake, N. Rifai, J. E. Buring, and P. M. Ridker, "Blood pressure, C-reactive protein, and risk of future cardiovascular events," *Circulation,* vol. 108, no. 24, pp. 2993-2999, 2003.

[106] H. D. Sesso, J. E. Buring, N. Rifai, G. J. Blake, J. M. Gaziano, and P. M. Ridker, "C-reactive protein and the risk of developing hypertension," *JAMA,* vol. 290, no. 22, pp. 2945-2951, 2003.

[107] Q. N. Dinh, G. R. Drummond, C. G. Sobey, and S. Chrissobolis, "Roles of inflammation, oxidative stress, and vascular dysfunction in hypertension," *BioMed Research International,* vol. 2014, 2014.

[108] K. J. Tracey, "Physiology and immunology of the cholinergic antiinflammatory pathway," *J Clin Invest,* vol. 117, no. 2, pp. 289-296, Feb 2007.

[109] B. Olshansky, "Vagus nerve modulation of inflammation: cardiovascular implications," *Trends Cardiovas Med,* vol. 26, no. 1, pp. 1-11, 2016.

[110] Y. Zhang *et al.*, "Chronic vagus nerve stimulation improves autonomic control and attenuates systemic inflammation and heart failure progression in a canine high-rate pacing model," *Circ-Heart Fail,* vol. 2, no. 6, pp. 692-699, Nov 2009.

[111] K. Gong, G. Song, J. Spiers, E. Kelso, and Z. Zhang, "Activation of immune and inflammatory systems in chronic heart failure: novel therapeutic approaches," *Int J Clin Pract,* vol. 61, no. 4, pp. 611-621, 2007.

[112] W. Li and B. Olshansky, "Inflammatory cytokines and nitric oxide in heart failure and potential modulation by vagus nerve stimulation," *Heart Fail Rev,* vol. 16, no. 2, pp. 137-145, 2011.

[113] S. von Haehling, J. C. Schefold, M. Lainscak, W. Doehner, and S. D. Anker, "Inflammatory biomarkers in heart failure revisited: much more than innocent bystanders," *Heart Fail Clin,* vol. 5, no. 4, pp. 549-560, 2009.

[114] G. Mancia, J. C. Romero, and J. T. Shepherd, "Continuous inhibition of renin release in dogs by vagally innervated receptors in the cardiopulmonary region," *Circ Res,* vol. 36, no. 4, pp. 529-535, 1975.

[115] World Health Organization, *The world health report 2002: reducing risks, promoting healthy life*. World Health Organization, 2002.

[116] S. Lalande and B. D. Johnson, "Diastolic dysfunction: A link between hypertension and heart failure," *Drugs of Today,* vol. 44, no. 7, pp. 503-513, Jul 2008.

[117] S. Julius and M. Valentini, "Consequences of the increased autonomic nervous drive in hypertension, heart failure and diabetes," *Blood Pressure,* vol. 7, no. SUPPL. 3, pp. 5-13, 1998 1998.

[118] H. Bettermann, D. Cysarz, and H. C. Kummell, "Heart rate variability: How to assess effects of mild therapies on autonomic control in small groups of mild and borderline hypertensives?," *Hypertension,* vol. 35, no. 2, pp. E6-+, Feb 2000.

[119] J. M. Ormaetxe, J. D. M. Alday, J. Almendral, M. A. Beobide, and M. Iriarte, "Prognostic significance of ventricular arrhythmias in the presence of pathological left-ventricular hypertrophy," *Eur Heart J,* vol. 14, pp. 73-75, Nov 1993.

[120] J. Almendral, J. P. Villacastin, A. Arenal, L. Tercedor, J. L. Merino, and J. L. Delcan, "Evidence favoring the hypothesis that ventricular arrhythmias have prognostic significance in left-ventricular hypertrophy secondary to systemic hypertension," *Am J Cardiol,* vol. 76, no. 13, pp. D60-D63, Nov 1995.

[121] A. Yildirir, M. K. Batur, and A. Oto, "Hypertension and arrhythmia: blood pressure control and beyond," *Europace,* vol. 4, no. 2, pp. 175-182, Apr 2002.

[122] G. Mancia *et al.*, "2007 Guidelines for the management of arterial hypertension - The task force for the management of arterial hypertension of the European society of hypertension (ESH) and of the European society of cardiology (ESC)," *Eur Heart J,* vol. 28, no. 12, pp. 1462-1536, Jun 2007.

[123] J. A. Armour, "The little brain on the heart," *Clev Clin J Med,* vol. 74, no. 1, 2007.

[124] M. A. Harman and T. J. Reeves, "Effecrs of efferent vagal stimulation on atrial and ventricular function in dogs," *Am J Physiol,* vol. 215, no. 5, pp. 1210-1217, 1968 1968.

[125] X. Xie *et al.*, "Intermittent Vagal Nerve Stimulation Alters the Electrophysiological Properties of Atrium in the Myocardial Infarction Rat Model," in *36th Annual International Conference of the IEEE-Engineering-in-Medicine-and-Biology-Society (EMBC),* Chicago, IL, 2014, pp. 1575-1578, 2014.

[126] K. Shinlapawittayatorn *et al.*, "Vagus nerve stimulation initiated late during ischemia, but not reperfusion, exerts cardioprotection via amelioration of cardiac mitochondrial dysfunction," *Heart Rhythm,* vol. 11, no. 12, pp. 2278-2287, Dec 2014.

[127] B. Veitenheimer and J. W. Osborn, "Role of spinal V1a receptors in regulation of arterial pressure during acute and chronic osmotic stress," *Am Physiol-Reg I,* vol. 300, no. 2, pp. R460-R469, Feb 2011.

[128] X. Xie, R. Visweswaran, P. A. Guzman, R. M. Smith, J. W. Osborn, and E. G. Tolkacheva, "The effect of cardiac sympathetic denervation through bilateral stellate ganglionectomy on electrical properties of the heart," *Am Physiol-Heart C,* vol. 301, no. 1, pp. H192-H199, Jul 2011.

[129] C. Bell and E. M. McLachlan, "Dependence of deoxycorticosterone salt hypertension in the rat on the activity of the adrenergic cardiac nerves," *Clinical Science,* vol. 57, no. 2, pp. 203-210, 1979 1979.

[130] M. Esler and D. Kaye, "Measurement of sympathetic nervous system activity in heart failure: the role of norepinephrine kinetics," *Heart Fail Rev,* vol. 5, no. 1, pp. 17-25, 2000-Mar 2000.

[131] M. Esler, G. Lambert, H. P. Brunner-La Rocca, G. Vaddadi, and D. Kaye, "Sympathetic nerve activity and neurotransmitter release in humans: translation from pathophysiology into clinical practice," *Acta Physiologica Scandinavica,* vol. 177, no. 3, pp. 275-284, Mar 2003.

[132] M. T. La Rovere, J. T. Bigger, F. I. Marcus, A. Mortara, P. J. Schwartz, and A. Investigators, "Baroreflex sensitivity and heart-rate variability in prediction of total cardiac mortality after myocardial infarction," *The Lancet,* vol. 351, no. 9101, pp. 478-484, Feb 14 1998.

[133] J. Nolan *et al.*, "Prospective study of heart rate variability and mortality in chronic heart failure - Results of the United Kingdom heart failure evaluation and assessment of risk trial (UK-Heart)," *Circulation,* vol. 98, no. 15, pp. 1510-1516, Oct 13 1998.

[134] R. A. Gray, A. M. Pertsov, and J. Jalife, "Spatial and temporal organization during cardiac fibrillation," *Nature,* vol. 392, no. 6671, pp. 75-78, Mar 1998.

[135] S. C. Hao *et al.*, "Effect of beta-adrenergic blockade on dynamic electrical restitution in vivo," *Am J Physiol-Heart C,* vol. 287, no. 1, pp. H390-H394, Jul 2004.

[136] S. E. Hoeks *et al.*, "Increase of 1-year mortality after perioperative beta-blocker withdrawal in endovascular and vascular surgery patients," *Euro J Vasc Endovasc,* vol. 33, no. 1, pp. 13-19, Jan 2007.

[137] G. M. De Ferrari *et al.*, "Chronic vagus nerve stimulation: a new and promising therapeutic approach for chronic heart failure," *Eur Heart J,* vol. 32, no. 7, pp. 847-855, Apr 2011.

[138] T. E. Lohmeier, R. Iliescu, T. M. Dwyer, E. D. Irwin, A. W. Cates, and M. A. Rossing, "Sustained suppression of sympathetic activity and arterial pressure during chronic activation of the carotid baroreflex," *Am J Physiol-Heart C,* vol. 299, no. 2, pp. H402-H409, Aug 2010.

[139] H. N. Sabbah, "Baroreflex activation for the treatment of heart failure," *Curt Cardiol Rep,* vol. 14, no. 3, pp. 326-333, Jun 2012.

[140] K. Heusser *et al.*, "Carotid baroreceptor stimulation, sympathetic activity, baroreflex function, and blood pressure in hypertensive patients," *Hypertension,* vol. 55, no. 3, pp. 619-626, Mar 1 2010.

[141] G. L. Bakris, M. K. Nadim, H. Haller, E. G. Lovett, J. E. Schafer, and J. D. Bisognano, "Baroreflex Activation Therapy provides durable benefit in patients with resistant hypertension: results of long-term follow-up in the Rheos Pivotal Trial," *J Am Soc Hypertens,* vol. 6, no. 2, pp. 152-158, Mar-Apr 2012.

[142] B. Olshansky, H. N. Sabbah, P. J. Hauptman, and W. S. Colucci, "Parasympathetic nervous system and heart failure - Pathophysiology and potential implications for therapy," *Circulation,* vol. 118, no. 8, pp. 863-871, Aug 19 2008.

[143] M. Honda, R. Komatsu, T. Isobe, M. Tabo, and T. Ishikawa, "Involvement of the autonomic nervous system in diurnal variation of corrected QT intervals in common marmosets," *J Pharmacol Sci,* vol. 121, no. 2, pp. 131-137, Feb 2013.

[144] P. J. Schwartz, G. E. Billman, and H. L. Stone, "Autonomic mechanisms in ventricular fibrillation induced by myocardial ischemia during exercise in dogs with healed myocardial infarction - an experimental preparation or sudden cardiac death," *Circulation,* vol. 69, no. 4, pp. 790-800, 1984 1984.

[145] G. Zuanetti, G. M. Deferrari, S. G. Priori, and P. J. Schwartz, "Protective effect of vagal stimulation on reperfustion arrhythmias in cats," *Circ Res,* vol. 61, no. 3, pp. 429-435, Sep 1987.

[146] E. Vanoli, G. M. Deferrari, M. Strambabadiale, S. S. Hull, R. D. Foreman, and P. J. Schwartz, "Vagal stimulation and prevension of sudden death in conscious dogs with a healed myocardial infarcation," *Circ Res,* vol. 68, no. 5, pp. 1471-1481, May 1991.

[147] Z. L. Qu, A. Garfinkel, P. S. Chen, and J. N. Weiss, "Mechanisms of discordant alternans and induction of reentry in simulated cardiac tissue," *Circulation,* vol. 102, no. 14, pp. 1664-1670, Oct 3 2000.

[148] I. Banville and R. A. Gray, "Effect of action potential duration and conduction velocity restitution and their spatial dispersion on alternans and the stability of arrhythmias," *J Cardiovasc Eletr,* vol. 13, no. 11, pp. 1141-1149, Nov 2002.

[149] E. Dupont *et al.*, "Altered connexin expression in human congestive heart failure," *J Mol Cell Cardiol,* vol. 33, no. 2, pp. 359-371, Feb 2001.

[150] M. J. A. Van Kempen, C. Fromaget, D. Gros, A. F. M. Moorman, and W. H. Lamers, "Spatial distribuation of Connexin 43 the major cardiac gap junction protein in the development of adult rat heart," *Circ Res,* vol. 68, no. 6, pp. 1638-1651, 1991 1991.

[151] D. A. Brown and B. O'Rourke, "Cardiac mitochondria and arrhythmias," *Cardiovas Res,* vol. 88, no. 2, pp. 241-249, Nov 2010.

[152] J. O. Foley and F. S. DuBois, "Quantitative studies of the vagus nerve in the cat. I. The ratio of sensory to motor fibers," *Jour Comp Neurol,* vol. 67, no. (1), pp. 49-64, 1937 1937.

[153] D. M. Woodbury and J. W. Woodbury, "EEffects of vagal stimulation on experimentally induced seizures in rats," *Epilepsia,* vol. 31, pp. S7-S19, 1990 1990.

[154] A. Zagon and A. A. Kemeny, "Slow hyperpolarization in cortical neurons: A possible mechanism behind vagus nerve simulation therapy for refractory epilepsy?," *Epilepsia,* vol. 41, no. 11, pp. 1382-1389, Nov 2000.

[155] E. Ben-Menachem, "Vagus-nerve stimulation for the treatment of epilepsy," *Lancet Neurology,* vol. 1, no. 8, pp. 477-482, Dec 2002.

[156] L. E. Fields, V. L. Burt, J. A. Cutler, J. Hughes, E. J. Roccella, and P. Sorlie, "The burden of adult hypertension in the United States 1999 to 2000 - A rising tide," *Hypertension,* vol. 44, no. 4, pp. 398-404, Oct 2004.

[157] World Health Organization, "Global brief on hypertension," *World Health Organization,* 2013.

[158] B. M. Egan, Y. Zhao, R. N. Axon, W. A. Brzezinski, and K. C. Ferdinand, "Uncontrolled and apparent treatment resistant hypertension in the United States, 1988 to 2008," *Circulation,* 111.030189, 2011.

[159] E. M. Annoni *et al.*, "Intermittent electrical stimulation of the right cervical vagus nerve in salt-sensitive hypertensive rats: effects on blood pressure, arrhythmias, and ventricular electrophysiology," *Physiological Reports,* vol. 3, no. 8, p. e12476, 2015.

[160] S. W. Lee *et al.*, "Chronic cyclic vagus nerve stimulation has beneficial electrophysiological effects on healthy hearts in the absence of autonomic imbalance," *Physiological Reports,* vol. 4, no. 9, 2016.

[161] E. M. Annoni and E. G. Tolkacheva, "Acute hemodynamic effects of vagus nerve stimulation in conscious hypertensive rats," in *40th Annual International Conference of the IEEE-Engineering-in-Medicine-and-Biology-Society (EMBC)*, Honolulu, HI, 2018.

[162] G. Bertinieri, M. Di Rienzo, A. Cavallazzi, A. Ferrari, A. Pedotti, and G. Mancia, "A new approach to analysis of the arterial baroreflex," *J Hypertens,* vol. 3, no. 3, pp. S79-81, 1985.

[163] W. B. White, "Importance of blood pressure control over a 24-hour period,"*J Manage Care Pharm,* vol. 13, no. 8 Supp B, pp. 34-39, 2007.

[164] W. B. White, "Ambulatory blood pressure monitoring: dippers compared with non-dippers," *Blood Pressure Monitoring,* vol. 5, pp. S17-23, 2000.

[165] K. Saku *et al.*, "Afferent vagal nerve stimulation resets baroreflex neural arc and inhibits sympathetic nerve activity," *Physiological Reports,* vol. 2, no. 9, p. e12136, 2014.

[166] M. W. Chapleau, "Baroreceptor Reflexes-Chapter 33," 2012.

[167] M. Inoko, Y. Kihara, I. Morii, H. Fujiwara, and S. Sasayama, "Transition from compensatory hypertrophy to dilated, failing left ventricles in Dahl salt-sensitive rats," *Am J Physiol-Heart C,* vol. 267, no. 6, pp. H2471-H2482, 1994.

[168] T. P. Nguyen *et al.*, "Increased susceptibility of spontaneously hypertensive rats to ventricular tachyarrhythmias in early hypertension," *J Physiol,* vol. 594, no. 6, pp. 1689-1707, 2016.

[169] K. Yoshida *et al.*, "Acute electrical vagal nerve stimulation exerts powerful anti-inflammatory effects through its nicotinic action in rats with pulmonary arterial hypertension," *The FASEB Journal*, vol. 31, no. 1 Supplement, pp. 697.6-697.6, 2017.

[170] J. Schultz, E. M. Annoni, and E. G. Tolkacheva, "Isolating low frequency oscillations in baroflex function in rats," in *40th Annual International Conference of the IEEE-Engineering-in-Medicine-and-Biology-Society (EMBC)*, Honolulu, HI, 2018.

[171] D. Ojeda *et al.*, "Sensitivity analysis of vagus nerve stimulation parameters on acute cardiac autonomic responses: Chronotropic, inotropic and dromotropic effects," *PloS one*, vol. 11, no. 9, p. e0163734, 2016.

[172] C. Höcht, "Blood pressure variability: prognostic value and therapeutic implications," *ISRN Hypertension*, vol. 2013, 2013.

[173] D. Clement, L. Jordaens, and G. Heyndrickx, "Influence of vagal nervous activity on blood pressure variability," *J Hypertens*, vol. 2, no. 3, pp. S391-3, 1984.

[174] E. M. Annoni and E. G. Tolkacheva, "Acute hemodynamic effects of vagus nerve stimulation in conscious hypertensive rats," in *40th Annual International Conference of the IEEE-Engineering-in-Medicine-and-Biology-Society (EMBC)*, Honolulu, HI, In press.

[175] H. Calkins *et al.*, "2012 HRS/EHRA/ECAS expert consensus statement on catheter and surgical ablation of atrial fibrillation: recommendations for patient selection, procedural techniques, patient management and follow-up, definitions, endpoints, and research trial design: a report of the Heart Rhythm Society (HRS) Task Force on Catheter and Surgical Ablation of Atrial Fibrillation." *Heart Rhythm*, vol. 9, no. 4, pp. 632-696. e21, 2012.

[176] W. He and Y. Chu, "Atrial fibrillation as a prognostic indicator of myocardial infarction and cardiovascular death: a systematic review and meta-analysis," *Scientific reports*, vol. 7, no. 1, p. 3360, 2017.

[177] M. R. Reynolds and V. Essebag, "Economic burden of atrial fibrillation: implications for intervention," *Am J Pharm Benefits*, vol. 4, no. 2, pp. 58-65, 2012.

[178] M. H. Kim, S. S. Johnston, B.-C. Chu, M. R. Dalal, and K. L. Schulman, "Estimation of total incremental health care costs in patients with atrial fibrillation in the United States," *Circ-Cardiovasc Qual*, vol. 4, no. 3, pp. 313-320, 2011.

[179] G. Y. H. Lip *et al.*, "Atrial fibrillation," vol. 2, 2016.

[180] A. Amin, A. Houmsse, A. Ishola, J. Tyler, and M. Houmsse, "The current approach of atrial fibrillation management," *Avicenna Journal of Medicine*, vol. 6, no. 1, p. 8, 2016.

[181] C. T. January *et al.*, "2014 AHA/ACC/HRS guideline for the management of patients with atrial fibrillation: a report of the American College of Cardiology/American Heart Association Task Force on Practice Guidelines and the Heart Rhythm Society," *J Am Coll Cardiol*, vol. 64, no. 21, pp. e1-e76, 2014.

[182] F. Luca *et al.*, "Pharmacological management of atrial fibrillation: One, none, one hundred thousand," *Cardiology Research and Practice,* vol. 2011, 2011.

[183] T.-F. Chao *et al.*, "Clinical outcome of catheter ablation in patients with nonparoxysmal atrial fibrillation clinical perspective: results of 3-year follow-up," *Circ-Arrhythmia Elec,* vol. 5, no. 3, pp. 514-520, 2012.

[184] P. Chowdhury, W. R. Lewis, R. A. Schweikert, and J. E. Cummings, "Ablation of atrial fibrillation: What can we tell our patients," *Cleve Clin J Med,* vol. 76, no. 9, pp. 543-550, 2009.

[185] T. J. Jensen, J. Haarbo, S. M. Pehrson, and B. Thomsen, "Impact of premature atrial contractions in atrial fibrillation," *PACE,* vol. 27, no. 4, pp. 447-452, 2004.

[186] J. W. Waks and M. E. Josephson, "Mechanisms of atrial fibrillation–reentry, rotors and reality," *Arrhythmia & Electrophysiology Review,* vol. 3, no. 2, p. 90, 2014.

[187] M. Haissaguerre *et al.*, "Spontaneous initiation of atrial fibrillation by ectopic beats originating in the pulmonary veins," *New Engl J Med,* vol. 339, no. 10, pp. 659-666, 1998.

[188] D. E. Krummen, V. Swarup, and S. M. Narayan, "The role of rotors in atrial fibrillation," *J Thorac Dis,* vol. 7, no. 2, pp. 142-151, Feb 2015.

[189] M. S. Guillem, A. M. Climent, M. Rodrigo, F. Fernández-Avilés, F. Atienza, and O. Berenfeld, "Presence and stability of rotors in atrial fibrillation: evidence and therapeutic implications," *Cardiovas Res,* vol. 109, no. 4, pp. 480-492, 2016.

[190] G. Moe and J. Abildskov, "Atrial fibrillation as a self-sustaining arrhythmia independent of focal discharge," *Am Heart J,* vol. 58, no. 1, pp. 59-70, 1959.

[191] G. K. Moe, "On the multiple wavelet hypothesis of atrial fibrillation," *Arch Int Pharmacodyn Ther,* vol. 140, pp. 183-188, 1962.

[192] M. Yamazaki and J. Jalife, "Pathophysiology of atrial fibrillation: from initiation to maintenance," *Journal of Arrhythmia,* vol. 28, no. 3, pp. 129-139, 2012.

[193] M. A. Allessie, "Experimental evaluation of Moe's multiple wavelet hypothesis of atrial fibrillation," *Cardiac Electrophysiology and Arrhythmias,* pp. 265-275, 1985.

[194] J. L. Cox, "The surgical treatment of atrial fibrillation. IV. Surgical technique," *J Thorac Cardiov Sur,* vol. 101, no. 4, pp. 584-592, 1991.

[195] A. T. Winfree, "Spiral waves of chemical activity," *Science,* vol. 175, no. 4022, pp. 634-636, 1972.

[196] J. M. Davidenko, P. F. Kent, D. R. Chialvo, D. C. Michaels, and J. Jalife, "Sustained vortex-like waves in normal isolated ventricular muscle," *Proceedings of the National Academy of Sciences,* vol. 87, no. 22, pp. 8785-8789, 1990.

[197] S. V. Pandit and J. Jalife, "Rotors and the dynamics of cardiac fibrillation," *Circ Res,* vol. 112, no. 5, pp. 849-862, Mar 2013.

[198] S. Zlochiver, V. Munoz, K. L. Vikstrom, S. M. Taffet, O. Berenfeld, and J. Jalife, "Electrotonic myofibroblast-to-myocyte coupling increases propensity to reentrant arrhythmias in two-dimensional cardiac monolayers," *Biophysical Journal,* vol. 95, no. 9, pp. 4469-4480, 2008.

[199] J. A. Zaman, N. S. Peters, and S. M. Narayan, "Rotor mapping and ablation to treat atrial fibrillation," *Curr Opin Cardiol,* vol. 30, no. 1, p. 24, 2015.

[200] J. Jalife, O. Berenfeld, and M. Mansour, "Mother rotors and fibrillatory conduction: a mechanism of atrial fibrillation," *Cardiovas Res,* vol. 54, no. 2, pp. 204-216, May 2002, Art. no. Pii s0008-6363(02)00223-7.

[201] D. Filgueiras-Rama *et al.*, "High-resolution endocardial and epicardial optical mapping in a sheep model of stretch-induced atrial fibrillation," *JoVE,* no. 53, 2011.

[202] M. Yamazaki *et al.*, "Heterogeneous atrial wall thickness and stretch promote scroll waves anchoring during atrial fibrillation," *Cardiovas Res,* vol. 94, no. 1, pp. 48-57, 2012.

[203] S. M. Narayan, D. E. Krummen, P. Clopton, K. Shivkumar, and J. M. Miller, "Direct or coincidental elimination of stable rotors or focal sources may explain successful atrial fibrillation ablation: on-treatment analysis of the CONFIRM trial (Conventional ablation for AF with or without focal impulse and rotor modulation)," *J Am Coll Cardiol,* vol. 62, no. 2, pp. 138-147, 2013.

[204] S. Narayan, D. Krummen, A. Donsky, V. Swarup, G. Tomassoni, and J. Miller, "Treatment of paroxysmal atrial fibrillation by targeted elimination of stable rotors and focal sources without pulmonary vein isolation: the precise rotor elimination without concomitant pulmonary vein isolation for subsequent elimination of PAF (PRECISE) trial," *Heart Rhythm,* vol. 10, no. 9 Supplement, p. 1414, 2013.

[205] P. Sanders *et al.*, "Spectral analysis identifies sites of high-frequency activity maintaining atrial fibrillation in humans," *Circulation,* vol. 112, no. 6, pp. 789-797, Aug 2005.

[206] R. Mandapati, A. Skanes, J. Chen, O. Berenfeld, and J. Jalife, "Stable microreentrant sources as a mechanism of atrial fibrillation in the isolated sheep heart," *Circulation,* vol. 101, no. 2, pp. 194-199, Jan 2000.

[207] F. Atienza *et al.*, "Real-time dominant frequency mapping and ablation of dominant frequency sites in atrial fibrillation with left-to-right frequency gradients predicts long-term maintenance of sinus rhythm," *Heart Rhythm,* vol. 6, no. 1, pp. 33-40, Jan 2009.

[208] M. Baumert, P. Sanders, and A. Ganesan, "Quantitative-electrogram-based methods for guiding catheter ablation in atrial fibrillation," *Proceedings of the Ieee,* vol. 104, no. 2, pp. 416-431, Feb 2016.

[209] S. M. Narayan, D. E. Krummen, K. Shivkumar, P. Clopton, W. J. Rappel, and J. M. Miller, "Treatment of atrial fibrillation by the ablation of localized sources CONFIRM (Conventional Ablation for Atrial Fibrillation With or Without Focal Impulse and Rotor Modulation) Trial," *J Am Coll Cardiol,* vol. 60, no. 7, pp. 628-636, Aug 2012.

[210] K. Nademanee *et al.*, "A new approach for catheter ablation of atrial fibrillation: Mapping of the electrophysiologic substrate," *J Am Coll Cardiol,* vol. 43, no. 11, pp. 2044-2053, Jun 2004.

[211] N. Habel *et al.*, "The temporal variability of dominant frequency and complex fractionated atrial electrograms constrains the validity of sequential mapping in human atrial fibrillation," *Heart Rhythm,* vol. 7, no. 5, pp. 586-593, May 2010.

[212] N. Sasaki *et al.*, "Localized rotors and focal impulse sources within the left atrium in human atrial fibrillation: A phase analysis of contact basket catheter electrograms," *Journal of Arrhythmia,* vol. 32, no. 2, pp. 141-144, Apr 2016.

[213] A. Yaksh *et al.*, "Atrial fibrillation: to map or not to map?," *Netherlands Heart Journal,* vol. 22, no. 6, pp. 259-266, 2014.

[214] N. M. de Groot, M. J. Schalij, K. Zeppenfeld, N. A. Blom, E. T. Van der Velde, and E. E. Van der Wall, "Voltage and activation mapping: how the recording technique affects the outcome of catheter ablation procedures in patients with congenital heart disease," *Circulation,* vol. 108, no. 17, pp. 2099-2106, 2003.

[215] S. Arunachalam, S. Kapa, S. Mulpuru, P. Friedman, and E. Tolkacheva, "Novel approaches for quantitative electrogram analysis for intraprocedural guidance for catheter ablation: A case of a patient with persistent atrial fibrillation," *Nuclear Medicine and Biomedical Imaging,* vol. 2, no. 2, 2017.

[216] F. Atienza and J. Jalife, "Reentry and atrial fibrillation," *Heart Rhythm,* vol. 4, no. 3, pp. S13-S16, 2007.

[217] R. Latchamsetty and A. G. Kocheril, "Review of dominant frequency analysis in atrial fibrillation," *Journal of Atrial Fibrillation,* vol. 2, no. 3, 2009.

[218] M. S. Guillem *et al.*, "Non-invasive localization of maximal frequency sites of atrial fibrillation by body surface potential mapping," *Circulation: Arrhythmia and Electrophysiology,* p. CIRCEP. 113.000167, 2013.

[219] M. Sohal *et al.*, "Is mapping of complex fractionated electrograms obsolete?," *Arrhythmia & Electrophysiology Review,* vol. 4, no. 2, p. 109, 2015.

[220] Y. Takahashi *et al.*, "Characterization of electrograms associated with termination of chronic atrial fibrillation by catheter ablation," *J Am Coll Cardiol,* vol. 51, no. 10, pp. 1003-1010, 2008.

[221] C. Schilling, "Analysis of Atrial Electrograms," *KIT Scientific Publishing,* 2012.

[222] A. S. Jadidi *et al.*, "Inverse relationship between fractionated electrograms and atrial fibrosis in persistent atrial fibrillation: combined magnetic resonance imaging and high-density mapping," *J Am Coll Cardiol,* vol. 62, no. 9, pp. 802-812, 2013.

[223] K. Konings, C. Kirchhof, J. Smeets, H. Wellens, O. C. Penn, and M. A. Allessie, "High-density mapping of electrically induced atrial fibrillation in humans," *Circulation,* vol. 89, no. 4, pp. 1665-1680, 1994.

[224] A. S. Jadidi *et al.*, "Functional nature of electrogram fractionation demonstrated by left atrial high-density mapping," *Circ-Arrhythmia Elec,* vol. 5, no. 1, pp. 32-42, 2012.

[225] A. Verma *et al.*, "Approaches to catheter ablation for persistent atrial fibrillation," *New Engl J Med,* vol. 372, no. 19, pp. 1812-1822, 2015.

[226] K. Umapathy *et al.*, "Phase mapping of cardiac fibrillation," *Circ-Arrhythmia Elec,* vol. 3, no. 1, pp. 105-114, 2010.

[227] R. Vijayakumar, S. K. Vasireddi, P. S. Cuculich, M. N. Faddis, and Y. Rudy, "Methodology considerations in phase mapping of human cardiac arrhythmias," *Circ-Arrhythmia Elec,* vol. 9, no. 11, p. e004409, 2016.

[228] M. Haissaguerre *et al.*, "Noninvasive panoramic mapping of human atrial fibrillation mechanisms: a feasibility report," *J Cardiovasc Electr,* vol. 24, no. 6, pp. 711-717, 2013.

[229] M. Rodrigo *et al.*, "Highest dominant frequency and rotor positions are robust markers of driver location during noninvasive mapping of atrial fibrillation: A computational study," *Heart Rhythm,* vol. 14, no. 8, pp. 1224-1233, 2017.

[230] S. P. Arunachalam, S. K. Mulpuru, P. A. Friedman, E. G. Tolkacheva, "Feasibility of visualizing higher regions of Shannon Entropy in atrial fibrillation patients," in *37th Annual International Conference of the IEEE Engineering in Medicine and Biology Society (EMBC),* Milan, Italy, 2015, pp. 4499-4502, 2015.

[231] A. N. Ganesan *et al.*, "Bipolar electrogram shannon entropy at sites of rotational activation: implications for ablation of atrial fibrillation," *Circ-Arrhythmia Elec,* p. CIRCEP. 112.976654, 2012.

[232] S. P. Arunachalam, E. M. Annoni, S. K. Mulpuru, P. A. Friedman, and E. G. Tolkacheva, "Novel multiscale frequency approach to identify the pivot point of the rotor," *Journal of Medical Devices-Transactions of the ASME,* vol. 10, no. 2, Jun 2016, Art. no. 020948.

[233] S. P. Arunachalam, E. M. Annoni, S. K. Mulpuru, P. A. Friedman, and E. G. Tolkacheva, "Kurtosis as a statistical approach to identify the pivot point of the rotor," in *Engineering in Medicine and Biology Society (EMBC), 2016 IEEE 38th Annual International Conference of the,* 2016, pp. 497-500: IEEE.

[234] S. Arunachalam, E. Annoni, and E. Tolkacheva, "Novel multiscale entropy approach for rotor pivot point identification," in *BMES Annual Meeting,* 2016.

[235] R. A. Gray *et al.*, "Mechanisms of cardiac fibrillation," *Science,* vol. 270, no. 5239, pp. 1222-1223, Nov 1995.

[236] A. M. Pertsov, J. M. Davidenko, R. Salomonsz, W. T. Baxter, and J. Jalife, "Spiral waves of excitation underlie reentrant activity in isolated cardiac muscle," *Circ Res,* vol. 72, no. 3, pp. 631-650, Mar 1993.

[237] F. H. Samie *et al.*, "A mechanism of transition from ventricular fibrillation to tachycardia - Effect of calcium channel blockade on the dynamics of rotating waves," *Circ Res*, vol. 86, no. 6, pp. 684-691, Mar 2000.

[238] J. M. Davidenko, "Spiral wave activity - a possible common mechanism for polymorphic and monomorphic ventricular tachycardia," *J Cardiovasc Electr,* vol. 4, no. 6, pp. 730-746, Dec 1993.

[239] F. H. Samie and J. Jalife, "Mechanisms underlying ventricular tachycardia and its transition to ventricular fibrillation in the structurally normal heart," *Cardiovas Res,* vol. 50, no. 2, pp. 242-250, May 2001.

[240] S. Mironov, J. Jalife, and E. G. Tolkacheva, "Role of conduction velocity restitution and short-term memory in the development of action potential duration alternans in isolated rabbit hearts," *Circulation,* vol. 118, no. 1, pp. 17-25, Jul 2008.

[241] A. Matiukas, A. M. Pertsov, P. Kothari, A. Cram, E. G. Tolkacheva, and Ieee, "Optical mapping of electrical heterogeneities in the heart during global ischemia," in *Annual International Conference of the IEEE-Engineering-in-Medicine-and-Biology-Society*, Minneapolis, MN, 2009, pp. 6321-+, 2009.

[242] R. Arora, M. K. Das, D. P. Zipes, and J. Wu, "Optical mapping of cardiac arrhythmias," *Indian Pacing and Electrophysiology Journal*, vol. 3, no. 4, p. 187, 2003.

[243] D. Rosenbaum and J. Jalife, *Optical Mapping of Cardiac Excitation and Arrhythmias*. Wiley-Blackwell, 2001.

Appendix A

Techniques

Animal Surgical Procedures

All experiments were approved by the University of Minnesota Animal Care and Use Committee and were conducted in accordance with Institutional and NIH guidelines (NIH publication No. 85-23, revised 1996).

Vagus Nerve Stimulator Implantation

VNS stimulators were implanted subcutaneously on the lower back of the rats as described previously [125, 126]. Briefly, the back and the neck were shaved, and the right cervical vagus nerve and common carotid artery bundle were isolated from the surrounding tissue through a small incision on the neck. Bipolar cuff electrodes were placed around the bundle. The pulse generator (8 cc, 14 g) was then implanted subcutaneously and positioned on the back of the rat. Parameters of the intermittent VNS for the study presented in Chapter 3 were set as follows: pulse frequency 20 Hz; pulse width 500 μs; output current 1.0 mA. The VNS therapy was delivered with a duty cycle of 15% with VNS on for 7 s followed by 66 s of VNS off. Parameters for VNS in the study presented in Chapters 4 and 5 were set as follows: pulse frequency 20 Hz; pulse width 500 μs; output current set individually for each rat resulting in a heart rate drop of no more than 5% while VNS in on. The VNS therapy was delivered with a duty cycle of 23% with VNS on for 14 s followed by 66 s of VNS off. Note each episode of VNS includes a 2-second ramp up and ramp down which are part of the 66 sec “Off” period but included in the “On” period for duty cycle calculations.

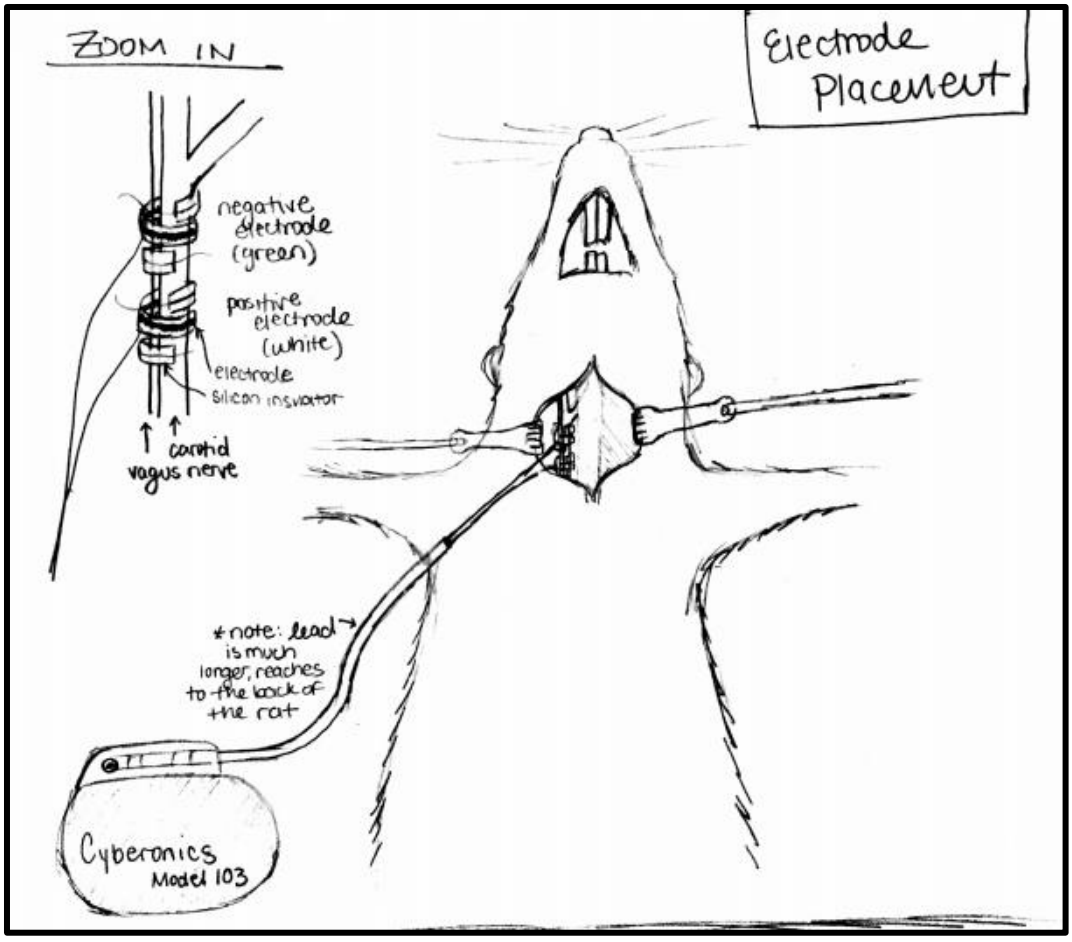

DSI Telemetry System Implantation

The DSI transmitter implantation was performed as described previously[48]. Briefly, the surgical regions, the chest and inner leg, were shaved and the transmitter pressure catheter was implanted into the descending aorta through the left femoral artery. The two ECG leads were fixed subcutaneously on the chest muscle. Following recovery, the rats were conscious and freely moving in their home cage for the duration of the in-vivo study. Continuous arterial blood pressure and ECG data acquisitions were performed at a sampling rate of 500 Hz with the use of commercially available telemetry system (DSI, Inc.). Each cage is placed on a receiver (Model RPC1, DSI Inc.) that was connected to a computer via a Data Exchange Matrix (DSI Inc.).

OPTICAL MAPPING

At the end of the in-vivo protocol, the rats were sacrificed and the hearts were extracted through

a thoracotomy for ex-vivo optical mapping studies. The hearts were cannulated through the aorta and Langendorff-perfused using a warm (37 +/- 1 °C), oxygenated Tyrode's solution (in mM: NaCl 130, CaCl2 1.8, KCl 4, MgCl2, 1.0, NaH2PO4 1.2, NaHCO3 24, C6H12O6 5.5, pH 7.4) under constant pressure [128]. Blebbistatin (10 μM) was added to the Tyrode's solution to reduce motion artifact and voltage sensitive dye, Di4-ANNEPS, was added (5 μg/mL) to the perfusate. The dye was excited using two continuous-excitation lasers with a wavelength of 532nm (Millenia Pro 5sJ, Spectra-Physics Inc., Mountain View, CA, USA). The voltage/action potentials from the epicardial surface of both ventricles were captured using two synchronized 14-bit CCD cameras (Little Joe CCD39, SciMeasure Analytical Systems Inc., GA, USA). The cameras captured the cardiac electrical signal at a rate of 1000 frames per second with 80x80 pixel resolution from approximately 80% of the ventricular surface.

The hearts were then paced to assess the electrophysiological changes during sinus rhythm, periodic pacing, and through VF induction. The HTN hearts were paced at a progressively decreasing basic cycle length (BCL), from 200 down to 100 ms in steps of 20 ms then from 90 ms down to 60 ms in steps of 10 ms or until ventricular tachycardia (VT) or ventricular fibrillation (VF) induction. At each BCL, 50 stimuli were applied to reach steady state, and the last 10 stimuli were recorded for analysis. If the hearts did not exhibit VT or VF during the dynamic pacing protocol, the VT/VF induction protocol was used.

Optical Mapping Analysis

Using the optical mapping videos, the following parameters regarding the electrophysiological properties of the Sham and VNS hearts were calculated at varying BCLs for both the right ventricle (RV) and left ventricle (LV) as previously described [128, 240]: action potential duration (APD), spatial heterogeneity of APD, slope of APD restitution, conduction velocity (CV), and VT/VF analysis.

APD: optical APD was measured at 80% repolarization (APD_{80}) and 2D maps were constructed to observe the spatial distribution of APDs on the epicardial surface of the RV and LV.

Spatial heterogeneity of APD: Spatial distribution of APD was estimated using the heterogeneity index, μ^{50}. This index was calculated as follows:

$$\mu = \frac{APD_{95} - APD_{5}}{APD_{50}}$$

Where APD_{95} and APD_5 are the 95th and 5th percentiles of the APD distribution respectively and APD_{50} is the median APD distribution.

Slope of APD restitution: At each pixel, the maximum slope of the APD restitution curve was calculated using a results from the dynamic pacing protocol. 2D slope maps were obtained for the RV and LV separately. These maps were used to compare arrhythmia susceptibility between the treated and untreated groups.

Conduction velocity: The local CV was measured as described previously[50]. The distributions of activation times for the spatial regions of 5x5 pixels were fitted to a plane. Gradients of activation times, g_x and g_y, were calculated for the plane along the x and y axes respectively. The magnitude of the local CV was calculated for each pixel as:

$$CV = \frac{1}{\sqrt{g_x^2 + g_y^2}}$$

Mean values and standard errors of CV were recorded at each BCL for the RV and LV.

VT/VF analysis: Episodes of VT or VF were captured using optical mapping. Three second videos of VT or VF were recorded and used to analyze the complexity of the cardiac arrhythmias in the Sham and VNS hearts. These episodes were evaluated to determine the number of domains and the corresponding DF for each domain by constructing 2D DF maps of the LV and RV.